Spindynamik komplexer itineranter Magnete

Spin dynamics of complex itinerant magnets

Dissertation

zur Erlangung des akademischen Grades
Doctor rerum naturalium (*Dr. rer. nat.*)

vorgelegt der

Naturwissenschaftlichen Fakultät II – Chemie und Physik
der Martin-Luther-Universität Halle-Wittenberg

von mgr inż. Paweł Adam Buczek, M.Sc.
geboren am 7.7.1981 in Rybnik, Polen

Gutachter:

1: PD Dr. Leonid M. Sandratskii, MPI Halle (Betreuer)
2: Prof. Dr. Wolfram Hergert, MLU Halle-Wittenberg
3: Prof. Dr. Julie Staunton, University of Warwick

Halle, den 27.4.2009
(Tag der Verteidigung)

Paweł Buczek

Spin dynamics of complex itinerant magnets

Abstract. In order to gain an insight into the nature of magnetic excitations in complex itinerant magnets, an implementation of the linear response density functional theory based on the Korringa-Kohn-Rostoker Green's function method was developed and tested. In the first part of the thesis an outline of the ground state formalism and the linear perturbation theory is provided. Subsequently, the computational scheme is described. First applications of the code are magnetic excitations in the bulk phases of cobalt, several Heusler alloys (NiMnSb, Co_2MnSi and Cu_2MnAl) and thin iron films, both supported on a W(110) substrate and free standing. While qualitatively the spin-dynamics of all these systems can be understood within the spin-polarized Fermi gas model, quantitatively their behavior can be quite different. The life-time of moderately long wave-length magnons is very short in the case of bcc Fe, but in the half-metallic magnets certain important decay mechanisms may become inoperative. Both the damping and the energies of magnons depend sensitively on the electronic structure, modified for example by the presence of a substrate, as demonstrated in the Fe/W(110) example. Special attention is paid to the relation between the dynamic approach and adiabatic spin dynamics based on the mapping onto the Heisenberg Hamiltonian. The latter treatment cannot account for the decay of spin-waves but it appears to be in most cases sufficient to give an estimate of the magnon dispersion relation; nonetheless, there exist limitations.

Zusammenfassung. Um Einblicke in die Natur magnetischer Anregungen in komplexen itineranten Magneten zu gewinnen, wurde eine Implementation der Dichtefunktionaltheorie mitsamt Lineare-Antwort-Formalismus, eingebettet in den Rahmen der Greensche-Funktion-Vielfachstreutheorie nach Korringa, Kohn und Rostoker, entwickelt und getestet. Im ersten Teil der vorliegenden Arbeit wird ein Überblick über den Grundzustandsformalismus und lineare Störungstheorie gegeben, anschließend wird das Berechnungsverfahren beschrieben. Erste Anwendungen des Codes sind magnetische Anregungen von Cobalt und verschiedenen Heuslerverbindungen (NiMnSb, Co_2MnSi und Cu_2MnAl) als Volumenmaterial sowie von dünnen Eisenschichten, frei oder auf W(110). Obwohl die Spindynamik dieser Systeme qualitativ gut durch das Modell des polarisierten Fermigases beschrieben wird, können quantitativ große Unterschiede auftreten. Die Lebensdauer von Magnonen mittlerer Wellenlängen reicht von extrem kleinen Werten in bcc Fe bis hin zu unendlich großen in halbmetallischen Magneten. Dämpfung und Energie der Magnonen hängen empfindlich von der elektronischen Struktur ab. Letztere wird zum Beispiel durch die Anwesenheit eines Substrats beeinflusst, wie am Beispiel von Fe/W(110) gezeigt wird. Ein weiterer Augenmerk liegt auf der Beziehung zwischen dem hier beschriebenen dynamischen Ansatz und der adiabatischen Spindynamik, welche durch Abbilden auf einen Heisenberg-Hamiltonian definiert ist. Letztere kann zwar nicht das Abklingen der Spinwellen erklären, jedoch gibt sie in den meisten Fällen eine hinreichend gute Näherung für die Dispersionsrelation der Magnonen; nichtsdestoweniger exisiteren für sie etliche Einschränkungen.

CONTENTS

INTRODUCTION

A sample exposed to an oscillating external field can absorb energy by changing its magnetic configuration. Such transitions are called *magnetic excitations* and their theoretical understanding is the subject of this thesis. The absorption can have a sharp resonant character, as presented in Fig. 1.1, and these excited long-living states have been named *spin-waves*. They will be of particular interest here.
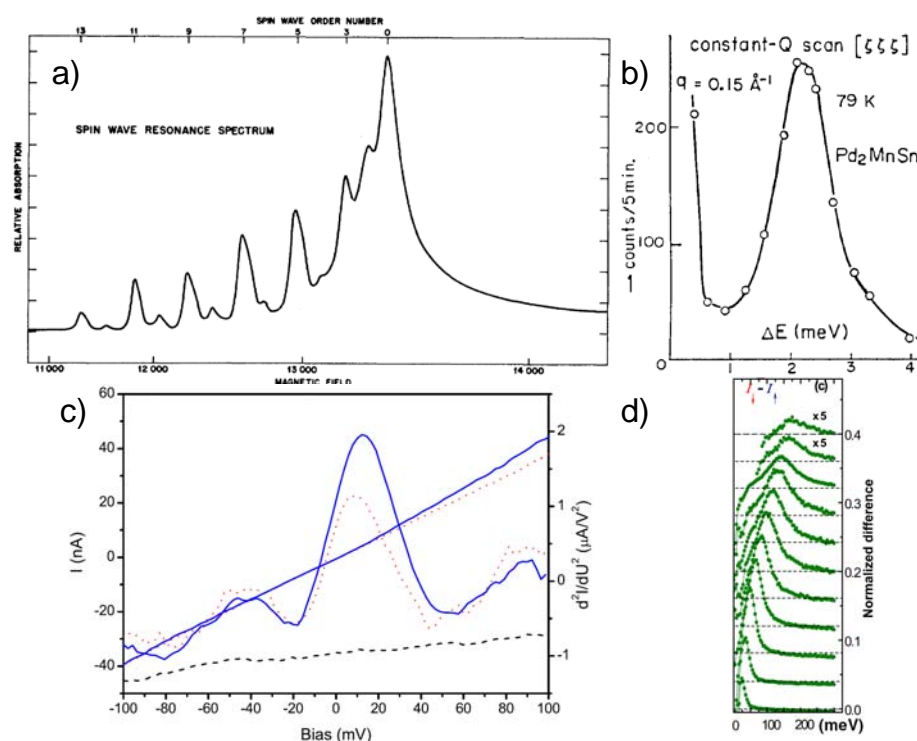
Figure 1.1: Four examples of experiments capable of detecting spin-waves: spin-wave resonance (a, 5600 Å permalloy film, Ref. [1]), inelastic neutron scattering (b, Heusler phase Pd_2MnSn, Ref. [2]), spin-polarized scanning tunneling spectroscopy (c, 3 and 4 monolayers of Co on Cu(111), Ref. [3]) and spin-polarized electron energy loss spectroscopy (SPEELS) (d, 2 monolayers of Fe on W(110), Ref. [4]). The absorption peaks have a well defined position – corresponding to the excitation energy – and a breadth larger than detectors' resolution, which signifies a finite life-time of the quasi-particles.

Not accidentally the thesis begins with a reference to experiment. The condensed matter theory allows us to believe that magnetism of solids is mainly an electronic property, in the simplest picture arising from combination of the Coulomb interaction and the antisymmetric Fermionic wave-function. The experiments involving magnetic excitations offer therefore a probe into the interacting electron gas in

solids, allowing the development and testing of models of this intricate physical object. The last five years witnessed the birth of new experimental techniques like spin-polarized electron energy loss spectroscopy (SPEELS) [5] and scanning tunneling (microscope) spectroscopy (STS) [3], which joined the time honored spin-wave resonance [6, 7, 8, 9] and inelastic neutron scattering (INS) [10]. These new methods offer exciting possibilities to study the magnetic excitations in nanostructures.

Magnetic excitations are indispensable in the theoretical language of magnetism. First of all, the spectrum of these excitations determines the thermodynamics of the magnetic materials and the magnetic transition temperature [11]. Furthermore, the magnetic excitations contribute to the electronic specific heat and the electrical and thermal conductivity. They couple to charge degrees of freedom [12], control the hot electrons' mean free path [13] and even are believed to provide a coupling mechanism in high temperature superconductors [14].

The very dependence of the transition temperature on properties of these excitations makes their studies interesting from the practical point of view, but other applications have also been suggested, e.g. the possibility of inter-chip communication based of spin-torque effect [15, 16]. Ever faster magnetic storage technologies gradually approach the limit where the production of magnetic excited states cannot be neglected.

A substantial part of this thesis, especially chapters 2 and 3, pertain to a rather general condensed matter system, but the *itinerant magnets* [17] are in the focal point of this work. In these materials spin-waves are identified as collective low-energetic modes. Another type of magnetic excitations are the particle-hole triplet states called *Stoner excitations*. The Stoner states are pronounced mostly at higher energies, corresponding roughly to the exchange splitting of electron states, but they can have non-vanishing contribution also in the spin-wave energy region and lead to the damping of the spin-wave states. In some materials, most notably in half-metals, spin-waves can exist in a gap of the Stoner continuum and their decay to these states is impossible. In our formalism such spin-waves live infinitely long. Of course in reality other – usually smaller – effects are still operative. They could be captured in a language of magnon-magnon or magnon-phonon interactions, to mention a few. The latter phenomena are not considered in this thesis. On the other hand, the high-energy magnons usually coexist with high density Stoner states and can be strongly damped. When the width of the spin-wave peak is comparable in magnitude to the peak's energy, the magnon cannot be regarded as a well defined excitations anymore.

Until now the main body of theoretical studies on magnetic excitations has been based on the adiabatic treatment of magnetic degrees of freedom [18]. In this approach one maps the system onto an effective Heisenberg Hamiltonian, which is much easier to study. The formalism has been formulated in two major flavors, namely the frozen magnon approximation [19] or magnetic force theorem [20]. The methods utilize density functional theory and do not involve adjustable parameters, yielding the dispersion relation of spin-waves. In this approach the presence of the Stoner continuum is neglected and no prediction regarding life-times can be made.

Damping can be captured in calculations of wave-vector and frequency-dependent magnetic susceptibility χ, where spin-waves and Stoner states are treated on an equal footing. The position of the singularities of χ in the complex energy plane determines energies and life times of magnetic excitations. Cooke *et al.* in 1980 [21] computed the susceptibility of Ni and Fe using the random phase approximation to susceptibility starting from an idealized band structure. The dynamic method became particularly powerful after a formulation using the parameter free linear response density functional theory developed in 1985 by Gross and Kohn [22, 23]. (Earlier work of Callaway, Laurent & Wang [24] contains already all important elements of the magnetic response in local approximation.) From this time on several works addressing the paramagnetic susceptibility appeared along this line [25, 26, 27, 28, 29]. In 1998 Savrasov presented the first calculation of the susceptibility for magnetically ordered systems using linear response density functional theory.

The approach presented in this thesis is formally equivalent to the work of Savrasov, but technically rather different because of the use of Green's functions. It is from the very beginning meant to address complex magnetic structures, including systems with broken translational symmetry like surfaces and in-

terfaces. In the latter case the damping was predicted to be more severe (e.g. [30]) and lead to a qualitative failure of adiabatic methods.

The structure of the thesis is as follows. Chapters 2 and 3 outline the formalism of the ground state and the linear response calculations. Chapter 4 treats the spin dynamics of the uniform polarized Fermi gas; the model is conceptually very important for understanding spin-waves in itinerant ferromagnets. Being exactly solvable, it provides us with a benchmark for testing the developed code. Chapter 5 describes the implementation of the linear response theory within the Hutsepot Korringa-Kohn-Rostoker environment. The fruit of two years of author's work on code development is summarized there, but the chapter is rather technical and can be skipped at first reading, possibly except Sec. 5.5, where several ways of interpreting the susceptibility matrix are discussed. Subsequent chapters describe first applications of the computational scheme, namely spin-waves of bulk cobalt (Chap. 6), several Heusler phases (Chap. 7) and iron in bulk and thin film geometry (Chap. 8). All results presented are new. The accompanying discussion features several recurring motives, among them the impact of the structural complexity and dimensionality on properties of magnetic excitations, the relation between dynamic and adiabatic approaches and the damping of spin-waves. A reader is encouraged to have a look on the appendices at the end of the thesis, which contain the conventions rather consistently used here. It is hoped that this work advances the understanding of dynamics of magnets.

FERMI SYSTEMS

We model a solid as an ensemble of Coulomb interacting electrons in an external potential at temperature T. Along the lines of linear response theory one assumes that the dominant part of the potential, say $V(\mathbf{x})$, is static but otherwise arbitrary and the time dependent part is small and can be treated in a perturbative way. As we will see the perturbative procedure requires the knowledge of the eigensystem of the Hamiltonian including only $V(\mathbf{x})$ and we start therefore with a formalism which allows to describe systems with time independent Hamiltonians.

In the framework of this thesis the mentioned external potential pertains to the interaction of electrons with positively charged motionless atomic nuclei; phonons are absent in our formalism. We assume that Hamiltonian conserves the number of particles in the system. Occasionally an additional external magnetic field can be introduced. The field couples only to the spin degrees of freedom; the formation of Landau levels (diamagnetic response) is neglected. Relativistic effects are not taken into account. One uses atomic Rydberg units (ARU) in this work, as specified in App. A.

The resultant solid state Hamiltonian in its first quantized version reads

$$
\begin{aligned}
H &= \sum_i \left(T(\mathbf{x}_i)\delta_{\alpha_i\beta_i} + V(\mathbf{x}_i)\delta_{\alpha_i\beta_i} - \mu_{\mathrm{B}}\mathbf{B}(\mathbf{x}_i)\cdot\boldsymbol{\sigma}_{\alpha_i\beta_i} \right) + \frac{1}{2}\sum_{i\neq j} U(\mathbf{x}_i,\mathbf{x}_j)\delta_{\alpha_i\beta_i}\delta_{\alpha_j\beta_j} \\
&= \left(-\sum_i \nabla_i^2 \delta_{\alpha_i\beta_i} - 2\sum_{n,i} \frac{Z_n}{|\mathbf{x}_i - \mathbf{R}_n|}\delta_{\alpha_i\beta_i} - \mu_{\mathrm{B}}\sum_i \mathbf{B}(\mathbf{x}_i)\cdot\boldsymbol{\sigma}_{\alpha_i\beta_i} \right) + \sum_{i\neq j} \frac{1}{|\mathbf{x}_i - \mathbf{x}_j|}\delta_{\alpha_i\beta_i}\delta_{\alpha_j\beta_j}
\end{aligned}
$$

$$(2.0.1)$$

i and j run from 1 to the number of particles N, n labels atomic nuclei located at positions $\mathbf{R}_n$, small Greek letter denote spin components, Pauli matrices $\boldsymbol{\sigma}$ are defined later in this chapter and U is the two body electron-electron interaction – Coulomb potential.

The material on many-body theory covered here is standard and can be found in many textbooks. I mostly enjoyed these [31, 32, 33]. Section 2.1 deals with the formalism of second quantization; it is not meant as a self contained exposition, rather as a slightly extended notation guide. The subsequent section 2.3 exposes the fundamentals of Green's function formalism. Section 2.4 presents basic notions of density functional theory and local density approximation (LDA).

2.1 Schrödinger equation in many-particle Hilbert space

Within the formalism of second quantization one introduces an orthonormal set of single particle orbitals $\varphi_j^0(\alpha\mathbf{x})$, where α is a spin variable. Many-particle Hilbert space can be spanned on the following *direct*

product states

$$|n_1 n_2 \cdots n_N\rangle = \prod_{j=1}^{N} \left(c_j^\dagger\right)^{n_j} |\mathbf{0}\rangle, \tag{2.1.1}$$

where $|\mathbf{0}\rangle$ denotes a vacuum state and $c_j^\dagger$ creates a particle on the orbital j; there are n_j of them in this state. Operator c_j removes the particle from the orbital. Our particles are electrons and therefore Fermions and Pauli principle applies. It is incorporated into the formalism by imposing the Fermionic anti-commutation rules on creation and destruction operators ($[a, b]_\pm \equiv ab \pm ba$)

$$\left[c_k, c_l^\dagger\right]_+ = \delta_{kl}, \quad [c_k, c_l]_+ = \left[c_k^\dagger, c_l^\dagger\right]_+ = 0. \tag{2.1.2}$$

This imply that there can be at most one electron occupying each orbital. Direct product states form an orthonormal basis and a general many-body wave function $|\Psi(t)\rangle$ is a superposition of these states normalized to one.

Operators acting in this space[1] are constructed from their first quantized counterparts by means of field operators (here given explicitly in the Schrödinger picture, see below)

$$\widehat{\psi}(\mathbf{x}\alpha) = \sum_j \varphi_j^0(\mathbf{x}\alpha)c_j, \quad \widehat{\psi}^\dagger(\mathbf{x}\alpha) = \sum_j \varphi_j^0(\mathbf{x}\alpha)^* c_j^\dagger. \tag{2.1.3}$$

A general one body operator (N denotes the number of particles)

$$J = \sum_{i=1}^{N} J_1(\mathbf{x}_i)_{\alpha_i \beta_i} \tag{2.1.4}$$

in its second quantized form reads[2]

$$\hat{J} = \int d\mathbf{x}\, \widehat{\psi}^\dagger(\mathbf{x}\alpha) J_1(\mathbf{x})_{\alpha\beta} \widehat{\psi}(\mathbf{x}\beta). \tag{2.1.5}$$

The Schrödinger equation in the second quantization language assumes the following form

$$\mathrm{i}\frac{\partial}{\partial t}|\Psi(t)\rangle = \hat{K}|\Psi(t)\rangle, \tag{2.1.6}$$

where $\hat{K}$ is a grand Hamiltonian. In this chapter it is assumed that it does not depend on time.

$$\hat{K} = \hat{H} - \mu\hat{N}, \tag{2.1.7}$$

where μ stands for chemical potential, $\hat{N}$ is the particle number operator

$$\hat{N} = \sum_s c_s^\dagger c_s \tag{2.1.8}$$

and $\hat{H}$ is a Hamiltonian.

Very often $\hat{K}$ is split into non-interacting part $\hat{K}_0$ (which can be treated exactly) and an interacting part $\hat{K}_1$ usually tractable only approximately. To facilitate a perturbative solution including the effect of $\hat{K}_1$ one introduces different representations (pictures) of operators and wave functions. In equation 2.1.6 these quantities are in the Schrödinger picture; operators which do not include time explicitly remain time

---

[1] Second quantized operators will be consequently denoted with a "hat" in this work.

[2] Summation over repeated spin indices is assumed throughout the work.

independent. In the Heisenberg picture the operators – unless they commute with grand Hamiltonian – acquire time dependence[3]

$$\hat{o}_K(t) = \mathfrak{e}^{i\hat{K}t}\hat{o}\mathfrak{e}^{-i\hat{K}t}, \quad |\Psi_K(t)\rangle = \mathfrak{e}^{i\hat{K}t}|\Psi(t)\rangle. \tag{2.1.9}$$

The interaction picture is defined as follows

$$\hat{o}_I(t) = \mathfrak{e}^{i\hat{K}_0 t}\hat{o}\mathfrak{e}^{-i\hat{K}_0 t}, \quad |\Psi_I(t)\rangle = \mathfrak{e}^{i\hat{K}_0 t}|\Psi(t)\rangle. \tag{2.1.10}$$

Below, several of the most important operators are explicitly given in the Schrödinger picture. The particle density operator reads

$$\hat{n}(\mathbf{x}) = \delta_{\alpha\beta}\widehat{\psi}^\dagger(\mathbf{x}\alpha)\widehat{\psi}(\mathbf{x}\beta), \tag{2.1.11}$$

while the magnetization density operator is given by

$$\hat{\boldsymbol{\sigma}}(\mathbf{x}) = \boldsymbol{\sigma}_{\alpha\beta}\widehat{\psi}^\dagger(\mathbf{x}\alpha)\widehat{\psi}(\mathbf{x}\beta), \tag{2.1.12}$$

where $\boldsymbol{\sigma} = (\sigma^x, \sigma^y, \sigma^z)$ stands for the vector of Pauli matrices

$$\sigma^x = \begin{pmatrix} 0 & 1 \\ 1 & 0 \end{pmatrix}, \quad \sigma^y = \begin{pmatrix} 0 & -i \\ i & 0 \end{pmatrix} \quad \text{and} \quad \sigma^z = \begin{pmatrix} 1 & 0 \\ 0 & -1 \end{pmatrix}. \tag{2.1.13}$$

The explicit form of the solid state Hamiltonian reads

$$\hat{H} = \int d^3\mathbf{x}\,\widehat{\psi}^\dagger(\alpha\mathbf{x})(T(\mathbf{x}) + V(\mathbf{x}))\widehat{\psi}(\alpha\mathbf{x})$$
$$+ \frac{1}{2}\iint d^3\mathbf{x}\,d^3\mathbf{x}'\,\widehat{\psi}^\dagger(\alpha\mathbf{x})\widehat{\psi}^\dagger(\beta\mathbf{x}')U(\mathbf{x}, \mathbf{x}')\widehat{\psi}(\beta\mathbf{x}')\widehat{\psi}(\alpha\mathbf{x}). \tag{2.1.14}$$

For example, the term associated with the magnetic field would read

$$\hat{H}_B = -\mu_\mathrm{B}\int d^3\mathbf{x}\,\hat{\boldsymbol{\sigma}}(\mathbf{x}) \cdot B(\mathbf{x}). \tag{2.1.15}$$

The expectation value (thermal average) of an operator is defined as

$$\langle \hat{o}\rangle = \mathrm{Tr}\,[\hat{\rho}_G \hat{o}] \equiv \mathfrak{e}^{\beta\Omega}\sum_j \langle j|\mathfrak{e}^{-\beta\hat{K}}\hat{o}|j\rangle, \tag{2.1.16}$$

where Ω is the grand canonical potential

$$\mathfrak{e}^{-\beta\Omega} = \sum_j \langle j|\mathfrak{e}^{-\beta\hat{K}}|j\rangle. \tag{2.1.17}$$

The one particle orbitals can be conveniently chosen as eigenvectors of K_0

$$K_0\varphi_j^0 = \left(\epsilon_j^0 - \mu\right)\varphi_j^0, \tag{2.1.18}$$

where ϵ_j^0 is the eigenenergy associated with state j. Let us note that here K_0 is not only in first-quantized form but also it is a single particle Hamiltonian. In the case of non-interacting particles, the Hamiltonian of the whole system reduces to the sum of single particle Hamiltonians. With such a choice of φ's the field operators in the interaction picture assume the following forms:

$$\widehat{\psi}_I(\mathbf{x}\alpha t) = \sum_j \varphi_j^0(\mathbf{x}\alpha)\mathfrak{e}^{-i(\epsilon_j^0 - \mu)t}c_j, \quad \widehat{\psi}_I^\dagger(\mathbf{x}\alpha t) = \sum_j \varphi_j^0(\mathbf{x}\alpha)^*\mathfrak{e}^{i(\epsilon_j^0 - \mu)t}c_j^\dagger. \tag{2.1.19}$$

In the non-interacting case the grand Hamiltonian $\hat{K}_0$ is readily expressed as

$$\hat{K}_0 = \sum_j \left(\epsilon_j^0 - \mu\right)c_k^\dagger c_k. \tag{2.1.20}$$

---

[3]Quantities in the Heisenberg picture bear subscript K, while they do not have any in the case of the Schrödinger picture. The interaction picture is denoted with I.

2.2 Fermi-Dirac function

The Fermi-Dirac distribution function

$$f_T(z) = \frac{1}{e^{\beta(z-\mu)} + 1} \tag{2.2.1}$$

is one of the most important tools in this work. In the non-interacting case the occupation of orbital j depends only on the energy of the state and can be expressed in terms of f_T

$$n_k^0 \equiv \mathrm{Tr}\left[\hat{\rho}_{G0} c_k^\dagger c_k\right] = f_T\left(\epsilon_k^0\right). \tag{2.2.2}$$

In the complex plane, $f_T(z)$ is a meromorphic function with poles given by Fermionic Matsubara frequencies

$$z_m = \mu + i\omega_m^f = z_{-m-1}^*,\ m \in \mathbb{Z}, \tag{2.2.3}$$

where $\omega_m^f = (2m+1)\frac{\pi}{\beta}$. One can prove that

$$\mathrm{Res}_{z=z_m}\left[f_T(z)\right] = -\frac{1}{\beta}. \tag{2.2.4}$$

f_T has one more symmetry we are going to exploit, namely

$$f_T\left(\epsilon + i2m\frac{\pi}{\beta}\right) = f_T(\epsilon),\ m \in \mathbb{Z},\ \epsilon \in \mathbb{R}. \tag{2.2.5}$$

The Fermi-Dirac function can be used to evaluate sums over Fermionic frequencies. If $h(z)$ is a complex function, by means of Cauchy theorem one can write

$$\frac{1}{\beta} \sum_{m \in S \subseteq \mathbb{Z}} h(z_m) = \frac{i}{2\pi} \oint_{\mathcal{C}} dz h(z) f_T(z). \tag{2.2.6}$$

The contour $\mathcal{C}$ shall be oriented counter clock-wise (CCW) and contain all $z_m, m \in S$ (i.e. the z_m's we want to sum over) and $h(z)$ must be analytic inside $\mathcal{C}$. If we want to set $S = \mathbb{Z}$, $h(z)$ must not have any branch cut crossing the whole complex plane.

At sufficiently low temperatures one can write

$$\int_{\mathbb{R}} dz h(z) f_T(z) \approx \int_{-\infty}^{\mu} dz h(z) + \frac{\pi^2}{6} \frac{1}{\beta^2} \frac{dh(z)}{dz}\bigg|_{z=\mu}. \tag{2.2.7}$$

This is the first term of so called Sommerfeld expansion.

2.3 Green's functions

Most of the systems of interacting bodies can be treated only in an approximate manner. One of the most powerful methods to construct a suitable approximation is Feynman's diagrammatic technique, which makes extensive use of a special propagator, the so called Green's function. From the Green's function G of an interacting system one can extract – among other observables – the total energy of the system and the particle and magnetization density; the poles of the Green's function determine quasiparticle energies and life-times. The Green's function G^0 of a non-interacting system can be calculated exactly. When the interaction is turned on one can express in a systematic manner series of corrections to G by means of G^0.

In this work, this line of treating interactions is not adopted, we work with density functional theory instead. However the formalism provides several useful tools. Basically, the exposition deals only with Green's function formalism for (effectively) non-interacting particles.

The retarded single particle real-time Green's function is defined as

$$\bar{G}^R_{\alpha\beta}(\mathbf{x}t, \mathbf{x}'t') \equiv -\mathrm{i}\theta(t - t')\left\langle \left[\widehat{\psi}_K(\mathbf{x}\alpha t), \widehat{\psi}^\dagger_K(\mathbf{x}'\beta t')\right]_+ \right\rangle. \tag{2.3.1}$$

In the non-interacting case it can be expressed through the eigensystem of H_0

$$\bar{G}^{0R}_{\alpha\beta}(\mathbf{x}, \mathbf{x}', t - t') = -\mathrm{i}\theta(t - t')\sum_j \varphi^0_j(\mathbf{x}\alpha)\varphi^0_j(\mathbf{x}'\beta)^* \mathrm{e}^{-\mathrm{i}(\epsilon^0_j - \mu)(t-t')}, \tag{2.3.2}$$

$$\bar{G}^{0R}_{\alpha\beta}(\mathbf{x}, \mathbf{x}', \omega) = \sum_j \frac{\varphi^0_j(\mathbf{x}\alpha)\varphi^0_j(\mathbf{x}'\beta)^*}{\omega - \left(\epsilon^0_j - \mu\right) + \mathrm{i}0^+} \equiv G_{\alpha\beta}(\mathbf{x}, \mathbf{x}', \omega + \mathrm{i}0^+) \tag{2.3.3}$$

and the latter object is so called bare Green's function

$$G_{\alpha\beta}(\mathbf{x}, \mathbf{x}', z) = \sum_j \frac{\varphi^0_j(\mathbf{x}\alpha)\varphi^0_j(\mathbf{x}'\beta)^*}{z - \epsilon^0_j}. \tag{2.3.4}$$

A perturbative scheme for contructing interacting Green's functions at finite temperatures can be devised, if one introduces a notion of imaginary time τ. The interaction picture of an operator in imaginary time reads

$$\hat{o}_I(\tau) = \mathrm{e}^{\hat{K}_0\tau}\hat{o}_S\mathrm{e}^{-\hat{K}_0\tau}. \tag{2.3.5}$$

while the Heisenberg picture is

$$\hat{o}_K(\tau) = \mathrm{e}^{\hat{K}\tau}\hat{o}_S\mathrm{e}^{-\hat{K}\tau}. \tag{2.3.6}$$

One defines so called temperature Green's function

$$\mathscr{G}_{\alpha\beta}(\mathbf{x}\tau, \mathbf{x}'\tau') \equiv -\mathrm{Tr}\left[\hat{\rho}_G \mathrm{T}_\tau\left[\widehat{\psi}_{K\alpha}(\mathbf{x}\tau)\widehat{\psi}^\dagger_{K\beta}(\mathbf{x}'\tau')\right]\right] \tag{2.3.7}$$

which in the non-interacting case can be explicitly written as

$$\mathscr{G}^0_{\alpha\beta}(\mathbf{x}\tau, \mathbf{x}'\tau') = -\sum_j \varphi^0_j(\mathbf{x}\alpha)\varphi^0_j(\mathbf{x}'\beta)^* \mathrm{e}^{-(\epsilon^0_j - \mu)(\tau - \tau')}\left(\theta(\tau - \tau')\left(1 - n^0_j\right) - \theta(\tau' - \tau)n^0_j\right). \tag{2.3.8}$$

($\theta(\tau)$ is the Heaviside step function, which is 1 for positive τ and 0 otherwise.) For every application it is necessary to consider variables τ and τ' only in a finite interval of length β and usually $\tau, \tau' \in [0, \beta]$. In the time independent case $\mathscr{G}^0_{\alpha\beta}(\mathbf{x}_1\tau_1, \mathbf{x}_2\tau_2)$ depends only on the difference $\tau = \tau_1 - \tau_2 \in [-\beta, \beta]$ and it is antiperiodic with period β in variable τ. One can represent $\mathscr{G}$ by means of Fourier series, $\mathscr{G}$ is non-zero only for Fermionic frequencies ω^f_m

$$\mathscr{G}^0_{\alpha\beta}\left(\mathbf{x}, \mathbf{x}', \omega^f_m\right) = \int_0^\beta d\tau \mathrm{e}^{\mathrm{i}\omega^f_m\tau}\mathscr{G}^0_{\alpha\beta}(\mathbf{x}, \mathbf{x}', \tau) = \sum_j \frac{\varphi^0_j(\mathbf{x}\alpha)\varphi^0_j(\mathbf{x}'\beta)^*}{\mu + \mathrm{i}\omega^f_m - \epsilon^0_j}$$

$$\equiv G_{\alpha\beta}(\mathbf{x}, \mathbf{x}', z_m). \tag{2.3.9}$$

One can see that $\bar{G}^{0R}$ and $\mathscr{G}$ are analytical continuations of each other and they are related through the bare Green's function. A similar statement is valid also in the interacting case, however the G cannot be simply expressed by means of single particle orbitals and energies.

One can prove that

$$\left(z\delta_{\alpha\beta} - H_0(\mathbf{x})_{\alpha\beta}\right)G_{\beta\gamma}(\mathbf{x}, \mathbf{x}', z) = \delta(\mathbf{x} - \mathbf{x}')\delta_{\alpha\gamma}, \tag{2.3.10}$$

where $z \in \mathbb{C}$. This is the fundamental equation relating every (effectively) non-interacting theory to the multiple scattering formalism. One can recognize that this is exactly the equation solved in the KKR method, outlined in Sec. 5.2.

There are several symmetries of G we are going to exploit. First of all the Green's function is a Hermitian operator

$$G_{\alpha\beta}(\mathbf{x}, \mathbf{x}', z) = G_{\beta\alpha}(\mathbf{x}', \mathbf{x}, z^*)^*, \quad z \in \mathbb{C}. \tag{2.3.11}$$

Let us close this section with remarking that the Green's function can be directly used to compute physical observables. In particular the magnetization and charge density are given by

$$\langle \hat{\boldsymbol{\sigma}}(\mathbf{x}) \rangle = \boldsymbol{\sigma}_{\alpha\beta}\mathscr{G}_{\beta\alpha}(\mathbf{x}\tau, \mathbf{x}\tau^+) = \frac{1}{\beta} \sum_{m \in \mathbb{Z}} \mathfrak{e}^{i\omega_m^f 0^+} \boldsymbol{\sigma}_{\alpha\beta} G_{\beta\alpha}(\mathbf{x}, \mathbf{x}, z_m)$$

$$= -\frac{1}{\pi} \int_{-\infty}^{\infty} d\epsilon f_T(\epsilon) \mathfrak{Im}\big[\boldsymbol{\sigma}_{\alpha\beta} G_{\beta\alpha}(\mathbf{x}, \mathbf{x}, \epsilon + i0^+)\big]. \tag{2.3.12}$$

2.4   Density functional theory

2.4.1   The context of DFT

There are several severe difficulties in calculating physical properties of any real electron system in solid state theory.

The most fundamental goes back to the very presence of interactions. At absolute zero the Fermionic non-interacting many body wave functions (in the first quantized form) are Slater determinants built from occupied single particle orbitals, while real many body wave functions of an interacting system are in general a superposition of Slater determinants based on many different sets of single particle orbitals. In the interacting case the single particle picture must be necessarily abandoned, electrons become correlated. One of the systematic ways of including correlations is the Feynman's diagrammatic technique. Unfortunately, the Coulomb interaction is strong and long ranged and can hardly be treated as a small perturbation. To obtain any meaningful results one must often sum infinite subsets of specially chosen diagrams and there exists no unequivocal choice of these series. The third problem is related to the fact that solids are usually of rather complicated structure and any method must be rather simple in order to be practically applicable to them.

To overcome the problem of the strength of Coulomb interaction one could use the Hedin's GW technique [34, 35]. In many systems, most notably in metals, electrons effectively do not interact via bare Coulomb potential, but the force is screened, much weaker. In this case one could build expansion not in bare Coulomb interaction but rather in W, the screened interaction. There are several problems, though. First of all in any practical applications one is restricted to – at best – the first few terms in the expansion. Second, the GW requires a self-consistency cycle, which is computationally too expensive, even for modern computers. At present GW is mainly used to *improve* – in a one-shot calculation – the existing approximate solutions, which should be reasonably close to real ones.

Dynamical mean field theory (DMFT) [36, 37] provides a way to treat exactly interacting particles in an idealized Hubbard model in the limit of the inifinite dimensions. There the Coulomb interaction is substituted by a matrix of adjustable parameters U. While DMFT allows for in depth understanding of strongly correlated systems it is still an oversimplified picture of real materials. It is also computationally demanding.

One can make a step towards a parameter free description of weakly correlated solids by reinstantiating the single particle picture, i.e. by assuming that particles do not interact and move in an effective potential which includes an averaged inter-particle interaction. The Hartree-Fock approximation (HFA) [38] is an example proceeding along this line. One constructs a trial many-body wave-function being a single Slater determinant and chooses the set of single particle orbitals which minimize the total energy

of the system, relying on Rayleigh-Ritz variational principle. HFA correctly accounts for Pauli exclusion principle and in the case of insulating materials and atoms the method gives qualitatively good results. In the metals however the description fails predicting for example vanishing density of states at the Fermi level; the main neglected effect here is the presence of the metallic screening partially accounted for in GWA. HFA is very complicated for solids, the reason being non-locality of the Hartree-Fock effective single particle potential. The effective inter-electron interaction in HFA approximation is called "exchange" and the effects beyond it are customarily named "correlations". Let us note that the term "correlations" is sometimes used more generically to describe all the effects arising due to the presence of interaction.

The first relatively easy and versatile scheme for calculating electronic properties of real materials came along the lines of density functional theory (DFT).

2.4.2   Hohenberg-Kohn theorem

In their seminal paper of 1964 Hohenberg and Kohn [39] managed to reformulate the many body problem to the determination of the ground state electronic density alone and thus they opened a possibility of constructing an easy calculational scheme; the density is obviously a much simpler object than a many body wave function.

One considers a system of N interacting electrons in a non-degenerate ground state in an external potential $V(\mathbf{x})$. Hohenberg-Kohn (HK) theorem states that the ground state density, $n(\mathbf{x})$, uniquely determines the potential $V(\mathbf{x})$ to within an additive constant. Since together with $V(\mathbf{x})$ the full Hamiltonian is known, the density determines all the physical properties of the system.

Furthermore, they proved that there exists a functional of the density, $F[n'(\mathbf{x})]$, defined for all non-degenerate ground state densities such that, for given $V(\mathbf{x})$, the quantity (the total energy of the system)

$$E_V[n'] \equiv \int d\mathbf{x} V(\mathbf{x}) n'(\mathbf{x}) + F[n'] \tag{2.4.1}$$

has its unique minimum for the correct ground state density, $n' = n$. If the functional F is known one can find the correct ground state density by minimizing it. The HK theory can be readily generalized to describe degenerate ground states [40].

For finite temperatures the ground state energy is replaced by the grand canonical potential Ω

$$\Omega_V^T[n'] \equiv \int d\mathbf{x} (V(\mathbf{x}) - \mu) n'(\mathbf{x}) + F^T[n'] \tag{2.4.2}$$

which ought to be minimum.

A generalization important from the point of view of this work is the possibility of formulating DFT in terms of spin densities. This makes the description of magnetic systems easier.

2.4.3   Kohn-Sham equations

In 1965 Kohn and Sham [41] suggested a method to obtain an exact, single-particle like, description of a many body problem. The free energy functional

$$\Omega_V^T[n] = T_s[n] - TS_s[n] + \int d\mathbf{x} (V(\mathbf{x}) - \mu) n(\mathbf{x}) + H[n] + \Omega_{\mathrm{xc}}[n] \tag{2.4.3}$$

is separated into the part corresponding to a non-interacting system with density n, which includes the kinetic energy T_s, entropy S_s and energy due to the external and chemical potential, in addition to the Hartree contribution

$$H[n] = \iint d\mathbf{x} d\mathbf{x}' \frac{n(\mathbf{x}) n(\mathbf{x}')}{|\mathbf{x} - \mathbf{x}'|} \tag{2.4.4}$$

and so called exchange-correlation functional $\Omega_{\mathrm{xc}}[n]$. Equation 2.4.3 can be understood as a definition of the latter; $\Omega_{\mathrm{xc}}[n]$ includes all the differences the interaction introduces to the energy and entropy of the system.

By extremizing the functional Ω Kohn and Sham recast the problem in the form of exact single particle self-consistent equations

$$\left(-\nabla^2 + v_{\mathrm{eff}}(\mathbf{x})\right)\phi_j(\mathbf{x}) = \epsilon_j\phi_j(\mathbf{x}), \tag{2.4.5}$$

which are called Kohn-Sham equations. The effective single-particle potential is a sum of an external, the Hartree and the so called exchange-correlation potential

$$v_{\mathrm{eff}}(\mathbf{x}) = V(\mathbf{x}) + 2\int d\mathbf{x}'\frac{n(\mathbf{x}')}{|\mathbf{x} - \mathbf{x}'|} + v_{\mathrm{xc}}(\mathbf{x}) \tag{2.4.6}$$

the latter being defined as a functional derivative of Ω_{xc} with respect to the density

$$v_{\mathrm{xc}}(\mathbf{x}) \equiv \frac{\delta\Omega_{\mathrm{xc}}[n(\mathbf{x})]}{\delta n(\mathbf{x})}. \tag{2.4.7}$$

It is important to note that the Kohn-Sham eigenfunctions and eigenenergies do not have any direct physical meaning, in particular the ϵ's cannot be interpreted as quasiparticle energies (even as their real parts). They are mathematical tools which are meant to yield the correct ground-state density

$$n(\mathbf{x}) = \sum_j f_T(\epsilon_j)|\phi_j(\mathbf{x})|^2. \tag{2.4.8}$$

The free energy can be computed using the Kohn-Sham energies as

$$\Omega = \sum_j f_T(\epsilon_j)\epsilon_j - TS_s - \mu N - H[n] - \int d\mathbf{x}v_{\mathrm{xc}}(\mathbf{x})n(\mathbf{x}) + \Omega_{\mathrm{xc}}[n], \tag{2.4.9}$$

where the entropy of the non-interacting system reads [42]

$$S_s = -k_{\mathrm{B}}\sum_j\left(f_j\ln f_j + (1 - f_j)\ln(1 - f_j)\right),\ f_j \equiv f_T(\epsilon_j). \tag{2.4.10}$$

Ω_{xc} at absolute zero will be denoted by E_{xc}.

For small temperatures one might be tempted to assume that $\Omega_{\mathrm{xc}} \approx E_{\mathrm{xc}}$, that is the temperature effects enter only through the smearing of the Fermi level introduced by f_T. A general discussion of this approximation goes beyond the scope of this thesis, but let us remark briefly that it fails badly for ferromagnets with large exchange splitting. The ferro-para transition in this so called Stoner picture is caused by exciting single spin-flips (Stoner states) decreasing gradually band splitting. The deviation of magnetization's direction (i.e. low energetic spin-waves) is neglected. In the Stoner picture the Curie temperature might be overestimated by an order of magnitude.

The KS equations are relatively easy to solve, since they have formally the form of a Schrödinger equation. Of course, they still retain all the complexity of many body problems buried in the specification of exchange-correlation functional. The enormous success of KS scheme lies in the existence of a simple and very practical approximation to E_{xc} based on uniform electron gas, i.e. local spin density approximation (LSDA).

The success is unexpected, since in real materials the density cannot be even approximately regarded as slow varying, and many authors argue that its predicting power comes from a certain subtle cancellation of errors. It is known that L(S)DA fullfils a series of exact sum rules. There are functionals which try to go beyond LSDA, e.g. the generalized gradient approximation (GGA) or hybrid functionals like Becke-Lee-Yang-Parr (BLYP). GGA is not clearly superior to LSDA in contrary to hybrid functionals, which

are however computationally too expensive to be used in electronic band calculations. In the materials featuring strong correlations LDA+U can be of some use, its disadvantage being introduction of tunable Coulomb repulsion U. Self-interaction correction (SIC) [43, 44] allows a parameter free description of correlated systems.

In this work we adopt LSDA mainly for its simplicity. The approximation is presented in the next subsection.

2.4.4   Local spin density approximation

The simplest formulation of spin density functional theory introduces spin up, $n_\uparrow$, and spin down, $n_\downarrow$, electronic densities. In the local approximation, at 0 K, exchange correlation functional is given by

$$E_{\mathrm{xc}} = \int d\mathbf{x} \epsilon_{\mathrm{xc}}(n_\uparrow(\mathbf{x}), n_\downarrow(\mathbf{x})) n(\mathbf{x}), \tag{2.4.11}$$

where n stands for the sum of the both components and ϵ_{xc} is the exchange-correlation energy per particle of a homogeneous, spin-polarized Fermi gas. $m = n_\uparrow - n_\downarrow$ will denote the value of local magnetization; its direction may generally vary in space. $n_{\uparrow,\downarrow}$ pertain to a local quantization axis.

The exchange correlation part of the effective KS potential is now a matrix in spin space and consists of two terms

$$v_{\mathrm{xc}}(\mathbf{x}) = \tilde{v}_{\mathrm{xc}}(\mathbf{x})\mathsf{I} - \mu_{\mathrm{B}}\mathbf{B}_{\mathrm{xc}}(\mathbf{x}) \cdot \boldsymbol{\sigma}. \tag{2.4.12}$$

The diagonal part of the xc potential is

$$\tilde{v}_{\mathrm{xc}}(\mathbf{x}) = \frac{\partial}{\partial n(\mathbf{x})}(\epsilon_{\mathrm{xc}}(n(\mathbf{x}), m(\mathbf{x}))n(\mathbf{x})) \tag{2.4.13}$$

and the exchange-correlation magnetic field reads

$$\mathbf{B}_{\mathrm{xc}}(\mathbf{x}) = -\frac{1}{\mu_{\mathrm{B}}}\frac{\partial}{\partial m(\mathbf{x})}(\epsilon_{\mathrm{xc}}(n(\mathbf{x}), m(\mathbf{x}))n(\mathbf{x}))\hat{\mathbf{m}} \equiv B_{\mathrm{xc}}\hat{\mathbf{m}} \tag{2.4.14}$$

pointing along the direction of local magnetization.

ϵ_{xc} is taken from Monte Carlo simulations of uniform electron gas and usually given through a relatively simple parameterizations, e.g. Refs. [45, 46] suggest that

$$\epsilon_{\mathrm{xc}} = \epsilon_{\mathrm{x}} + \epsilon_{\mathrm{c}}, \quad B_{\mathrm{xc}} = B_{\mathrm{x}} + B_{\mathrm{c}}, \tag{2.4.15}$$

where the exchange energy per particle (from HFA) and the corresponding magnetic field read respectively

$$\epsilon_{\mathrm{x}} = -3\left(\frac{3}{4\pi}\right)^{1/3}\frac{n_\uparrow^{4/3} + n_\downarrow^{4/3}}{n}, \quad -\mu_{\mathrm{B}}B_{\mathrm{x}} = -\left(\frac{6}{\pi}\right)^{1/3}\left(n_\uparrow^{1/3} - n_\downarrow^{1/3}\right). \tag{2.4.16}$$

The following notation will be used

$$r_s = \left(\frac{3}{4\pi n}\right)^{1/3}, \quad \zeta = \frac{n_\uparrow - n_\downarrow}{n_\uparrow + n_\downarrow}. \tag{2.4.17}$$

The correlation energy per particle (Perdew-Wang parameterization) is given by

$$\epsilon_{\mathrm{c}} = \epsilon_{\mathrm{c}}(r_s, 0) + \alpha_{\mathrm{c}}(r_s)\frac{f(\zeta)}{f''(0)}\left(1 - \zeta^4\right) + (\epsilon_{\mathrm{c}}(r_s, 1) - \epsilon_{\mathrm{c}}(r_s, 0))f(\zeta)\zeta^4, \tag{2.4.18}$$

where

$$f(\zeta) = \frac{(1+\zeta)^{4/3} + (1-\zeta)^{4/3} - 2}{2^{4/3} - 2}. \tag{2.4.19}$$

The corresponding correlation magnetic field reads

$$-\mu_{\mathrm{B}} B_{\mathrm{c}} = \frac{\partial \epsilon_{\mathrm{c}}}{\partial \zeta} = \alpha_{\mathrm{c}}(r_s) A(\zeta) + (\epsilon_{\mathrm{c}}(r_s, 1) - \epsilon_{\mathrm{c}}(r_s, 0)) B(\zeta), \tag{2.4.20}$$

where

$$A(\zeta) = 9\zeta^3 + \frac{3}{2}\big(-1 - 3\zeta^3 + 4\zeta^4\big)(1-\zeta)^{1/3} + \frac{3}{2}\big(1 - 3\zeta^3 - 4\zeta^4\big)(1+\zeta)^{1/3}, \tag{2.4.21a}$$

$$B(\zeta) = \frac{1}{2^{1/3} - 1}\left(-4\zeta^3 + \frac{2}{3}\zeta^3\big((3 - 4\zeta)(1-\zeta)^{1/3} + (3 + 4\zeta)(1+\zeta)^{1/3}\big)\right). \tag{2.4.21b}$$

$\alpha_{\mathrm{c}}(r_s)$, $\epsilon_{\mathrm{c}}(r_s, 1)$ and $\epsilon_{\mathrm{c}}(r_s, 0)$ are as functions of r_s given by relatively simple approximating formulas.

<div align="center">❧</div>

This ends the first chapter devoted to the ground state description of interacting Fermion systems in the presence of an external static potential. We have provided ourselves with necessary tools to address in the following chapter the weak time-dependent perturbations of quantum mechanical ensembles.

LINEAR RESPONSE THEORY

Linear response theory allows to find the response of a system to a weak external perturbation. One proves that such a response is completely determined by the ground state properties of the unperturbed ensemble. On one hand the fact simplifies considerably the necessary calculations, on the other it tells us that small external perturbation probes the "natural" excitations – and fluctuations – of the system. Indeed, the response function χ, which relates the response of the system to the perturbing force, carries information about the energies and probabilities of transitions induced by the external field and as such it can be used to study excited states. The imaginary part of χ is proportional to energy absorbed from the external field and determines cross-sections in scattering experiments.

This chapter is meant to present the fundamentals of the linear response theory. It opens with a rather general exposition, where we will focus on the construction, interpretation and general properties of susceptibilities, including the fluctuation-dissipation theorem, which gives a deep insight into the relevance of the formalism. Next, we will proceed to the magnetization response to show how it can be used to study magnetization dynamics. Our starting point will be field theory, but we will mention its techniques only briefly concentrating mainly on the response functions of noninteracting systems, since they are essential when formulating linear response theory in terms of DFT. Exposition and discussion of the latter formalism – central in this thesis – will be the last part of the chapter.

The modern form of linear response theory is often attributed to Ryōgo Kubo [47, 48] and called Kubo formalism. This chapter follow closely the exposition of Fetter & Walecka [31].

3.1 Generalized susceptibility

Let us consider a driving force $\Xi_\beta^{\mathrm{ex}}(t)$ which couples to the system through an operator $\hat{o}_{\beta S}$, so that the perturbation Hamiltonian reads

$$\hat{H}_K^{\mathrm{ex}}(t) = \hat{o}_{\beta K}(t)\Xi_\beta^{\mathrm{ex}}(t). \tag{3.1.1}$$

We assume that $\hat{o}_{\beta S}$ is Hermitian and has no explicit time dependence.

Let $\langle \hat{o} \rangle$ denote the expectation value of an operator $\hat{o}$ computed using the unperturbed but interacting Hamiltonian $\hat{H}$ and let $\langle \hat{o} \rangle_{\mathrm{ex}}(t)$ stand for the expectation value in the presence of the perturbation.

The linear (leading) response of the operator $\hat{o}_\alpha$ in field Ξ_β^{ex} reads

$$\delta\langle \hat{o}_\alpha \rangle_{\mathrm{ex}}(t) \equiv \langle \hat{o}_\alpha \rangle_{\mathrm{ex}}(t) - \langle \hat{o}_\alpha \rangle \tag{3.1.2}$$

$$= -\mathrm{i} \int dt' \mathrm{Tr}\left[\hat{\rho}_G\left[\hat{o}_{\alpha H}(t), \hat{o}_{\beta H}(t')\right]_-\right]\theta(t - t')\Xi_\beta^{\mathrm{ex}}(t')$$

$$= \int dt' \chi_{\alpha\beta}(t - t')\Xi_\beta^{\mathrm{ex}}(t') \tag{3.1.3}$$

and the retarded correlation function between operators $\hat{o}_\alpha$ and $\hat{o}_\beta$,

$$\mathrm{i}\chi_{\alpha\beta}(t - t') \equiv \left\langle \left[\hat{o}_{\alpha H}(t), \hat{o}_{\beta H}(t')\right]_-\right\rangle \theta(t - t'), \tag{3.1.4}$$

is called generalized susceptibility. We have used the fact that for time independent operators χ depends only on the time difference.

The Fourier transform of χ reads

$$\chi_{\alpha\beta}(\omega) = \sum_{js} \mathfrak{e}^{-\beta(K_s - \Omega)}\left(\frac{\langle j|\hat{o}_\alpha|s\rangle\langle s|\hat{o}_\beta|j\rangle}{\omega - (K_s - K_j) + \mathrm{i}0^+} - \frac{\langle j|\hat{o}_\beta|s\rangle\langle s|\hat{o}_\alpha|j\rangle}{\omega - (K_j - K_s) + \mathrm{i}0^+}\right), \tag{3.1.5}$$

where we double sum over all eigenstates of interacting grand Hamiltonian $\hat{K}$, $\hat{K}|l\rangle = K_l|l\rangle$. All the matrix elements are evaluated at $t - t' = 0$. This form is sometimes called Lehmann representation and provides us with clear physical interpretation of the generalized susceptibility. Its poles correspond to transitions between states which have non-vanishing matrix elements on operators $\hat{o}_\alpha$ and $\hat{o}_\beta$.

3.2 Fluctuation-dissipation theorem

In his famous paper from 1928 [49] Harry Nyquist showed that the irreversible dissipation of energy into heat is related to reversible fluctuations in thermal equilibrium. Nyquist considered specific example of a current flowing through a resistor. The general quantum-mechanical version of fluctuation-dissipation theorem was proved by Callen and Welton in 1951 [50]. The central concept of their paper is the *loss tensor*

$$-\frac{1}{\pi}\chi_{\alpha\beta}^L(\omega) \equiv \frac{\mathrm{i}}{2\pi}\left(\chi_{\alpha\beta}(\omega) - \chi_{\beta\alpha}^*(\omega)\right)$$

$$= \left(1 - \mathfrak{e}^{-\beta\omega}\right)\int dE \mathfrak{e}^{-\beta(E-\Omega)}\rho(E)\rho(E + \omega)\langle E|\hat{o}_\alpha|E + \omega\rangle\langle E + \omega|\hat{o}_\beta|E\rangle, \tag{3.2.1}$$

where ρ stands for the density of states in energy space, $|E\rangle$ is the eigenstate associated with energy E and the formula was derived starting from Eq. 3.1.5. Let us consider now a correlation function between operators $\hat{o}_\alpha$ and $\hat{o}_\beta$

$$A_{\alpha\beta}(t - t') = \left\langle \hat{o}_\alpha(t)\hat{o}_\beta(t')\right\rangle \tag{3.2.2}$$

and its Fourier transformation

$$A_{\alpha\beta}(\omega) = \int dE \mathfrak{e}^{-\beta(E-\Omega)}\rho(E)\rho(E + \omega)\langle E|\hat{o}_\alpha|E + \omega\rangle\langle E + \omega|\hat{o}_\beta|E\rangle. \tag{3.2.3}$$

Upon combining the above equations we obtain the fluctuation-dissipation theorem

$$A_{\alpha\beta}(\omega) = -\frac{1}{\pi}\chi_{\alpha\beta}^L(\omega)\frac{1}{1 - \mathfrak{e}^{-\beta\omega}}. \tag{3.2.4}$$

The above formula can be used to compute the fluctuations of the observable associated with the operator $\hat{o}_\alpha$

$$\langle \hat{o}_\alpha^2\rangle = -\frac{1}{\pi}\int_{-\infty}^{\infty} d\omega \chi_{\alpha\alpha}^L(\omega)\frac{1}{1 - \mathfrak{e}^{-\beta\omega}}. \tag{3.2.5}$$

Now one proves that the power P absorbed from the sinusoidally oscillating field associated with the perturbing Hamiltonian

$$\hat{H}_K^{\mathrm{ex}}(t) = \sin\omega t \sum_\alpha \hat{o}_{\alpha K}(t)\Xi_\alpha^{\mathrm{ex}} \tag{3.2.6}$$

reads

$$P = -\frac{\omega}{2} \sum_{\alpha\beta} (\Xi^{\mathrm{ex}}_\alpha)^* \chi^L_{\alpha\beta}(\omega) \Xi^{\mathrm{ex}}_\beta. \tag{3.2.7}$$

This is somewhat less general version of the theorem.

3.3 Magnetization and density response

We are particularly interested in transverse fluctuations of magnetization, since it involves *spin-flip processes* which are accessed in SPEELS and many neutron scattering experiments. They can be studied through the analysis of transverse magnetic susceptibility, therefore in this section we turn our attention to charge and magnetization density response. First, we consider general density-density susceptibility, gradually focusing on the transverse magnetic response of a collinear magnet.

We consider time dependent perturbation Hamiltonian including oscillating electrostatic potential and magnetic field coupled to the spin degree of freedom

$$\hat{H}^{\mathrm{ex}}_K(t) = \sum_{i=0}^{3} \int d\mathbf{x}\, \hat{\sigma}^i_K(\mathbf{x}t) \Xi_i(\mathbf{x}t), \tag{3.3.1}$$

where $\sigma^0_{\alpha\beta} \equiv \delta_{\alpha\beta}$ corresponds to the density operator, $\sigma^{1,2,3} \equiv \sigma^{x,y,z}$ are standard Pauli matrices and the driving potential is defined as a four-vector

$$\Xi(\mathbf{x}t) = (-|e|\mathcal{V}(\mathbf{x}t), -\mu_{\mathrm{B}}\mathbf{B}(\mathbf{x}t)), \tag{3.3.2}$$

where $\mathcal{V}$ stands for the external electrostatic potential and $\mathbf{B}$ for the external magnetic field.

We look for the susceptibility function which relates the induced charge and magnetization density to the driving force Ξ

$$\delta n^i(\mathbf{x}, \omega) = \sum_{j=0}^{3} \int d\mathbf{x}'\, \chi^{ij}(\mathbf{x}, \mathbf{x}', \omega) \Xi_j(\mathbf{x}', \omega) \tag{3.3.3}$$

and we define $\delta n^i(\mathbf{x}, \omega)$ as FT of

$$\delta n^i(\mathbf{x}, t) \equiv \left\langle \hat{\sigma}^i(\mathbf{x}t) \right\rangle_{\mathrm{ex}} - n^i_{\mathrm{GS}}(\mathbf{x}),\ i = 0, x, y, z \tag{3.3.4}$$

and $n^i_{\mathrm{GS}}(\mathbf{x})$ stands for the unperturbed (ground state) density. Using the results of section 3.1 we obtain the retarded susceptibility

$$\chi^{ij}_R(\mathbf{x}, \mathbf{x}', t - t') = -\mathrm{i}\theta(t - t') \left\langle \left[\hat{\sigma}^i_H(\mathbf{x}t), \hat{\sigma}^j_H(\mathbf{x}'t') \right]_- \right\rangle. \tag{3.3.5}$$

In practice the real time temperature susceptibility is rather hard to compute and one introduces *temperature corelation function*

$$\tilde{\chi}^{ij}(\mathbf{x}, \mathbf{x}', \tau - \tau') = -\left\langle \mathrm{T}_\tau \left[\hat{\sigma}^i_K(\mathbf{x}\tau) \hat{\sigma}^j_K(\mathbf{x}'\tau') \right] \right\rangle + \left\langle \hat{\sigma}^i(\mathbf{x}) \right\rangle \left\langle \hat{\sigma}^j(\mathbf{x}') \right\rangle, \tag{3.3.6}$$

which is much easier to calculate. The susceptibilities χ_R and $\tilde{\chi}$ are analytic continuations of each other.

3.3.1   Transverse magnetic susceptibility

The retarded correlation functions between raising and lowering magnetic operators defined in the previous chapter

$$\chi_R^+\big(\mathbf{x}, \mathbf{x}', t - t'\big) = -\mathrm{i}\theta(t - t')\Big\langle \big[\hat{\sigma}_H^+(\mathbf{x}t), \hat{\sigma}_H^-(\mathbf{x}'t')\big]_-\Big\rangle \tag{3.3.7}$$

is of natural use when studying transverse spin excitations. The above correlator allows us to follow the evolution of magnetic disturbance between two time-space points $(\mathbf{x}t)$ and $(\mathbf{x}'t')$. At 0 K and in the case of s uniform system the Lehmann representation of χ^+,

$$\chi_R^+(\mathbf{q}, \omega) = \sum_j \left(\frac{|\langle j|\hat{\sigma}^+(\mathbf{q})|0\rangle|^2}{\omega - (K_0 - K_j) + \mathrm{i}0^+} - \frac{|\langle j|\hat{\sigma}^-(-\mathbf{q})|0\rangle|^2}{\omega - (K_j - K_0) + \mathrm{i}0^+} \right), \tag{3.3.8}$$

where $|0\rangle$ denotes the ground state, is particularly easy to interpret. Its poles determine the spectrum of states which can be coupled to the ground state by lowering and raising operators, i.e. it allows us to study excited states involving spin-flip. The $\mathbf{q}$ dependence allows us to control additionally the shape of the magnetization change.

One proves (see e.g. [51]) that in a ferromagnet without anisotropy in the long wave-length limit the analytic structure of χ^+ is dominated by the spin-wave pole

$$\chi_R^+(\mathbf{q}, \omega) \sim \frac{1}{\omega - Dq^2 + \mathrm{i}0^+}, \tag{3.3.9}$$

which means that it diverges for $q = 0$ and $\omega = 0$, which corresponds to the fact that uniform rotation of magnetization in the absence of anisotropy does not cost any energy. This is an example of *Goldstone mode*.

3.3.2   Scattering experiments

The inelastic neutron-scattering cross section of magnetic excitations is given by [52, 10]

$$\frac{\partial^2 \sigma}{\partial\Omega\partial\omega} = -\frac{2}{\pi}\frac{1}{\mathfrak{e}^{-\beta\omega} - 1}\left(\frac{2\gamma e^2}{mc^2}\right)^2 \frac{k}{k'}\Big|F(\mathbf{q})^2\Big| \sum_{ij}\Big(\delta_{ij} - \hat{k}_i\hat{k}_j\Big)\mathfrak{Im}\chi^{ij}(\mathbf{q}, \omega), \tag{3.3.10}$$

where γ is the gyromagnetic ratio of the neutron, m stands for the electron mass, $\mathbf{k}$ and $\mathbf{k}'$ are incident and final wave vectors of the neutron, $\mathbf{q} \equiv \mathbf{k} - \mathbf{k}'$ stands for the momentum transfer, and $F(\mathbf{q})$ is the atomic form factor.

Analogous expression [53] is obtained for the cross-section in spin-polarized electron energy loss spectroscopy (SPEELS) [54, 55, 56, 13, 57, 5]. We remark here that despite this similarity the scattering of neutrons and electrons is governed by different physical processes. In the case of thermal neutrons the coupling mechanism is provided by the interaction of the magnetic moment of a neutron with the oscillating magnetic field of a spin-wave. For SPEELS the interaction is of the exchange type and no magnetic interaction is involved. Somewhat pictorially this can be presented as follows. A spin-polarized electron with a spin antiparallel to the majority spin orientation may create a magnon by exchanging with another electron with majority spin. During the process the sample becomes negatively charged and the electron is ejected with somewhat smaller energy. The difference is the excitation energy. The means free paths are different for the scattering electrons and neutrons. Electrons cannot penetrate deeper than couple of atomic layers into the sample, which makes SPEELS surface sensitive technique. Neutrons probe essentially the bulk magnetic modes, because of much smaller cross-section of the process.

3.3.3   Response of a non-interacting system

The response of an ensemble of non-interacting electrons can be determined starting from Eq. 3.3.5

$$
\chi_{R0}^{ij}\big(\mathbf{x},\mathbf{x}',t-t'\big) = \\
-\mathrm{i}\theta\big(t-t'\big)\sum_{km}\big(n_k^0-n_m^0\big)\sigma_{\alpha\beta}^i\sigma_{\gamma\delta}^j\varphi_k^0(\mathbf{x}\alpha)^*\varphi_m^0(\mathbf{x}\beta)\varphi_m^0\big(\mathbf{x}'\gamma\big)^*\varphi_k^0\big(\mathbf{x}'\delta\big)\mathfrak{e}^{\mathrm{i}\left(\epsilon_k^0-\epsilon_m^0\right)(t-t')}. \quad (3.3.11)
$$

Its FT reads

$$
\chi_{R0}^{ij}\big(\mathbf{x},\mathbf{x}',\omega\big) = \sum_{km}\sigma_{\alpha\beta}^i\sigma_{\gamma\delta}^j\big(n_k^0-n_m^0\big)\frac{\varphi_k^0(\mathbf{x}\alpha)^*\varphi_m^0(\mathbf{x}\beta)\varphi_m^0(\mathbf{x}'\gamma)^*\varphi_k^0(\mathbf{x}'\delta)}{\omega+\epsilon_k^0-\epsilon_m^0+\mathrm{i}0^+}. \quad (3.3.12)
$$

It can be shown that in the non-interacting case the imaginary time susceptibility can be expressed as

$$
\tilde{\chi}_0^{ij}\big(\mathbf{x},\mathbf{x}',\tau-\tau'\big) = \mathscr{G}_{\delta\alpha}^0\big(\mathbf{x}'\tau',\mathbf{x}\tau\big)\mathscr{G}_{\beta\gamma}^0\big(\mathbf{x}\tau,\mathbf{x}'\tau'\big)\sigma_{\alpha\beta}^i\sigma_{\gamma\delta}^j \quad (3.3.13)
$$

and aided by eq. 2.3.8 one obtains

$$
\tilde{\chi}_0^{ij}\big(\mathbf{x},\mathbf{x}',\tau-\tau'\big) = -\sum_{km}\sigma_{\alpha\beta}^i\sigma_{\gamma\delta}^j\varphi_k^0(\mathbf{x}\alpha)^*\varphi_m^0(\mathbf{x}\beta)\varphi_m^0\big(\mathbf{x}'\gamma\big)^*\varphi_k^0\big(\mathbf{x}'\delta\big) \quad (3.3.14)
$$

$$
\times\mathfrak{e}^{(\epsilon_k-\epsilon_m)(\tau-\tau')}\big(\theta\big(\tau-\tau'\big)\big(1-n_m^0\big)n_k^0+\theta\big(\tau'-\tau\big)\big(1-n_k^0\big)n_m^0\big). \quad (3.3.15)
$$

As a product of two Fermionic Green's functions $\tilde{\chi}_0^{ij}(\tau-\tau')$ is periodic with period β in variable $\tau-\tau'$; its imaginary time Fourier transform consists only of bosonic frequencies and reads

$$
\tilde{\chi}_0^{ij}\big(\mathbf{x},\mathbf{x}',\omega_n^b\big) = \sum_{km}\sigma_{\alpha\beta}^i\sigma_{\gamma\delta}^j\big(n_k^0-n_m^0\big)\frac{\varphi_k^0(\mathbf{x}\alpha)^*\varphi_m^0(\mathbf{x}\beta)\varphi_m^0(\mathbf{x}'\gamma)^*\varphi_k^0(\mathbf{x}'\delta)}{\mathrm{i}\omega_n^b+\epsilon_k^0-\epsilon_m^0}. \quad (3.3.16)
$$

Let us introduce the following function of a general complex variable

$$
\chi_0^{ij}\big(\mathbf{x},\mathbf{x}',z\big) = \sum_{km}\sigma_{\alpha\beta}^i\sigma_{\gamma\delta}^j\big(n_k^0-n_m^0\big)\frac{\varphi_k^0(\mathbf{x}\alpha)^*\varphi_m^0(\mathbf{x}\beta)\varphi_m^0(\mathbf{x}'\gamma)^*\varphi_k^0(\mathbf{x}'\delta)}{z+\epsilon_k^0-\epsilon_m^0}; \quad (3.3.17)
$$

we see that the temperature and real time susceptibilities are indeed analytic continuations of each other

$$
\tilde{\chi}_0^{ij}\big(\mathbf{x},\mathbf{x}',\omega_n^b\big) = \chi_0^{ij}\big(\mathbf{x},\mathbf{x}',\mathrm{i}\omega_n^b\big), \quad (3.3.18)
$$

$$
\chi_{R0}^{ij}\big(\mathbf{x},\mathbf{x}',\omega\big) = \chi_0^{ij}\big(\mathbf{x},\mathbf{x}',\omega+\mathrm{i}0^+\big). \quad (3.3.19)
$$

By means of eq. 3.3.13, the definition of bare Green's function 2.3.4 and the convolution theorem B.1.12 we arrive at the following equation

$$
\chi_0^{ij}\big(\mathbf{x},\mathbf{x}',\mathrm{i}\omega_n^b\big) = \frac{1}{\beta}\sum_{m\in\mathbb{Z}}\sigma_{\alpha\beta}^i\sigma_{\gamma\delta}^j G_{\beta\gamma}\big(\mathbf{x},\mathbf{x}',z_m\big)G_{\delta\alpha}\big(\mathbf{x}',\mathbf{x},z_{m-n}\big), \quad (3.3.20)
$$

which is the base for the numerical construction of the non-interacting Kohn-Sham susceptibility. $\chi_0^{ij}(\mathbf{x},\mathbf{x}',z)$ has the following symmetries providing $x\in\mathbb{R}_+$

$$
\chi_0^{ij}\big(\mathbf{x},\mathbf{x}',\mathrm{i}x\big)\in\mathbb{R}, \quad (3.3.21\mathrm{a})
$$

$$
\chi_0^{ij}\big(\mathbf{x},\mathbf{x}',-x+\mathrm{i}0^+\big) = \chi_0^{ij}\big(\mathbf{x},\mathbf{x}',x+\mathrm{i}0^+\big)^*. \quad (3.3.21\mathrm{b})
$$

They can be also deduced from the general property that $\chi^{ij}(\mathbf{x},t)$ is real.

3.3.4 Collinear magnetic structures

Collinear magnets are systems for which a one global spin quantization axis can be chosen and Green's function can be diagonalized in the same spin basis everywhere in space

$$G^0\left(\mathbf{x}, \mathbf{x}', z\right) = \begin{pmatrix} G^0_\uparrow(\mathbf{x}, \mathbf{x}', z) & 0 \\ 0 & G^0_\downarrow(\mathbf{x}, \mathbf{x}', z) \end{pmatrix}. \tag{3.3.22}$$

If the system is magnetized the direction of magnetization defines the z spin direction. The strong statement that the system is collinear can be made usually only about non-interacting systems.

In this case the density-density response χ_0^{ij} features several symmetries, which can be summarized as follows

$$\chi_0 = \begin{pmatrix} \chi_0^{00} & 0 & 0 & \chi_0^{0z} \\ 0 & \chi_0^{xx} & \chi_0^{xy} & 0 \\ 0 & -\chi_0^{xy} & \chi_0^{xx} & 0 \\ -\chi_0^{0z} & 0 & 0 & \chi_0^{zz} \end{pmatrix}. \tag{3.3.23}$$

Let us note that the response to the transverse (lying in the xy-spin-plane) magnetic field is transverse and does not involve charge density response as opposed to longitudinal magnetic field (along z-spin direction). In the paramagnetic case the whole susceptibility matrix becomes isotropic

$$\chi_{0\text{param}}^{ij} \sim \delta_{ij}. \tag{3.3.24}$$

Generally, in the collinear case the transverse susceptibility matrix is always isotropic, having a structure of a rotation matrix. This means that if one rotates rigidly the direction of the driving field the direction of magnetization response will be rotated by the same angle. It is therefore often convenient to introduce circular coordinates for magnetization response and magnetic field

$$m_\pm = m_x \pm \mathrm{i} m_y, \quad B_\pm = m_x \pm \mathrm{i} m_y. \tag{3.3.25}$$

It easy to see that they are connected through the following relation

$$m_\pm(\mathbf{x}, \omega) = \int d\mathbf{x}' \chi^\pm\left(\mathbf{x}, \mathbf{x}', \omega\right) B_\pm\left(\mathbf{x}', \omega\right), \tag{3.3.26}$$

where the circular components of the susceptibility are defined as

$$\chi^\pm = \chi^{xx} \mp \mathrm{i}\chi^{xy}. \tag{3.3.27}$$

3.3.5 Random phase approximation

Using the methods of field theory [31] one proves that the susceptibility of an interacting system can be computed as

$$\tilde{\chi}(\mathbf{q}, \omega_n^b) = \frac{\Pi(\mathbf{q}, \omega_n^b)}{1 - V(\mathbf{q})\Pi(\mathbf{q}, \omega_n^b)}, \tag{3.3.28}$$

where $\Pi(\mathbf{q}, \omega_n^b)$ is called proper polarization and for simplicity we considered a uniform system and charge-charge response. A theory of exactly the same structure is obtained for the general density-density response and inhomogeneous systems. Π is generally not known exactly and can be approximated by a selected set of Feynman diagrams.

A radical and simple but widely used treatment is to approximate Π with its non-interacting counterpart, Π_0, which coincides with the non-interacting susceptibility, χ_0. This method is called random phase approximation (RPA).

3.4   Linear response DFT

Runge and Gross formulated time dependent variant of density functional theory in 1984 [58] proving that under mild general conditions there is a one-to-one correspondence between the time-dependent charge and magnetization density $\langle \hat{\sigma}^i(\mathbf{x}t) \rangle$ and the time-dependent external potential $v(\mathbf{x}t)$. A time-dependent analog of KS equations can be devised [59]. The method is in principle capable of describing arbitrarily large excitations, including non-linear effects like higher harmonic generation.

In 1985 Gross and Kohn laid foundations of linear response time-dependent density functional theory framework [22, 23], which is applicable when the perturbing Hamiltonian is small. In order to construct the response functions in the linear response DFT (LRDFT) we must know only the ground state properties of the system.

The heart of the LRDFT is the assumption that the density perturbation is "non-interacting v-representable", that is one can write

$$\delta n^i(\mathbf{x}, \omega) = \sum_{j=0}^{3} \int d\mathbf{x}' \chi_{\mathrm{KS}}^{ij}(\mathbf{x}, \mathbf{x}', \omega) \delta v_{\mathrm{eff}}^j(\mathbf{x}', \omega), \tag{3.4.1}$$

where $\chi_{\mathrm{KS}}^{ij}(\mathbf{x}, \mathbf{x}', \omega)$ the retarded response function of the noninteracting Kohn-Sham ground state corresponding to unperturbed $v_{\mathrm{eff}}(\mathbf{x})$

$$\chi_{\mathrm{KS}}^{ij}(\mathbf{x}, \mathbf{x}', \omega) = \sum_{km} \sigma_{\alpha\beta}^i \sigma_{\gamma\delta}^j (f_k - f_m) \frac{\phi_k(\mathbf{x}\alpha)^* \phi_m(\mathbf{x}\beta) \phi_m(\mathbf{x}'\gamma)^* \phi_k(\mathbf{x}'\delta)}{\omega + (\epsilon_k - \epsilon_m) + \mathrm{i}0^+}, \tag{3.4.2}$$

where ϕ's and ϵ's denote KS eigensystem. The effective perturbing potential includes, in addition to the driving field, "many-body" potentials

$$\delta v_{\mathrm{eff}}^i(\mathbf{x}, \omega) = \Xi^i + 2\delta_{i0} \int d\mathbf{x}' \frac{\delta n^0(\mathbf{x}')}{|\mathbf{x} - \mathbf{x}'|} + \delta v_{\mathrm{xc}}^i(\mathbf{x}, \omega). \tag{3.4.3}$$

The second term in the above expression represents time-dependent Hartree response. The third term, being a perturbation to exchange correlation potential, is expressed as a functional of $\delta n^i(\mathbf{x})$

$$\delta v_{\mathrm{xc}}^i(\mathbf{x}, \omega) = \sum_{j=0}^{3} \int d\mathbf{x}' F_{\mathrm{xc}}^{ij}(\mathbf{x}, \mathbf{x}', \omega) \delta n^j(\mathbf{x}', \omega). \tag{3.4.4}$$

The exchange-correlation kernel is determined by the unperturbed ground-state density. Combining equations 3.3.3, 3.4.1, 3.4.3 and 3.4.4 we obtain the following self-consistency condition

$$\chi^{ij}(\mathbf{x}, \mathbf{x}', \omega) = \chi_{\mathrm{KS}}^{ij}(\mathbf{x}, \mathbf{x}', \omega) +$$
$$\sum_{k,l=0}^{3} \iint d\mathbf{x}_1 d\mathbf{x}_2 \chi_{\mathrm{KS}}^{ik}(\mathbf{x}, \mathbf{x}_1, \omega) \left(F_{\mathrm{xc}}^{kl}(\mathbf{x}_1, \mathbf{x}_2, \omega) + \frac{2\delta_{k0}\delta_{l0}}{|\mathbf{x}_1 - \mathbf{x}_2|} \right) \chi^{lj}(\mathbf{x}_2, \mathbf{x}', \omega). \tag{3.4.5}$$

The equation is referred to as "Dyson equation", because of its characteristic form.

F_{xc} can be formally obtained as a functional derivative of exchange-correlation potential with respect to the density

$$F_{\mathrm{xc}}^{ij}[n_{\mathrm{GS}}](\mathbf{x}, \mathbf{x}', t - t') = \frac{\delta v_{\mathrm{xc}}^i(\mathbf{x}, t)}{\delta n^j(\mathbf{x}'t')} \bigg|_{\Xi = \mathbf{0}, n = n_{\mathrm{GS}}}. \tag{3.4.6}$$

If F_{xc} were known, equation 3.4.5 would allow us to compute the exact response function of the interacting system. The structure of the above equation resembles strongly random phase approximation discussed in

the previous section. It is important however to note that equation 3.4.5 is exact, while RPA corresponds to a specific approximation for proper polarization function. Of course one still has to solve a true many body problem and some approximations are necessary. They are introduced via specification of F_{xc}.

The philosophy of Kohn-Sham scheme provides us with an intuitive insight into the LRDFT Dyson equation. In KS scheme interparticle interaction is mapped into a ficticious effective external potential, which is determined by the density distribution coming from all particles in the system. Suppose we perturb our system with an external potential inducing certain transitions between occupied and unoccupied KS states. The transitions lead to a change in the density distribution and therefore the effective potential seen by the electrons is modified; one can say that the non-interacting KS system is exposed not only to the external potential but also to an additional effective field being a result of the fluctuating environment. As in the case of ground-state calculations, this philosophy must lead to a self-consistent scheme, expressed exactly through Dyson equation.

We are going to construct F_{xc} based on the ground state functional given by LSDA. Before moving to detailed specification of F_{xc} let us point several limitations of this line of its construction. We are essentially unable to describe any retardation effects, since the ground state xc functional is based on time independent densities. The response of the exchange-correlation potential is necessarily adiabatic, given by the instantaneous charge and magnetization densities. This is equivalent to neglecting the frequency dependence of the kernel, $F_{\mathrm{xc}}(\omega) \simeq F_{\mathrm{xc}}(0)$. Such an approach can be criticized, but one can anticipate it to work well, when the characteristic energies we want to describe are small, like in the case of magnons. There have been attempts to introduce the frequency dependence back into the kernel. One possibility is to use the homogeneous electron gas kernel, making the assumption that the induced density is slowly varying function of space, i.e. analogous to the approximation made in traditional static LDA [22, 23]. As stated by Vignale *et al.* [60] due to the so called "harmonic potential theorem" violation it is impossible to retain the locality of the kernel, while making it frequency dependent. Onida *et al.* discuss several other possibilities [61].

So the kernel is local in LDA, determined by the local values of densities, and adiabatic

$$F_{\mathrm{xc}}\big(\mathbf{x}, \mathbf{x}', t - t'\big) \sim \delta\big(\mathbf{x} - \mathbf{x}'\big)\delta\big(t - t'\big). \tag{3.4.7}$$

It is called adiabatic LDA (ALDA).

3.4.1 Transverse magnetic susceptibility

In the context of this thesis it is not necessary to elaborate further the full structure of Dyson equation. We focus our attention on the transverse susceptibility with the adiabatic LDA kernel.

When sticking to non-relativistic LDA, the KS system for a ferromagnet, a ferrimagnet or an antiferromagnet forms a collinear magnetic structure. The noninteracting KS response to a transverse magnetic field is therefore transverse and does not involve a charge response. Within the LDA the true interacting response has the same property.

To see it let us focus on the exchange-correlation kernel. The derivation can be found in [62]. As we pointed out in the chapter devoted to DFT, the ith component of the exchange-correlation magnetic field reads

$$B_{\mathrm{xc}}^{i} = B_{\mathrm{xc}}\frac{m_i}{m} \tag{3.4.8}$$

and its functional derivative with respect to jth component of the magnetization is

$$\frac{\delta B_{\mathrm{xc}}^{i}}{\delta m_j} = B_{\mathrm{xc}}\frac{\partial}{\partial m_j}\frac{m_i}{m} + \frac{\delta B_{\mathrm{xc}}}{\delta m_j}\frac{m_i}{m} = \frac{B_{\mathrm{xc}}}{m}\Big(\delta_{ij} - \frac{m_i m_j}{m^2}\Big) + \frac{\delta B_{\mathrm{xc}}}{\delta m}\frac{m_i m_j}{m^2}. \tag{3.4.9}$$

The first term gives the response in the direction perpendicular to $\hat{\mathbf{m}}$ (the transverse response), while the second along the direction of ground state magnetization. We see that the induced transverse magnetization gives rise to an additional effective exchange-correlation magnetic field, which is also transverse. This

is an important property since it allows us to decouple the Dyson equation for the transverse magnetic susceptibility from the one for the longitudinal and the charge response.

Summing up, the Dyson equation for the transverse susceptibility reads

$$\chi^{\pm}(\mathbf{x}, \mathbf{x}', \omega) = \chi_{\mathrm{KS}}^{\pm}(\mathbf{x}, \mathbf{x}', \omega) + \int d\mathbf{x}_1 \chi_{\mathrm{KS}}^{\pm}(\mathbf{x}, \mathbf{x}_1, \omega) K_{\mathrm{xc}}(\mathbf{x}_1) \chi^{\pm}(\mathbf{x}_1, \mathbf{x}', \omega). \tag{3.4.10}$$

The use of circular coordinates allows us to work with a complex scalar equation instead of a matrix one in spin indices ij. The real exchange-correlation kernel function amounts to

$$K_{\mathrm{xc}}(\mathbf{x}) = -\mu_{\mathrm{B}} \frac{B_{\mathrm{xc}}(\mathbf{x})}{m(\mathbf{x})}, \tag{3.4.11}$$

where $B_{\mathrm{xc}}(\mathbf{x})$ and $m(\mathbf{x})$ are local values of the exchange-correlation magnetic fields and magnetization density respectively. They can easily be found once a LDA parameterization is given. Care must be exercised for the systems with vanishing magnetization, since in this case K_{xc} must be determined properly as a limit.

If one casts the spatial dependence of $\chi^{\pm}$, $\chi_{\mathrm{KS}}^{\pm}$ and K_{xc} in an orthonormal basis, the Dyson equation becomes a matrix one

$$\chi^{\pm}(\omega) = \chi_{\mathrm{KS}}^{\pm}(\omega) + \chi_{\mathrm{KS}}^{\pm}(\omega) K_{\mathrm{xc}} \chi^{\pm}(\omega) \tag{3.4.12}$$

with a solution

$$\chi^{\pm}(\omega) = \left(\mathsf{I} - \chi_{\mathrm{KS}}^{\pm}(\omega) K_{\mathrm{xc}} \right)^{-1} \chi_{\mathrm{KS}}^{\pm}(\omega). \tag{3.4.13}$$

K_{xc} matrix contains necessary matrix elements corresponding to the integral appearing in the original Dyson equation.

3.4.2   Spin rotational invariance

In the absence of magnetic anisotropy one expects the system to be rotationally invariant, but in magnetically ordered systems the original symmetry in spin space is destroyed by the spontaneous ordering along the z-axis described by the appearance of a static exchange-correlation field [63, 64]. The original symmetry is dynamically restored by the appearance of low-frequency Goldstone mode. In this section we want to show that the LRDFT formalism, exposed in the preceeding sections, exhibits a zero frequency spin-wave mode, conserving the spin rotational invariance.

We want to prove that there exists an infinitesimal static transverse magnetic field $B_0(\mathbf{x})$, pointing everywhere in the same direction, say along x-axis, for which the magnetic response is macroscopic. This corresponds to a divergence of susceptibility, i.e. to the presence of Goldstone mode. Physically this means that applying B_0 introduces a magnetic anisotropy to the system; if it is indeed rotationally invariant and B_0 correctly chosen, all spins align along B_0, minimizing their energy. For uniform systems, B_0 is a uniform field, but in the general case it varies in space. From the mathematical point of view $B_0(\mathbf{x})$ represents an eigenvector of $\chi^{\pm}$ matrix associated with a diverging eigenvalue.

We guess that $B_0(\mathbf{x}) \sim B_{\mathrm{xc}}(\mathbf{x})$, and let us take $B_0(\mathbf{x}) = \alpha B_{\mathrm{xc}}(\mathbf{x})$, where α is small. We first consider the response of the non-interacting KS system. The problem is static. The sum of xc magnetic field and the external field is $B_{\mathrm{xc}}(\mathbf{x})(\alpha, 0, 1)$ and one sees that for small α this corresponds to the rigid rotation of the effective magnetic field without the change of its length. (The change of the length of the new field is $O(\alpha^2)$.) We end up with original KS ground state system rotated in spin-space. The change of the z component of the magnetization is $O(\alpha^2)$, the induced transverse magnetization is along x and simply equals $\alpha m(\mathbf{x})$, where $m(\mathbf{x})$ stands for the ground-state value of the magnetization. We obtain the first important information:

$$\alpha m = \chi_0(\omega = 0) \alpha B_{\mathrm{xc}}. \tag{3.4.14}$$

Matrix notation is used for susceptibilities, m and B_{xc} should be understood as vectors in the orthonormal basis.

Using the same arguments as above, we note that the additional effective exchange-correlation transverse magnetic field appearing as a consequence of the induced transverse magnetization $\alpha m(\mathbf{x})$ is $B_{\mathrm{xc}}(\mathbf{x})(\alpha, 0, 0)$, i.e.

$$\alpha B_{\mathrm{xc}} = K_{\mathrm{xc}} \alpha m. \tag{3.4.15}$$

We see that the ground state magnetization is an eigenvector of matrix $\chi_0(0)K_{\mathrm{xc}}$ associated with an eigenvalue 1, so the matrix

$$\mathsf{I} - \chi_0(0)K_{\mathrm{xc}} \tag{3.4.16}$$

is singular. This is turn means that the response to field of the shape of ground-state xc field, i.e. $B_{\mathrm{xc}}(\mathbf{x})(1, 0, 0)$, is infinite. This proves that our formalism features Goldstone mode.

A few remarks are now in order. First, the same argument of the existence of a Goldstone mode applies to ferromagnets, but not to paramagnets, since in the latter case the is no effective xc field and the argumentation becomes invalid. The biggest eigenvalue of $\chi_0(0)K_{\mathrm{xc}}$ is essentially the Stoner enhancement factor and is smaller than one. Second, strictly speaking, the linear response theory breaks down in the vicinity of Goldstone mode, since however small the perturbing field is, the response is macroscopic. Finally, when dealing with periodic (uniform) systems Goldstone mode is necessarily associated with $\mathbf{q} = \mathbf{0}$, because $B_{\mathrm{xc}}(\mathbf{x})$ is a periodic (constant) function of $\mathbf{x}$.

3.5 Adiabatic spin dynamics

3.5.1 Heisenberg Hamiltonian

The characteristic energy $\omega(\mathbf{q})$ of long-wavelength magnons is usually small compared to the Stoner spin splitting Δ and this fact can be used to decouple the slow evolution of the directions of the magnetic moments and the fast electron dynamics, involving Stoner transitions. Such approach can be regarded as a time analogue of the WKB approximation [18, 65, 66]. Fast electronic degrees of freedom are integrated out and one arrives at a semiclassical equation of motion for the orientations of magnetic moments

$$\partial_t \mathbf{S}_p = -\gamma \mathbf{S}_p \times \mathbf{B}_{\mathrm{eff}}, \tag{3.5.1}$$

where $\mathbf{S}_p$ is an integral of the magnetization density $\mathbf{m}(\mathbf{r})$ over the atomic cell around the atomic site p, $\gamma \equiv g\mu_{\mathrm{B}}$, where g is the gyromagnetic ratio of the electron and equal to 2 in Dirac's theory and $\mathbf{B}_{\mathrm{eff}}$ is the effective magnetic field, which in addition to the external magnetic field includes the exchange interaction between moments. The procedure is effectively a mapping of the many body system onto well known Heisenberg Hamiltonian (HH)

$$\mathcal{H} = -\frac{1}{2} \sum_{pr} J_{pr} \mathbf{e}_p \cdot \mathbf{e}_r, \tag{3.5.2}$$

where $\mathbf{e}_p \equiv \mathbf{S}_p / S_p$ (S_p is the length of the moment and is always positive) and J_{pr} are so called exchange parameters. (We adopt a convention that $J_{pp} = 0$.) J's are formally proportional to the second derivative of E with respect to transverse magnetization and explicitly given in Ref. [18]. The approach is called adiabatic; in this context it means that the electrons relax to a constrained ground state given by the directions of $\mathbf{e}_p$'s essentially instantaneously.

One proceeds now as follows. First, one extracts the effective coupling constants J_{pr} from preferably *ab initio* band structure calculations and in the second step Hamiltonian 3.5.2 is used to study magnetization dynamics, including the determination of the spin-wave dispersion relation, the transition temperature, etc.
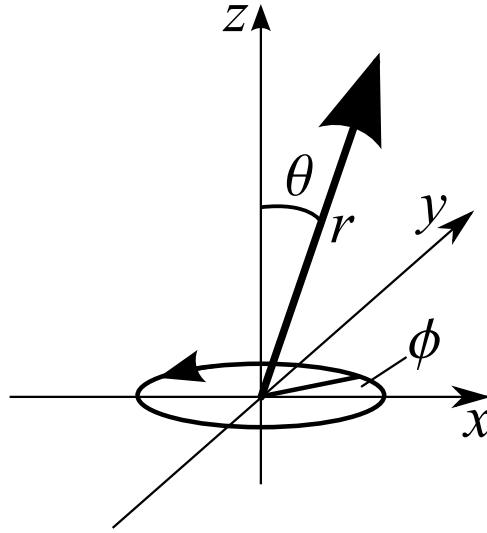
Figure 3.1: Angles determining the state of a magnetic moment. The polar angle θ is measured with respect to quantization axis z, azimuthal angle ϕ determines the phase of the moment. In the presence of the external magnetic field $(0, 0, B_0)$ the moment precesses clockwise around the z-axis with Larmor frequency $\omega_L \equiv \gamma B_0$. When the moment is tilted such that its z-component changes by $\theta^2 S/2 = 2$ (effectively one spin is flipped), the energy of the system increases by ω_L. It is assumed that S is large, i.e. one deals with a classical spin.

There are several computational schemes taking advantage of the outlined adiabatic spin dynamics. Using the so called *magnetic force theorem* (MFT) [20] one can determine directly the exchange parameters J_{pr}. The *frozen magnon approach* (described in detail below) is a formally equivalent technique allowing to find directly the energies of different magnetic configurations. The matrix J_{pr} can be also extracted from the knowledge of the *static* magnetic susceptibility [66]. Bruno [67] pointed out that the exchange parameters based on MFT and the susceptibility calculations are not equivalent − J's based on MFT contain a systematic error, which asserts itself once the adiabatic parameter $\varpi \equiv \omega(\mathbf{q})/\Delta$ ceases to be small − and suggested an improved version of MFT reproducing correctly the static susceptibility. Later it was argued [62] that while the "renormalized" MFT better reproduces static properties of magnets, the "old" exchange integrals should be used to determine spin-wave excitation spectra. It should be stressed that both approaches are equivalent in the $\varpi \rightarrow 0$ regime.

The adiabatic decoupling is exact in the limit of small magnon energy ($\varpi \rightarrow 0$), i.e. it allows to determine correctly the spin-wave stiffness constant D. For the higher energies (larger $\mathbf{q}$'s) one expects that he coupling to the Stoner continuum, apart from leading to a decay of spin-waves, can also cause a renormalization of the magnon energy. In the latter case the description of spin dynamics based on magnetic susceptibility $\chi(\mathbf{q}, \omega)$ is more reliable. On the other hand, the adiabatic approach leads to computationally inexpensive schemes and is of practical and conceptual importance.

3.5.2   Spin-waves of collinear magnets in the adiabatic approximation

Diagonalization of Heisenberg Hamiltonian

The effective field in the Heisenberg model reads

$$\mathbf{B}^p_{\mathrm{molec}} = \frac{1}{\mu_B S_p} \sum_r J_{pr} \mathbf{e}_r, \tag{3.5.3}$$

so we obtain the following equation of motion (EOM) for the directions of magnetic moments

$$S_p \partial_t \mathbf{e}_p(t) = -2\mathbf{e}_p \times \sum_r J_{pr} \mathbf{e}_r. \tag{3.5.4}$$

We assume now that the ground state is collinear. The EOM is non linear, but it can be linearized upon assumption that the deviations of moments from their ground state directions are small. In this case one obtains

$$\partial_t e_p^+(t) = 2\mathrm{i} S_p^{-1} \sum_r J_{pr} \left(e_p^+(t) e_r - e_p e_r^+(t)\right), \tag{3.5.5}$$

where $e_p^+ \equiv e_p^x + \mathrm{i} e_p^y$ measures the deviation of the moment and $e_p = +1$ when the moment in the ground state points upwards and -1 otherwise. We look now for a steady state solution of the EOM

$$e_p^+(t) = e_p^+ \mathfrak{e}^{\mathrm{i}\omega t} \tag{3.5.6}$$

and obtain the following eigenvalue problem for the "torque matrix"

$$\omega_\lambda e_{\lambda p}^+ = \sum_r T_{pr} e_{\lambda r}^+, \quad T_{pr} \equiv 2S_p^{-1} \delta_{pr} \sum_l J_{pl} e_l - 2S_p^{-1} e_p J_{pr}. \tag{3.5.7}$$

The index λ labels eigenvalues. The eigenmodes are spin-waves in our understanding: $e_{\lambda p}^+$ are interpreted as the mode's amplitudes on different sites and ω_λ is the magnon frequency.

The configuration of moments given by $e_{\lambda p}^+$ has energy higher than the ground state energy by

$$\Delta E_\lambda = \sum_{pr} \left(e_{\lambda p}^+\right)^* \mathcal{E}_{pr} e_{\lambda r}^+ = \frac{1}{4} \omega_\lambda \sum_p S_p e_p \left|e_{\lambda p}^+\right|^2, \tag{3.5.8}$$

where

$$\mathcal{E}_{pr} \equiv \frac{1}{2} \left(\delta_{pr} \sum_l J_{pl} e_l - J_{pr}\right) = \frac{1}{4} S_p e_p T_{pr}. \tag{3.5.9}$$

(The expression for ΔE given by Eq. 3.5.8 is valid for general e_p^+, not necessarily an eigenvector of T_{pr}.) Since the magnon corresponds to an effective flip of one spin

$$-\frac{1}{2} \sum_p S_p e_p \left|e_{\lambda p}^+\right|^2 = \pm 2. \tag{3.5.10}$$

The $-$ sign corresponds to the decrease of the total moment of the system (ω_λ positive) and $+$ to the decrease (ω_λ negative). The latter case arises for example in the antiferromagnetic case as one of the equivalent solutions. In any case $\Delta E_\lambda = |\omega|_\lambda > 0$ as expected for a system excited from the ground state.

In the case of translationally invariant systems the eigensolutions are plane waves

$$e_{\lambda p \mathbf{R}}^+ = e_{\lambda p}^+(\mathbf{q}) \mathfrak{e}^{\mathrm{i}\mathbf{q} \cdot \mathbf{R}}, \tag{3.5.11}$$

where p runs now over the atoms in the primitive cell now and $\mathbf{R} \in \mathcal{L}$. The amplitudes $e_{\lambda p}^+(\mathbf{q})$ are found as eigenvectors of

$$T_{pr}(\mathbf{q}) \equiv 2S_p^{-1} \delta_{pr} \sum_l J_{pl}(\mathbf{0}) e_l - 2S_p^{-1} e_p J_{pr}(\mathbf{q}), \quad J_{pr}(\mathbf{q}) = \sum_M J_{\mathbf{R}p0r} \mathfrak{e}^{-\mathrm{i}\mathbf{q} \cdot \mathbf{R}}. \tag{3.5.12}$$

There are so many distinct magnon branches $\omega_\lambda(\mathbf{q})$ as there are inequivalent atoms in the cell. One proves that one of these branches is acoustic, i.e. features quadratic dispersion relation for small q's. The energy of this mode vanishes for $\mathbf{q} = \mathbf{0}$; this is the Goldstone mode arising naturally due to the absence of anisotropy.

It is important to remark that the J's obtained from the "magnetic force theorem" of Liechtenstein [20] are two times smaller than those used in this section.

Let us finally determine the transverse magnetic susceptibility associated with the Heisenberg model. If one applies a small transverse field $B_p^+(\mathbf{q})\mathfrak{e}^{\mathbf{iq}\cdot\mathbf{R}}\mathfrak{e}^{\mathrm{i}\omega t}$, the induced magnetization is transverse and changes as $S_p e_p^+(\mathbf{q})\mathfrak{e}^{\mathbf{iq}\cdot\mathbf{R}}\mathfrak{e}^{\mathrm{i}\omega t}$ and can be found from the following equation

$$\sum_r S_r^{-1}(\delta_{pr}\omega - T_{pr}(\mathbf{q}))S_r e_r^+(\mathbf{q}) = \gamma e_p \frac{1}{\mu_\mathrm{B}}\left(-\mu_\mathrm{B} B_p^+(\mathbf{q})\right), \tag{3.5.13}$$

so the inverse of the dynamic transverse magnetic susceptibility in the understanding of this thesis reads

$$\left(\chi^{-1}(\omega, \mathbf{q})\right)_{pr} = \mu_\mathrm{B} e_p \gamma^{-1} S_r^{-1}(\omega\delta_{pr} - T_{pr}(\mathbf{q})). \tag{3.5.14}$$

It corresponds to the enhanced susceptibility. Since the magnon spectrum in the adiabatic approximation is fully determined by T it can be extracted from the static enhanced susceptibility [66].

Spin spiral calculations

In another but equivalent version of MFT one determines the spin-wave frequency as the *additional* energy needed for deformation of the ground state magnetization to the characteristic "spin-spiral" form specified above. In the electron band calculation the energy is obtained by means of spin-space symmetry groups [68, 19].

The state of a magnetic moment on a particular site is determined by two angles, see Fig. 3.1. The polar angle θ is measured with respect to quantization axis z, the azimuthal angle ϕ determines the phase of the moment. A frozen magnon configuration is given by specifying polar angles θ_i on each site in the unit cell and spin-wave vector $\mathbf{q}$ determining in turn the azimuthal angles

$$\phi_i = \mathbf{q}\cdot\mathbf{s}_i, \tag{3.5.15}$$

where $\mathbf{s}_i$ is the position of the ith atom in the unit cell. To estimate the dispersion relation $\omega(\mathbf{q})$ the energy of frozen magnon configuration $E(\{\theta_i\}, \mathbf{q})$ is computed and compared to undeformed configuration $E(\{\theta_i\}, \mathbf{0})$. The energies of the spin-wave excitations can now be estimated for small θ's as

$$\omega(\mathbf{q}) = \frac{2}{\Delta M}(E(\{\theta_i\}, \mathbf{q}) - E(\{\theta_i\}, \mathbf{0})), \tag{3.5.16}$$

where

$$\Delta M = \sum_\lambda \frac{\theta_\lambda^2}{2}M_\lambda \approx \sum_\lambda (1 - \cos\theta_\lambda)M_\lambda \tag{3.5.17}$$

can be regarded for small θ as a change of the system's magnetization. Note that the above normalization simply counts the number of magnons (each magnon lowers the magnetization by $2\mu_\mathrm{B}$).

A few remarks are now in order. For systems with many non-equivalent magnetic atoms the choice of θ_i is non-trivial. The angles can be guessed or determined self-consistently, separately for every vector $\mathbf{q}$. In the frozen-magnon scheme based on spin-spiral calculations, it is impossible to incorporate the magnetic anisotropy directly. Once the dispersion relation is computed one can extract coupling constant J's of the HH and subsequently employ this Hamiltonian to study magnetic properties as described in previous subsections.

<div align="center">☙</div>

All the necessary formalism has been exposed and in the proceeding chapters we will try to apply it to evaluation of dynamical susceptibility of itinerant electron systems.

UNIFORM ELECTRON GAS

The model of a *uniform electron gas* (UEG)[1], presented in this chapter, is conceptually very important for this thesis, since it provides us with a good semi-qualitative picture of the ground state and the dynamics of an itinerant ferromagnet. It contains all the relevant concepts (like the presence of band splitting, Stoner states, spontaneous symmetry breaking and Goldstone modes, etc.) being not obscured by the complex details of unit cells, thus allowing an intuitive insight into the machinery of linear response density functional theory (LRDFT). Apart from the conceptual aspects, the model is to a great extent solvable analytically and the results can be used to benchmark numerical implementations, cf. Sec. 5.7.

The Coulomb interacting electron gas even in the absence of spatially varying external potential, is not exactly solvable. The *model of a ground state* presented in Sec. 4.1 is believed to be qualitatively similar to the one found in weakly correlated itinerant magnets. We discuss the major assumptions behind the picture, remarking briefly that the general ground state of UEG in the whole range of electronic densities must necessarily be more complex than the one suggested by density functional theory in the LDA.

Based on the ground state, the susceptibility is constructed using the two step LRDFT scheme of the previous chapter. First, in Sec. 4.2, the Kohn-Sham susceptibility is found and subsequently in Sec. 4.3 one solves the susceptibility Dyson equation. At the end of the latter section main qualitative differences to be expected in real materials are mentioned.

Most of the material presented in this chapter is not new and can be found in [11], Chap. 3. The most important original contributions are the explicit derivation of non-enhanced susceptibility formula (author is not aware of any textbook containing it) and making connection between PFEG and real itinerant magnets at the end of Sec. 4.3.

4.1   Ground state

We adopt here a *jellium*-like picture in which the positive nuclear charges form an uniform background. We assume that the ground state densities are uniform and that the Stoner condition is satisfied, i.e. it is energetically favorable for the UEG to become spin-polarized. Furthermore the ground state is assumed to be collinear and ferromagnetic. The temperature is 0 K.

One immediately sees that essentially it cannot be the most general picture. Even if one assumes the uniform positive background, the system, could develop (spin-) density wave ground state by decreasing the electron-electron interaction while gaining on the interaction with the background. Similarly non-collinearity could be expected. Such viable scenarios are plenty in numbers, but the one chosen seems to be a good starting point for studying collinear itinerant magnets.

The Hartree potential is neutralized by the interaction with the background. The exchange-correlation scalar potential is uniform and can be gauged out, serving as a reference (zero) energy. The effective

---

[1]It will be sometimes referred to as *polarized Fermi gas* (PFEG).

exchange-correlation magnetic field is also uniform and points up along the z-axis. The single particle energies and orbitals are solutions of the Kohn-Sham equation[2]

$$\left(-\nabla^2 \mathsf{I} + \Delta\sigma^z\right)\psi = \epsilon\psi, \tag{4.1.1}$$

where half of the band splitting reads

$$\Delta = -\mu_\mathrm{B} B. \tag{4.1.2}$$

The spatial part of ψ is a plane wave

$$\psi_\mathbf{k}(\mathbf{x}) = \frac{1}{\sqrt{\Omega}}\mathrm{e}^{\mathrm{i}\mathbf{k}\cdot\mathbf{x}}, \tag{4.1.3}$$

where Ω stands for the volume of the world[3]. Single particle orbitals are labeled by a composite quantum number $\mathbf{k}\sigma$ and their energies read

$$\epsilon(\mathbf{k}\sigma) = k^2 + \sigma\Delta, \tag{4.1.4}$$

where the spin index $\sigma = 1$ for the electrons with spin up ($\uparrow$) and -1 for those with spin down ($\downarrow$). If $B > 0$ the down (-1) channel is the majority channel. Without loss of generality we will always consider this case.

The density of states in $\mathbf{k}$-space is constant and reads

$$\frac{\Omega}{(2\pi)^3}, \tag{4.1.5}$$

while in the energy space it depends on σ

$$\rho_\sigma(\epsilon) = \begin{cases} \frac{\Omega}{(2\pi)^2}\sqrt{\epsilon - \sigma\Delta} & \epsilon \geq \sigma\Delta \\ 0 & \epsilon < \sigma\Delta. \end{cases} \tag{4.1.6}$$

The particle density n and splitting Δ determine chemical potential μ

$$n = N/\Omega = \frac{1}{\Omega}\sum_\sigma \int_{-\infty}^{\mu} f_T(\epsilon)\rho_\sigma(\epsilon)d\epsilon \equiv \sum_\sigma n_\sigma, \tag{4.1.7}$$

where n_σ is the particle density in the given spin channel and N stands for the number of particles. The magnetization is defined as

$$m = -\zeta n = \sum_\sigma \sigma n_\sigma \tag{4.1.8}$$

and ζ is called polarization.

If $B = 0$ (Fig. 4.1a) the highest occupied state (paramagnetic Fermi energy, ϵ_F) can be expressed in terms of n as

$$\epsilon_\mathrm{F} \equiv k_\mathrm{F}{}^2 = \left(3\pi^2 n\right)^{2/3}. \tag{4.1.9}$$

As Δ increases there are more and more particles in down the channel (Fig. 4.1b). Th up channel becomes empty when the splitting reaches a critical value Δ_c, which can be determined from the following condition (Fig. 4.1c)

$$\mu = \Delta \equiv \Delta_c = \epsilon_\mathrm{F}/2^{1/3}. \tag{4.1.10}$$

---

[2]It is assumed that Δ is the self-consistent value.
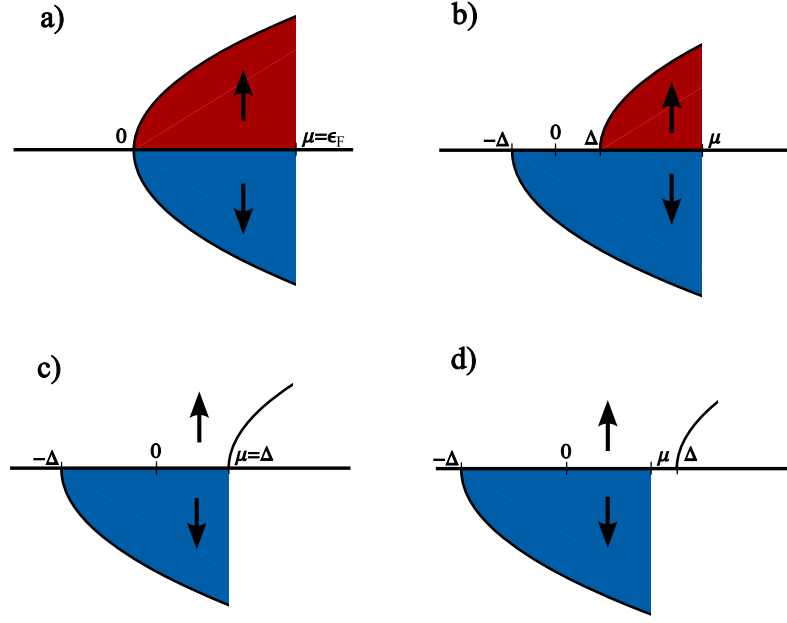[3]We use Born-von Kármán boundary conditions.

Figure 4.1: PFEG for different relative values of chemical potential and splitting. For vanishing splitting the system is essentially paramagnetic (a). Form small Δ it acquires a finite polarization, but both channel are populated (b). When the critical splitting is reached (c) the up states become unoccupied. For larger values of splitting we deal with a half-metal (d).

For larger splitting the system is half-metallic, Fig. 4.1d.

The chemical potential is rather complicated function of n and Δ

$$\mu(n, \Delta) = \begin{cases} \tilde{\mu}(n, \Delta) & \Delta < \Delta_c \\ 2^{2/3}\epsilon_F - \Delta & \Delta \geq \Delta_c; \end{cases} \qquad (4.1.11)$$

for practical purposes $\tilde{\mu}(n, \Delta)$ is evaluated numerically. There are several other handy relations

$$\zeta = \begin{cases} \left(\frac{\mu+\Delta}{\epsilon_F}\right)^{3/2} - 1 & \Delta < \Delta_c \\ 1 & \Delta \geq \Delta_c, \end{cases} \qquad (4.1.12a)$$

$$\mu = \frac{\epsilon_F}{2}\left((1+\zeta)^{2/3} + (1-\zeta)^{2/3}\right), \qquad (4.1.12b)$$

$$\Delta = \frac{\epsilon_F}{2}\left((1+\zeta)^{2/3} - (1-\zeta)^{2/3}\right). \qquad (4.1.12c)$$

Finally, the highest occupied k state in the given spin channel is given by

$$k_\sigma = k_F(1 - \sigma\zeta)^{1/3}. \qquad (4.1.13)$$

4.2 Non-interacting susceptibility

Based on the result of the previous chapter we can express the Fourier-transformed susceptibility of the polarized non-interacting electron gas as

$$\chi_0^{\mp}(\mathbf{q}, \omega + i\eta) = \frac{1}{(2\pi)^3} \int_{\mathbf{k}\in\mathbb{R}^3} d^3\mathbf{k} \frac{f_T(\epsilon_\downarrow(\mathbf{k})) - f_T(\epsilon_\uparrow(\mathbf{q}+\mathbf{k}))}{\omega + i\eta + \epsilon_\downarrow(\mathbf{k}) - \epsilon_\uparrow(\mathbf{q}+\mathbf{k})} \equiv \sum_{\sigma=\pm 1} I_\sigma, \qquad (4.2.1)$$

where

$$I_\sigma = -\frac{\sigma}{(2\pi)^3} \int_{\mathbf{k}\in\mathbb{R}^3} d^3\mathbf{k}\, \frac{\theta(k_\sigma - k)}{\omega - 2\mathbf{q}\cdot\mathbf{k} + \sigma q^2 - 2\Delta + i\eta} \tag{4.2.2}$$

and we used the fact that at 0 K f_T reduces to the Heaviside function. The integrals can be evaluated in spherical coordinates, with z-axis along $\mathbf{q}$

$$I_\sigma = -\frac{\sigma}{(2\pi)^3} \int_0^{k_\sigma} k^2 dk \int_0^{2\pi} d\phi \int_0^\pi \frac{d\theta \sin\theta}{\omega - 2qk\cos\theta + \sigma q^2 - 2\Delta + i\eta}. \tag{4.2.3}$$

The integral over θ reduces to

$$-\frac{1}{2qk} \int_{-1}^1 \frac{dx}{(p_\sigma - i\eta')/k + x} = -\frac{1}{2qk} \ln\frac{p_\sigma - i\eta' + k}{p_\sigma - i\eta' - k} \tag{4.2.4}$$

by means of substitution $x = \cos\theta$, where

$$p_\sigma = \frac{2\Delta - \omega - \sigma q^2}{2q}, \quad \eta' = \frac{\eta}{2q}. \tag{4.2.5}$$

Now we obtain

$$I_\sigma = \frac{\sigma}{(2\pi)^2} \frac{1}{2q} \int_0^{k_\sigma} k dk \ln\frac{p_\sigma - i\eta' + k}{p_\sigma - i\eta' - k} \tag{4.2.6}$$

and the integral in the above expression equates to

$$k_\sigma(p_\sigma - i\eta') + \frac{1}{2}\left(k_\sigma^2 - (p_\sigma - i\eta')^2\right)\ln\frac{p_\sigma - i\eta' + k_\sigma}{p_\sigma - i\eta' - k_\sigma}. \tag{4.2.7}$$

Finally the susceptibility reads

$$\chi_0^\mp(\mathbf{q}, \omega + i\eta) = \sum_{\sigma=\pm 1} \frac{\sigma}{(2\pi)^2} \frac{1}{2q}\left(k_\sigma(p_\sigma - i\eta') + \frac{1}{2}\left(k_\sigma^2 - (p_\sigma - i\eta')^2\right)\ln\frac{p_\sigma - i\eta' + k_\sigma}{p_\sigma - i\eta' - k_\sigma}\right). \tag{4.2.8}$$

In the case of retarded susceptibility ($\eta \to 0^+$) one obtains

$$\chi_0^\mp(\mathbf{q}, \omega + i0^+) = \sum_{\sigma=\pm 1} \frac{\sigma}{(2\pi)^2} \frac{1}{2q}\left(k_\sigma p_\sigma + \frac{1}{2}(k_\sigma^2 - p_\sigma^2)\left(\ln\left|\frac{k_\sigma + p_\sigma}{k_\sigma - p_\sigma}\right| + i\pi\theta(k_\sigma - |p_\sigma|)\right)\right), \tag{4.2.9}$$

using the following identity ($\alpha \in \mathbb{R} \setminus \{0\}$)

$$\ln\frac{\alpha + 1 \pm 0^+}{\alpha - 1 \pm 0^+} = \ln\left|\frac{\alpha + 1}{\alpha - 1}\right| \mp i\pi\theta(1 - |\alpha|). \tag{4.2.10}$$

The imaginary part remains finite when one of the following conditions is satisfied (Figure 4.2)

$$\omega_{-1} > \omega > \omega_1, \quad \omega_2 > \omega > \omega_{-2}, \text{ with} \tag{4.2.11a}$$

$$\omega_{\pm 1} = (q \mp k_\downarrow)^2 - k_\downarrow^2 + 2\Delta, \tag{4.2.11b}$$

$$\omega_{\pm 2} = -(q \mp k_\uparrow)^2 + k_\uparrow^2 + 2\Delta. \tag{4.2.11c}$$

The imaginary part vanish for $\omega = 0$. For the half-metallic PFEG there appears a gap $\Delta - \mu$ in the spectrum of Stoner states.
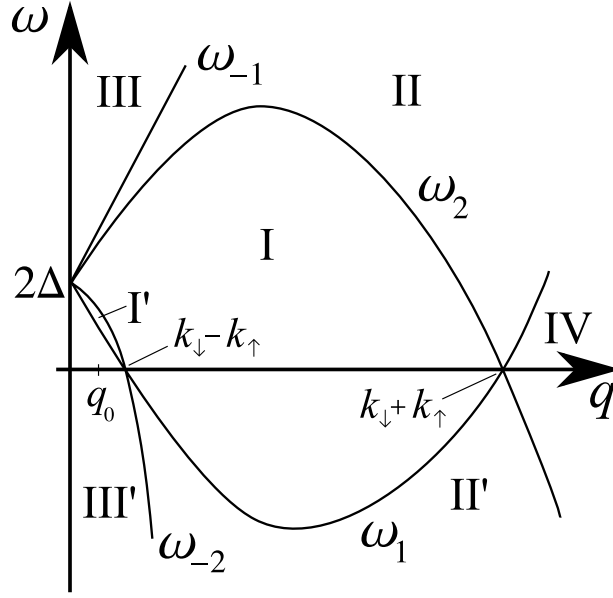
Figure 4.2: q-ω plane with regions where Stoner states exist (I, I' and II). The spin-waves can appear only in the region III' for $\omega > 0$. Please see text for the definition of the ω symbols. The picture comes from [11].

The finite imaginary part of the non-enhanced susceptibility signifies the presence of singularities (Stoner states), which in this case form a branch cut on the real axis (corresponding to the characteristic logarithmic behavior). An example of the frequency dependence of the susceptibility for vector $q_0 < k_\downarrow - k_\uparrow$ marked in Fig. 4.2 is presented in Fig. 4.3a. The imaginary part is finite only in a limited domain, being negative for $\omega > 0$. (We remind that the spectral power is given by $(-1/\pi)\Im\chi(\omega + i0^+)$.) The real part changes its sign as it crosses the singular region. The intensity is strongly peaked for $q = 0$ and $\omega = 2\Delta$.

For vanishing splitting the static susceptibility reduces to the well-known Lindhard dielectric function

$$\chi^{\mp}_{0\Delta=0}(\mathbf{q}, 0) = -\frac{k_{\mathrm{F}}}{4\pi^2}\mathrm{Lh}\left(\frac{q}{2k_{\mathrm{F}}}\right), \tag{4.2.12a}$$

$$\mathrm{Lh}(x) = \frac{1}{2} + \frac{1 - x^2}{4x}\log\left|\frac{1 + x}{1 - x}\right|. \tag{4.2.12b}$$

The static uniform susceptibility of the paramagnetic non-interacting electron gas equals $-\frac{1}{4\pi^2}k_{\mathrm{F}}$.

Because of the continuous translational invariance the susceptibility depends only on single wave-vector $\mathbf{q}$. Additionally the invariance with respect to spatial rotations reduces this dependence to the absolute value of the vector q.

4.3   Spin-waves in PFEG model

The enhanced susceptibility is readily obtained from the susceptibility Dyson equation

$$\chi(q, z) = \chi_0(q, z) + \chi_0(k, \omega)K_{\mathrm{xc}}\chi(k, \omega), \tag{4.3.1a}$$

$$\chi(q, z) = \frac{\chi_0(q, z)}{1 - K_{\mathrm{xc}}\chi_0(q, z)}. \tag{4.3.1b}$$

The exchange correlation kernel K_{xc} is a simple scalar constant in adiabatic local density approximation and to satisfy the spin rotational invariance it must read

$$K_{xc} = \frac{1}{\chi_0(0,0)} \in \mathbb{R}. \tag{4.3.2}$$

We immediately see that the enhanced susceptibility can develop a singularity beside the Stoner continuum, providing that the denominator vanishes

$$1 - K_{xc}\chi_0(q, \omega_0(q)) = 0. \tag{4.3.3}$$

Since K_{xc} is necessarily real, $\chi_0(q, \omega_0(q))$ must be real, too. This in turn means that $\omega_0(q) \in \mathbb{R}$ and it is located outside the Stoner continuum. The singularity therefore will be a simple pole located on the real axis. The behavior of the enhanced susceptibility in the small neighborhood of $\omega_0(q)$ can be determined as follows

$$\begin{aligned}\chi(q,z) &\approx \frac{\chi_0(q,\omega_0(q))}{1 - K_{xc}\chi_0(q,\omega_0(q)) - K_{xc}\chi_0'(q,\omega_0(q))(z-\omega_0(q))} \\ &= -\frac{\chi_0(q,z)/(K_{xc}\chi_0'(q,\omega_0(q)))}{z-\omega_0(q)}. \end{aligned} \tag{4.3.4}$$

(The expression above is -1st term of the Laurent expansion about the spin-wave pole $\omega_0(\mathbf{q})$.) Figure 4.3b presents the imaginary part of the enhanced susceptibility for $q = q_0$ from Figure 4.2. The spin-waves can appear only in the region III' for $\omega > 0$. For small q's the spin-waves feature a quadratic dispersion relation. Their intensity decreases with increasing q and vanishes when they contact the Stoner continuum. Substantial spectral power is transferred from the Stoner states to the spin-wave peak; the first become strongly renormalized, featuring enhanced intensity close to their contact point with the spin-waves instead of $q = 0$ and $\omega = 2\Delta$ point in the non-interacting case. The model is qualitatively very close to the picture of magnetic excitations in most ferromagnetic metals, e.g. MnSi is believed to be described well by the PFEG model [69]. Below we will discuss briefly, what differences might occur.
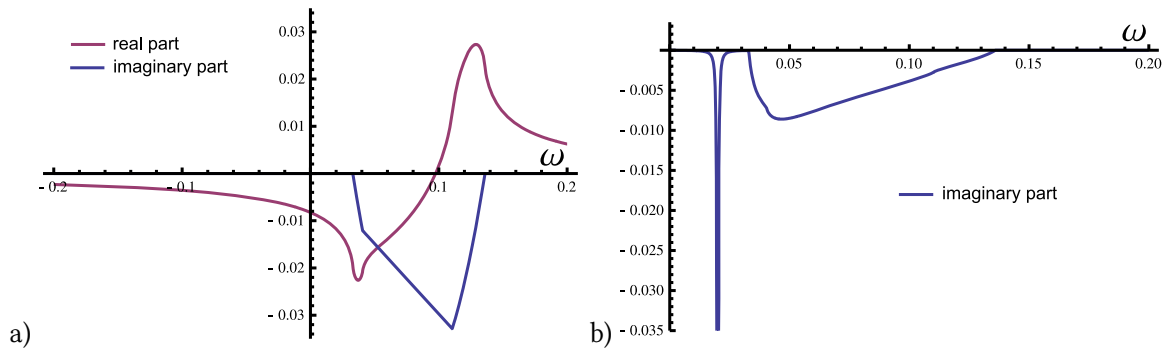

a)   b)

Figure 4.3: Non-enhanced (a) and enhanced (b) retarded susceptibility for wave-vector q_0 from Fig. 4.2. Susceptibility is given in Kb. In figure (a) one can distinguish regions III', I', I, II and II (going in the direction of growing frequency) divided by discontinuities of 1st derivative of $\mathfrak{Im}\chi_0(\mathbf{q}_0, \omega + \mathrm{i}0^+)$. Note the strong renormalization of Stoner continuum upon the action of the Dyson equation.

The spectral density of (non-enhanced) Stoner states in PFEG model is either zero or substantial (the imaginary part being comparable to the real part), therefore no well defined spin-waves peaks are expected in the Stoner region. In real materials however one can imagine that for certain $\omega_0(\mathbf{q}) \in \mathbb{R}$

$$1 - K_{xc}\mathfrak{Re}\left[\chi_0\left(\mathbf{q}, \omega_0(\mathbf{q}) + \mathrm{i}0^+\right)\right] = 0 \tag{4.3.5}$$

and in addition the imaginary part of $\chi_0(\mathbf{q}, \omega_0(\mathbf{q}) + i0^+)$ is small comparing to its real part. The susceptibility around $\omega_0(\mathbf{q})$ will assume than the form

$$\chi(\mathbf{q}, z) \approx -\frac{\chi_0(\mathbf{q}, z)/(K_{xc}\chi_0'(\mathbf{q}, \omega_0(\mathbf{q}) + i0^+))}{z - (\omega_0(\mathbf{q}) + \Sigma(\mathbf{q}))}, \qquad (4.3.6)$$

where the magnon self-energy would be

$$\Sigma(\mathbf{q}) = \frac{1 - K_{xc}\chi_0(\mathbf{q}, \omega_0(\mathbf{q}) + i0^+)}{K_{xc}\chi_0'(\mathbf{q}, \omega_0(\mathbf{q}) + i0^+)}. \qquad (4.3.7)$$

The function *appears to have effectively a new pole* at $\omega_0(\mathbf{q}) + \Sigma(\mathbf{q})$. Since the self-energy has a non-vanishing imaginary part, the spin-wave features a finite life-time. Additionally, the real part of Σ causes energy renormalization. In fact there is no *additional* singularity introduced by the Dyson equation. Rather, the originally small Stoner continuum becomes strongly enhanced near $\omega_0(\mathbf{q})$. Where the non-interacting Stoner states' density is pronounced such a single pole approximation must fail; the susceptibility retains its logarithmic singular behavior.

In ALDA the hybridization with Stoner states mentioned above is the only mechanism of broadening of spin-waves. It seems to describe well the collective modes in simple magnetic materials (Fe, Ni, Co) where broadened but yet well-defined spin-wave peaks exist in the wide range of wave-vectors. In this materials the density of Stoner states is not the only factor determining the magnons' life-time. As suggested by Cooke [21] the detailed structure of K_{xc} matrix, giving the overlap between Stoner and magnon states, is important as well.

Outside the Stoner continuum spin-waves leave infinitely long. Functionals beyond ALDA could account for the broadening of the spin-wave peaks also outside the continuum [60], capturing effects which could be interpreted as magnon-magnon or magnon-plasmon interaction, to mention just the two examples. Non-electronic degreed of freedom, most notably phonons, provide additional decay channel.

In nearly ferromagnetic paramagnets Stoner continuum can also become strongly enhanced and such a quasi spin-wave peak acquires even a certain dispersion. These states are called paramagnons. They were first considered by Doniach [70] in a model system, but they exist in real materials as well, examples being Pd, V, Y and Sc and $Cr_{95}V_5$ [29, 71, 25, 72].

Let us finally remark that, there is only one spin-wave branch in the PFEG model. In materials with many non-equivalent magnetic atoms in the unit cell many branches are expected. The effect originates from the internal dynamics within the unit cell, necessarily absent in the spatially uniform model.

IMPLEMENTATION

This chapter deals with the implementation of the formalism of the linear response density functional theory using Korringa-Kohn-Rostoker Green's function method based on Hutsepot environment. First, the construction of the KKR Green's function is outlined and subsequently one moves to the description of susceptibility calculations. A basis set is discussed, the construction of the non-enhanced susceptibility, solution of Dyson equation and finally, in Sec. 5.5, the possibilities of extracting useful information from the enhanced susceptibility matrix.

5.1   The structure of space

$\mathbf{x}$ or $\mathbf{r}$ denotes general spatial coordinate. For our purposes it is convenient to introduce so called cell centered coordinates. A set of *sites* $\{\mathbf{S}_N\}$ is defined and the position $\mathbf{r}$ is measured with respect to the the site $\mathbf{S}_N$, which is the one closest to $\mathbf{r}$

$$\mathbf{r}_N = \mathbf{r} - \mathbf{S}_N. \tag{5.1.1}$$

The site index $N = N(\mathbf{r})$ is determined almost uniquely by $\mathbf{r}$ by means of Voronoi tessellation of the set of all $\mathbf{S}_N$[1].

When a systems is periodic the general site coordinates can be decomposed into lattice vector $\mathbf{R}_n$ determining given primitive cell and the position of the basis atom $\mathbf{s}_\alpha$

$$\mathbf{S}_N = \mathbf{R}_n + \mathbf{s}_\alpha. \tag{5.1.2}$$

Small Latin letters $(m, n, \ldots)$ label lattice vectors, while small Greek letters $(\alpha, \beta, \ldots)$ denote basis vectors within the cell. The general index N is therefore understood as a pair (n, α).

5.2   The construction of the KKR Green's function

As it has been mentioned in Chap. 2 the Green's function of a non-interacting system is the resolvent of the single particle Schrödinger equation 2.3.10

$$(z - H_0(\mathbf{x}))G(\mathbf{x}, \mathbf{x}') = \delta(\mathbf{x} - \mathbf{x}'). \tag{5.2.1}$$

One of the method to determine the Green's function is to treat the problem as a genuine scattering of an electron off the effective potential and this formulation is known as the Korringa-Kohn-Rostoker scheme

---

[1]The word "almost" is used to indicate exceptions where a point $\mathbf{r}$ may be equally close to two or more sites. This happens on the boundaries of the Voronoi cells.

or multiple scattering theory [73, 74, 75]. Any practical implementation of the method is as involved as any other band technique and its detailed description is not relevant in the context of the thesis, it is however necessary to sketch how the Green's function is constructed.

In the multiple scattering theory one divides the space into non-overlapping space-filling polyhedra, so called atomic cells, since in the most cases their centers correspond to the positions of atomic nuclei. From the very beginning we resort ourselves to the atomic sphere approximation (ASA) [76], where the polyhedra are approximated by means of overlapping spheres and it is assumed that the potentials in the spheres are spherically symmetric. Now, the construction of the Green's function is split into two parts. First, the scattering off a single atomic cell is concerned. By solving a radial Schrödinger equation for the single scatterer one obtains the so called scattering (or t-) matrix and a pair of regular and irregular solutions [77]. Next, the multiple scattering off the centers is taken into account through the construction of so called "backscattering" operator. There exists an equivalent formulation in which the multiple scattering effects are described by so called "scattering path operator", but it is not used in this work.

G is a general matrix in spin space, $G_{\alpha\beta}$, but in the case of collinear magnetic system it has only diagonal components and often the notation G_σ will be used, where $\sigma = \uparrow, \downarrow$. The Green's function is represented as a sum

$$G(\mathbf{r}, \mathbf{r}', z) = \bar{G}(\mathbf{r}, \mathbf{r}', z) + \tilde{G}(\mathbf{r}, \mathbf{r}', z). \tag{5.2.2}$$

$\tilde{G}$ represent the scattering due to a single site, while $\bar{G}$ corresponds to the multiple scattering part. Spatial dependence of the Green's function is expressed by means of spherical harmonics and the regular and irregular solutions

$$\bar{G}_\sigma(\mathbf{r}, \mathbf{r}', z) = \sum_{LL'} G_{\sigma LL'}^{MN}(z) R_{\sigma L}^M(r_M, z) R_{\sigma L'}^N(r'_N, z) \mathcal{Y}_L(\hat{\mathbf{r}}_M) \mathcal{Y}_{L'}(\hat{\mathbf{r}}'_N), \tag{5.2.3}$$

$$\tilde{G}_\sigma(\mathbf{r}, \mathbf{r}', z) = \sqrt{z} \sum_L \delta_{MN} R_{\sigma L}^M(r_M^<, z) H_{\sigma L}^M(r_M^>, z) \mathcal{Y}_L(\hat{\mathbf{r}}_M) \mathcal{Y}_L(\hat{\mathbf{r}}'_M). \tag{5.2.4}$$

$G_{\sigma LL'}^{MN}(z)$ stands for the backscattering operator, R and H are the regular and irregular solutions respectively. $r_M^> = \max(r_M, r'_M)$, while $r_M^< = \min(r_M, r'_M)$. The spatial dependence of radial solutions is given on a mesh. M is the index of the site closest to $\mathbf{r}$ and N of the one closest to $\mathbf{r}'$.

In what follows we use special super-matrix notation: site and angular indices are merged into a single composite index $\lambda = (M, L)$. A special notation is used for such entities, e.g. $\mathsf{G}_{\sigma\lambda\lambda'}$ stands for $G_{\sigma LL'}^{MN}$ and often the λ-indices are not explicitly written. $\circ$ denotes standard matrix multiplication of two such super-matrices.

To determine the backscattering operator one introduces a concept of a reference system. A reference system is a space with a potential chosen in such a way so its backscattering operator G_r and the t-matrices t_r can be easily determined. If

$$\mathsf{t}_\Delta \equiv \mathsf{t} - \mathsf{t}_r, \tag{5.2.5}$$

where t stands for the scattering matrix of our original system, then the desired backscattering operator reads

$$\mathsf{G}(z) = -\mathsf{t}_\Delta^{-1}(z) + \mathsf{t}_\Delta^{-1}(z) \circ (\mathsf{I} - \mathsf{t}_\Delta(z) \circ \mathsf{G}_r(z))^{-1}. \tag{5.2.6}$$

$\mathsf{G}_r(z)$ is called structure constant.

The matrices in the above expressions are in general infinite. First of all, the L index assumes an arbitrary large values, but L-truncation, although it leads to many complications, can be safely handled. Now, unless one works with a cluster of atoms placed in vacuum, one must deal with an infinite number of sites. Let us look closer at the latter problem.

Up to now a real space formulation was used. One can exploit the discrete translational symmetry of a system (if there exists one) and use the Fourier transformed backscattering operators

$$G^{\alpha\beta}_{\sigma LL'}(\mathbf{k}) = \sum_n \mathfrak{e}^{-\mathbf{i}\mathbf{k}\cdot\mathbf{R}_n} G^{n\alpha 0\beta}, \tag{5.2.7}$$

where $\mathbf{R}_n$ are the lattice vectors and it sufficient to consider $\mathbf{k}$ in the first Brillouin zone. Small Greek letters ($\alpha\beta$) label atoms, which are non-equivalent taking into account discrete translational symmetry. Since t-matrices are diagonal in site space, equation 5.2.6 can be rewritten as

$$\mathsf{G}(z,\mathbf{k}) = -\mathsf{t}^{-1}_\Delta(z) + \mathsf{t}^{-1}_\Delta(z) \circ (\mathsf{I} - \mathsf{t}_\Delta(z) \circ \mathsf{G}_r(z,\mathbf{k}))^{-1}. \tag{5.2.8}$$

In the latter case the composite index $\lambda = (\alpha, L)$ contains only non-equivalent sites, what solves the above mentioned problem of infinite matrices for 3D periodic solids. In this case an empty space can be used as the reference system and one speaks about conventional structure constant and the conventional KKR method.

For the same reason we see immediately that the scheme cannot be used in a straightforward way for layered systems or clusters immersed in a matrix of another material, since in the latter case one faces inversion of an infinite matrix $\mathsf{I} - \mathsf{t}_\Delta(z) \circ \mathsf{G}_r(z, \mathbf{k})$. (It is often called *KKR matrix*.) Obviously one must content himself with the knowledge of Green's function restricted to a given finite number of site pairs (within the film or the cluster). Additionally, there must be some assumptions made upon the (semi-)infinite system outside the region of interest. Usually we assume that the potential deep within the substrate or matrix correspond to the potential of the bulk. Under these conditions one can obtain the backscattering operator in the interesting region, providing that such a choice of the reference system is made, which reduces the reference backscattering operator $G^{MN}_{r\sigma LL'}$ to block tridiagonal form [78, 79, 80, 81]. In other words the $G^{MN}_{r\sigma LL'}$ must be screened, that is vanish if sites M and N are sufficiently far apart from each other. It turns out that a sufficiently strong repulsive constant potential is a good choice for the reference system and one can find all the necessary fragments of the inverse of tridiagonal matrices in this case.

We are going to use similar trick to solve the susceptibility Dyson equation in the case of layered systems and further details regarding the technique and usage of tridiagonal matrices are presented there.

When a system has a discrete translational symmetry it is convenient to write the Green's function in the following form

$$G(\mathbf{x}, \mathbf{x}') = G(\mathbf{r}, \mathbf{r}', \mathbf{R}). \tag{5.2.9}$$

Here $\mathbf{x}, \mathbf{x}' \in \mathbb{R}^3$ while $\mathbf{r}$ and $\mathbf{r}'$ belong to the primitive cell of the system closest to the origin and $\mathbf{R} \in \mathcal{L}$ is the lattice vector closest to the the difference $\mathbf{x} - \mathbf{x}'$. Partially Fourier transformed Green's function reads

$$G(\mathbf{r}, \mathbf{r}', \mathbf{k} \in \Omega_{\mathrm{BZ}}) = \sum_{\mathbf{R}\in\mathcal{L}} \mathfrak{e}^{-\mathbf{i}\mathbf{k}\cdot\mathbf{R}} G(\mathbf{r}, \mathbf{r}', \mathbf{R}). \tag{5.2.10}$$

5.3   Non-interacting susceptibility

The non-interacting susceptibility at Bosonic poles can be calculated from Eq. 3.3.20. Using the Brillouin convolution theorem one obtains for the partially Fourier transformed quantities the following formula

$$\chi^0_{ij}(\mathbf{r}, \mathbf{r}', \mathbf{q}, \mathbf{i}\omega^b_n) = \frac{1}{\beta} \sum_{m\in\mathbb{Z}} \sigma^i_{\alpha\beta} \sigma^j_{\gamma\delta} \frac{1}{\Omega_{\mathrm{BZ}}} \int_{\Omega_{\mathrm{BZ}}} d^D\mathbf{k} G_{\beta\gamma}(\mathbf{r}, \mathbf{r}', \mathbf{k}, z_m) G_{\delta\alpha}(\mathbf{r}', \mathbf{r}, \mathbf{k} - \mathbf{q}, z_{m-n}), \tag{5.3.1}$$

which is the starting point for the numerical implementation.

One should consider several points. First of all we need to represent the spatial dependence of χ, i.e. we must choose a suitable basis. Second, we note that the equation involves two convolutions, one over the energy and the second over the Brillouin zone. In this section these points are addressed from the numerical point of view and directly implementable formulas are developed.

5.3.1   Spatial basis

The representation of susceptibility $\chi(\mathbf{r}, \mathbf{r}', z)$ is like in the case of KKR Green's function based on the cell centered coordinates. An approximation similar to ASA is used; atomic cells are substituted by spheres centered at positions of nuclei. Angular dependence inside every sphere is given by means of spherical harmonics. The radial dependence is based on Chebyshev polynomials. We will call this basis Y-Ch.

$$\chi(\mathbf{r}, \mathbf{r}', z) = \frac{1}{r_M r'_N} \sum_{LL'\mu\mu'} \chi_{LL'\mu\mu'}^{MN}(z) \mathfrak{Ch}_\mu\big(\xi_{[0,R_M]}(r_M)\big) \mathfrak{Ch}_{\mu'}\big(\xi_{[0,R_N]}(r'_N)\big) \mathcal{Y}_L(\hat{\mathbf{r}}_M)\mathcal{Y}_{L'}(\hat{\mathbf{r}}'_N). \quad (5.3.2)$$

R_M stands for the radius of the atomic sphere ascribed to site M and $\xi_{[0,R]}(r)$ is the Chebyshev reduced argument function (cf. App. C). $\chi(\mathbf{r}, \mathbf{r}', z)$ in the above expression is a matrix connecting all components of charge or magnetization densities and fields.

Let us note the additional prefactor $(rr')^{-1}$ in addition to two Chebyshev polynomials. This convention helps to stabilize the Chebyshev approximation procedure it is also convenient when solving the Dyson equation. These two points will be discussed later in a greater detail.

The basis is necessarily infinite, in practice one must use a finite number of spherical harmonics and Chebyshev polynomials. The basis functions are real and energy independent. This properties are helpful since all analytic symmetries of the susceptibility are straightforwardly reflected in the susceptibility matrix $\left(\chi_{LL'\mu\mu'}^{MN}(z)\right)_{ij}$. Finally, the basis is separable and the fact simplifies greatly the solution of the susceptibility Dyson equation.

If there exists discrete translational symmetry one can transform the susceptibility matrix to $\mathbf{k}$-space

$$\chi_{LL'\mu\mu'}^{\alpha\beta}(\mathbf{q}, z) = \sum_n \mathfrak{e}^{-i\mathbf{q}\cdot\mathbf{R}_n} \chi_{LL'\mu\mu'}^{n\alpha0\beta}(z). \quad (5.3.3)$$

The construction of $\left(\chi_{LL'\mu\mu'}^{\alpha\beta}(\mathbf{q}, i\omega_n^b)\right)_{ij}$ is the ultimate goal of our computations.

5.3.2   Energy convolution

By reshuffling the terms in the sums, using the symmetries of the Green's function and the fact that the Pauli matrices are Hermitian one can rewrite the Eq. 5.3.1 as

$$\chi_{ij}^0\big(\mathbf{r}, \mathbf{r}', \mathbf{q}, i\omega_n^b\big) = \frac{1}{\beta} \sum_{m=0}^{n-1} S_{ij}\big(\mathbf{r}, \mathbf{r}', \mathbf{q}, z_m, z_{m-n}\big) +$$

$$\frac{1}{\beta} \sum_{m=0}^{\infty} S_{ij}\big(\mathbf{r}, \mathbf{r}', \mathbf{q}, z_{m+n}, z_m\big) + \left(\frac{1}{\beta} \sum_{m=0}^{\infty} S_{ij}\big(\mathbf{r}, \mathbf{r}', -\mathbf{q}, z_{m+n}, z_m\big)\right)^*, \quad (5.3.4)$$

where

$$S_{ij}\big(\mathbf{r}, \mathbf{r}', \mathbf{q}, c_1, c_2\big) = \sigma_{\alpha\beta}^i \sigma_{\gamma\delta}^j \frac{1}{\Omega_{\mathrm{BZ}}} \int_{\Omega_{\mathrm{BZ}}} d^D\mathbf{k}\, G_{\beta\gamma}\big(\mathbf{r}, \mathbf{r}', \mathbf{k}, c_1\big) G_{\delta\alpha}\big(\mathbf{r}', \mathbf{r}, \mathbf{k}-\mathbf{q}, c_2\big). \quad (5.3.5)$$

Since the spin matrices are Hermitian, the convolution has the following symmetry

$$S_{ij}\big(\mathbf{r}, \mathbf{r}', \mathbf{q}, c_1, c_2\big) = S_{ij}\big(\mathbf{r}, \mathbf{r}', -\mathbf{q}, c_2^*, c_1^*\big)^*. \quad (5.3.6)$$

The first sum in Eq. 5.3.4 is finite and is valuated term-by-term. The two infinite sums will be split and partially summed term-by-term (up to M-th Fermionic pole) and partially transformed to Fermi-Dirac integrals by means of Eq. 2.2.6.

Let us consider a closed counter clock-wise (CCW) contour C which consists of a straight segment parallel to real axis stretching from $\mu - R + i\omega_{M+1}^b$ to $\mu + R + i\omega_{M+1}^b$ and a semicircular closure of radius

R such that when we let R to approach infinity the contour will enclose all the poles of f_T of indices greater than M. We have

$$\frac{1}{\beta} \sum_{m=M+1}^{\infty} S_{ij}(\mathbf{r}, \mathbf{r}', \mathbf{q}, z_{m+n}, z_m) = \frac{\mathrm{i}}{2\pi} \oint_C f_T(z) S_{ij}(\mathbf{r}, \mathbf{r}', \mathbf{q}, z + \mathrm{i}\omega_n^b, z) dz \qquad (5.3.7)$$

and similarly for the second sum. (It is important that the conjugation operation is performed at the very end, since S_{ij}^* in in general not analytic and Cauchy theorem does not hold.) It can be shown that the contribution to the integrals coming from the semicircular closure vanishes when $R \to \infty$.
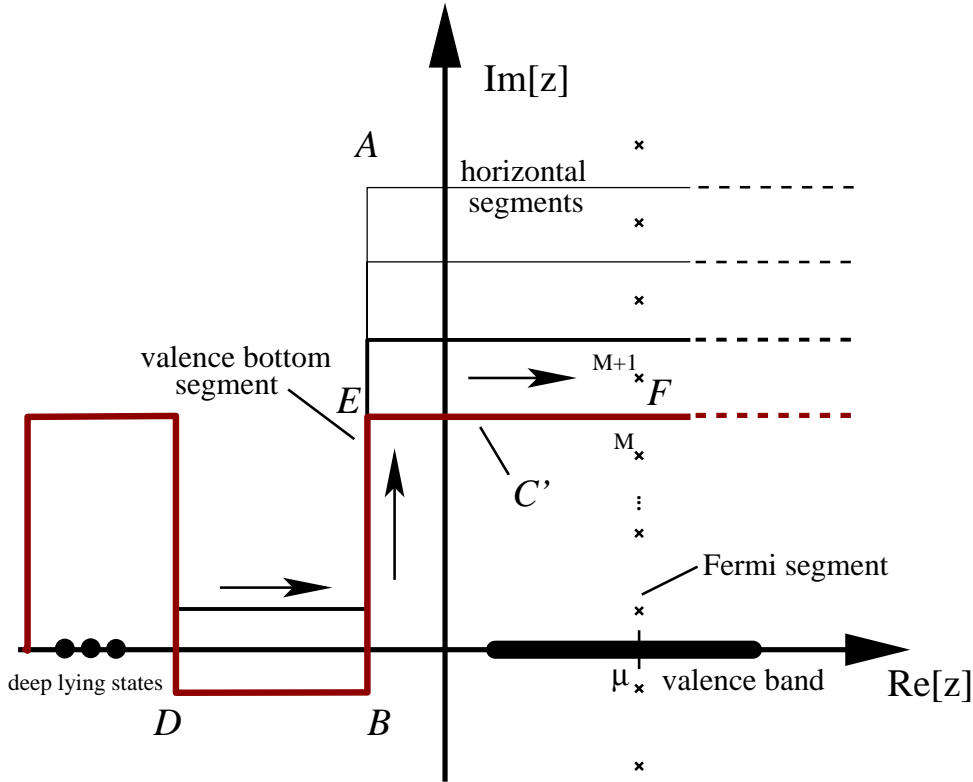
Figure 5.1: The general scheme of Matsubara energy convolution. The terms in convolution sums, which are not summed explicitly, are converted to complex integrals. Around the valence band one uses a rectangular contour BEF which starts close to the real axis below the bottom of valence band at $E_b - \mathrm{i}\omega_n^b/2$, continues vertically to $E_b + \mathrm{i}\omega_{M+1}^b$ and then horizontally up to Fermi energy. Similar box contours are used around deeply lying states. The contributions from the segments parallel to the real axis below the valence band (e.g. DB) vanish. For the energies above the chemical potential the Sommerfeld procedure is used and the integration is performed only up to μ. Arrows mark the orientation of contours.

In the next step the segment parallel to the real axis is deformed continuously to contour C' (see Fig. 5.1), that is below the bottom of valence band it runs parallel to the real axis in the lower complex semi-plane, containing points of complex parts equal to $-\mathrm{i}\omega_n^b/2$. Around the deep lying poles of Green's function it comes back to the upper semi-plane. We show now that the contributions to the integrals coming from the segments parallel to the real axis vanish. Let us say that the segment stretches from $E_1 - \mathrm{i}\omega_n^b/2$ to $E_2 - \mathrm{i}\omega_n^b/2$. The contribution from the first sum reads

$$\frac{\mathrm{i}}{2\pi} \int_{E_1}^{E_2} d\epsilon f_T\left(\epsilon - \frac{\mathrm{i}\omega_n^b}{2}\right) S_{ij}\left(\mathbf{r}, \mathbf{r}', \mathbf{q}, \epsilon + \frac{\mathrm{i}\omega_n^b}{2}, \epsilon - \frac{\mathrm{i}\omega_n^b}{2}\right), \qquad (5.3.8)$$

while the contribution from the conjugated term is

$$\left(\frac{\mathrm{i}}{2\pi}\int_{E_1}^{E_2}d\epsilon\, f_T\left(\epsilon-\frac{\mathrm{i}\omega_n^b}{2}\right)S_{ij}\left(\mathbf{r},\mathbf{r}',-\mathbf{q},\epsilon+\frac{\mathrm{i}\omega_n^b}{2},\epsilon-\frac{\mathrm{i}\omega_n^b}{2}\right)\right)^* \tag{5.3.9}$$

$$=-\frac{\mathrm{i}}{2\pi}\int_{E_1}^{E_2}d\epsilon\, f_T\left(\epsilon-\frac{\mathrm{i}\omega_n^b}{2}\right)S_{ij}\left(\mathbf{r},\mathbf{r}',\mathbf{q},\epsilon+\frac{\mathrm{i}\omega_n^b}{2},\epsilon-\frac{\mathrm{i}\omega_n^b}{2}\right), \tag{5.3.10}$$

where the symmetry 5.3.6 and the fact that $f_T\left(\epsilon-\mathrm{i}\omega_n^b/2\right)\in\mathbb{R}$ were used. The two contributions cancel each other. Since the energies of single particle states are bounded from below the integration below the Fermi energy is limited to a finite number of segments around the poles of the KKR Green's function.

Unfortunately the integration for energies above the Fermi level cannot be reduced to a finite one by means of the trick since the energies of single particle states are not bounded from above. However for sufficiently small temperatures the Fermi-Dirac distribution function is still very similar to a step function and one can use Sommerfeld procedure (eq. 2.2.7). Let E_b be an energy below the bottom of the valence band and above the deeper lying states. Above E_b we let the contour to be parallel to real axis and we place it in the middle between two Fermionic poles, so it contains points of the form $\epsilon+\mathrm{i}\omega_{M+1}^b$. The part of the integral stretching from the bottom of the valence band to infinity reads

$$\int_{E_b}^{\infty}d\epsilon\, f_T\left(\epsilon+\mathrm{i}\omega_{M+1}^b\right)S_{ij}\left(\mathbf{r},\mathbf{r}',\mathbf{q},\epsilon+\mathrm{i}\omega_{M+1}^b,\epsilon+\mathrm{i}\omega_{M+n+1}^b\right)=$$

$$\int_{E_b}^{\mu}d\epsilon\, f_T(\epsilon)S_{ij}\left(\mathbf{r},\mathbf{r}',\mathbf{q},\epsilon+\mathrm{i}\omega_{M+1}^b,\epsilon+\mathrm{i}\omega_{M+n+1}^b\right)+\text{Sommerfeld corrections} \tag{5.3.11}$$

where the periodicity of Fermi-Dirac function was used, cf. eq. 2.2.5.

The general integration scheme is presented in Fig. 5.1. A few remarks are now in order. One could be tempted to think that the infinite sums could be approximated by summing only up to a certain Fermionic frequency, but this would lead to an effect similar to Gibb's ringing. Matsubara formalism boils essentially down to Fourier series decomposition of a Green's function in the imaginary time. Around $\tau=0$ the function features discontinuity and Fourier series cannot approximate it uniformly and as long as the number of Fourier components is finite the region around the discontinuity is poorly represented. Therefore it is important to include all the poles, which is done by converting some parts of the sum into integrals. In addition the contour is chosen such that to keep away from the singularities of Green's function, which lie on the real axis and coincide with the Kohn-Sham energies.

5.3.3 Y-Ch matrix elements

Let us look closer at the product of two Green's functions in the equation 5.3.5. Upon substituting the KKR form of G we obtain

$$\frac{1}{\Omega_{\text{BZ}}}\int_{\Omega_{\text{BZ}}}d^D\mathbf{k}\, G_{\sigma_1}\left(\mathbf{r},\mathbf{r}',\mathbf{k},c_1\right)G_{\sigma_2}\left(\mathbf{r}',\mathbf{r},\mathbf{k}-\mathbf{q},c_2\right)$$

$$=\sum_{L_1L_2L_3L_4}\mathcal{Y}_{L_1}(\hat{\mathbf{r}}_\alpha)\mathcal{Y}_{L_2}\left(\hat{\mathbf{r}}'_\beta\right)\mathcal{Y}_{L_3}\left(\hat{\mathbf{r}}'_\beta\right)\mathcal{Y}_{L_4}(\hat{\mathbf{r}}_\alpha)\times$$

$$(^{\sigma_1\sigma_2}C_{L_1L_2L_3L_4}^{\alpha\beta}(c_1,c_2,\mathbf{q})R_{\sigma_1L_1}^\alpha(r_\alpha,c_1)R_{\sigma_1L_2}^\beta\left(r'_\beta,c_1\right)R_{\sigma_2L_3}^\beta\left(r'_\beta,c_2\right)R_{\sigma_2L_4}^\alpha(r_\alpha,c_2)+$$

$$\delta_{\alpha\beta}\delta_{L_1L_2}\sqrt{c_1}R_{\sigma_1L_1}^\alpha\left(r_\alpha^<,c_1\right)H_{\sigma_1L_1}^\alpha\left(r_\alpha^>,c_1\right)B_{\sigma_2L_3L_4}^\alpha(c_2)R_{\sigma_2L_3}^\alpha\left(r'_\alpha,c_2\right)R_{\sigma_2L_4}^\alpha(r_\alpha,c_2)+$$

$$\delta_{\alpha\beta}\delta_{L_3L_4}B_{\sigma_1L_1L_2}^\alpha(c_1)R_{\sigma_1L_1}^\alpha(r_\alpha,c_1)R_{\sigma_1L_2}^\alpha\left(r'_\alpha,c_1\right)\sqrt{c_2}R_{\sigma_2L_3}^\alpha\left(r_\alpha^<,c_2\right)H_{\sigma_2L_3}^\alpha\left(r_\alpha^>,c_2\right)+$$

$$\delta_{\alpha\beta}\delta_{L_1L_2}\delta_{L_3L_4}\sqrt{c_1c_2}R_{\sigma_1L_1}^\alpha\left(r_\alpha^<,c_1\right)H_{\sigma_1L_1}^\alpha\left(r_\alpha^>,c_1\right)R_{\sigma_2L_3}^\alpha\left(r_\alpha^<,c_2\right)H_{\sigma_2L_3}^\alpha\left(r_\alpha^>,c_2\right)). \tag{5.3.12}$$

The first term comes from the convolution of two backscattering operators

$$^{\sigma_1\sigma_2}C_{L_1L_2L_3L_4}^{\alpha\beta}(c_1,c_2,\mathbf{q})=\frac{1}{\Omega_{\text{BZ}}}\int_{\Omega_{\text{BZ}}}d^D\mathbf{k}\, G_{\sigma_1L_1L_2}^{\alpha\beta}(c_1,\mathbf{k})G_{\sigma_2L_3L_4}^{\beta\alpha}(c_2,\mathbf{k}-\mathbf{q}) \tag{5.3.13}$$

while the next two terms involve diagonal part of it

$$B_{\sigma LL'}^{\alpha}(z) = \frac{1}{\Omega_{\text{BZ}}} \int_{\Omega_{\text{BZ}}} d^D\mathbf{k} G_{\sigma LL'}^{\alpha\alpha}(z, \mathbf{k}). \tag{5.3.14}$$

5.3.4 Remarks

The calculation of the non-enhanced susceptibility is based on the direct implementation of the formulae given in the previous sections. Every energy pair contribution S_{ij} might be seen as a sum of four components. Only the one involving the convolution of backscattering operators ${}^{\sigma_1\sigma_2}C_{L_1L_2L_3L_4}^{\alpha\beta}(c_1, c_2, \mathbf{q})$ lead to the $\mathbf{q}$-dependence of the susceptibility. Only this term is non-local in site space. The other three terms are local and $\mathbf{q}$-independent and must be computed only once for every Bosonic frequency.

We can anticipate now the general flow of computations. For every necessary energy pair (c_1, c_2) and a given spin configuration (σ_1, σ_2) one performs a Brillouin zone integration (convolution) to obtain the B and C matrices. The next step involves 2D-Chebyshev approximation of the radial dependence given by the products of four radial solutions. In the next step one uses Gaunt coefficients to express fours of spherical harmonics by means of pairs. Then S_{ij}'s (or rather $\chi_{LL'\mu\mu'}^{\alpha\beta}(\mathbf{q}, i\omega_n^b)$) matrix corresponding to them) are constructed by combining different spin configurations and, as it has been mentioned, in the last stage the energy summations and integrals are performed.

The accurate determination of non-enhanced susceptibility is the most time consuming part of calculations, due to the necessary Brillouin zone integrations. The number of $\mathbf{k}$-points necessary to achieve a given level of accuracy, depends strongly on the imaginary parts of $c_{1,2}$ arguments, decreasing rapidly as one moves away from the real axis and the Fermi energy. At the beginning of calculations a scan of complex plane is made. For a set of complex numbers a convolution of backscattering operators is performed for increasing density of $\mathbf{k}$-mesh. The mesh is made denser until all the elements of array ${}^{\sigma_1\sigma_2}C_{L_1L_2L_3L_4}^{\alpha\beta}(c_1, c_2, \mathbf{0})$ converge with a specified accuracy ($10^{-3} \div 10^{-5}$). Similar convergence test is performed for $B_{\sigma LL'}^{\alpha}(z)$. Very close to the real axis one needs typically $8 \cdot 10^6$ $\mathbf{k}$-points (3D case). For the energy $\epsilon_{\text{F}} + 0.1i$ this number does not exceed 1000.

At present a uniform $\mathbf{k}$-mesh is used. It is likely however that the integrands might feature strong peaks in the Brillouin zone and some kind of adaptive integration scheme (for example based on tetrahedron method) would be more preferable.

The 2D-Chebyshev approximation of the radial part might potentially lead to problems. The single site contribution to the Green's function is singular close to the center of the atomic cell, what can be immediately seen when taking into account the asymptotics of H and R

$$H_L(r) \sim r^{-l-1}, \; R_L(r) \sim r^l, \quad r \to 0. \tag{5.3.15}$$

This problem is solved in our calculations by including this divergence explicitly in the basis. In this way one has to perform approximation of a function without singularities. Unfortunately even in this case the radial dependence still doesn't not have a continuous first derivative; the single scattering part of Green's function feature an essential cusp which gives rise to the Dirac's delta on the right hand side of Eq. 5.2.1. Chebyshev polynomials cannot approximate uniformly such functions, but experience shows that the cusp can still be reasonably well reproduced.

The transformation leading to 5.3.4 was possible only under the assumption that spin matrices $\sigma^{i,j}$ were Hermitian in spin space. One therefore works usually with $\chi_{xx,xy}$ and constructs $\chi_{\pm}$ only at the very end of the calculations.

If the temperature T is small compared to the width of the valence band one can completely neglect Sommerfeld corrections. All integrals are simply performed up to the Fermi energy and for smaller energies one takes $f_T \equiv 1$. One must stress that the introduction of temperature is here only a numerical trick, allowing to move away from Green's function singularities near the Fermi energy. The smearing of Fermi level introduces change of order $k_{\text{B}}T/\Delta \approx 2.1 \cdot 10^{-3}$ for $T = 50$K and $\Delta = 0.15$ corresponding to the band slitting of Fe. Our calculations describe still essentially low temperature state.

For sufficiently small frequencies the susceptibility is primarily determined by the transitions within valence band and complex integration around deeper lying states can be neglected.

The energy dependence of the screened structure constants, t-matrices and radial solutions can be approximated on the complex plane by means of Chebyshev polynomials, which allows to significantly reduce the computational time of energy integrations.

5.4   Susceptibility Dyson equation

We want to solve numerically the susceptibility Dyson equation 3.4.10

$$\chi(\mathbf{r}, \mathbf{r}', \mathbf{q}, z) = \chi_0(\mathbf{r}, \mathbf{r}', \mathbf{q}, z) + \int_{\Omega_{\text{WS}}} d\mathbf{r}_1 \chi_0(\mathbf{r}, \mathbf{r}_1, \mathbf{q}, z) K_{\text{xc}}(\mathbf{r}_1) \chi(\mathbf{r}_1, \mathbf{r}', \mathbf{q}, z), \qquad (5.4.1)$$

which means we want to construct $\chi_{LL'\mu\mu'}^{\alpha\beta}$ representing the interacting susceptibility in Y-Ch basis for every interesting $z \in \mathbb{C}$ and $\mathbf{q}$.

The exchange-correlation kernel is represented as follows

$$K_{\text{xc}}(\mathbf{r}) = \mathcal{W}(\xi(R_\alpha, r_\alpha)) \sum_{L\mu} K_{\text{xc}}^{\alpha L\mu} \mathcal{Y}_L(\hat{\mathbf{r}}_\alpha) \mathfrak{Ch}_\mu(\xi(R_\alpha, r_\alpha)). \qquad (5.4.2)$$

Let us note additional Chebyshev weight included in order to simplify the solution.

Using Y-Ch representation for susceptibility matrices and the above representation for the xc kernel the integral Dyson equation is transformed to an algebraic equation

$$\chi_{LL'\mu\mu'}^{\alpha\beta} = \chi_{0LL'\mu\mu'}^{\alpha\beta} + \sum_{\gamma_1 L_1 \mu_1 \gamma_2 L_2 \mu_2} \chi_{0LL_1\mu\mu_1}^{\alpha\gamma_1} M_{\gamma_2 L_2 \mu_2}^{\gamma_1 L_1 \mu_1} \chi_{L_2 L'\mu_2\mu'}^{\gamma_2 \beta}, \qquad (5.4.3)$$

where the matrix M is constructed based on exchange-correlation kernel and overlap integrals

$$M_{\gamma_2 L_2 \mu_2}^{\gamma_1 L_1 \mu_1} = \delta_{\gamma_1 \gamma_2} \sum_{L\mu} {}^{\gamma_1} c_{\mu\mu_1\mu_2}^{LL_1 L_2} K_{\text{xc}}^{\gamma_1 L\mu}, \qquad (5.4.4)$$

$$^{\gamma_1} c_{\mu\mu_1\mu_2}^{LL_1 L_2} = \int_{4\pi} d\hat{\mathbf{r}} \mathcal{Y}_L(\hat{\mathbf{r}}) \mathcal{Y}_{L_1}(\hat{\mathbf{r}}) \mathcal{Y}_{L_2}(\hat{\mathbf{r}}) \times \qquad (5.4.5)$$

$$\int_0^{R_\gamma} dr \mathcal{W}(\xi(R_\gamma, r)) \mathfrak{Ch}_\mu(\xi(R_\gamma, r)) \mathfrak{Ch}_{\mu_1}(\xi(R_\gamma, r)) \mathfrak{Ch}_{\mu_2}(\xi(R_\gamma, r)). \qquad (5.4.6)$$

The triples of indices $(\alpha L\mu)$ can be combined into one composite index. As a consequence all matrices appearing in the algebraic Dyson equation become two dimensional and if there is a finite number of non-equivalent atoms, $\chi_{LL'\mu\mu'}^{\alpha\beta}$ can be obtained by matrix inversion

$$\chi = (\mathsf{I} - \chi_0 \mathsf{M})^{-1} \chi_0 \equiv \mathsf{D}^{-1} \chi_0. \qquad (5.4.7)$$

D is called Dyson matrix. This approach is directly implemented in the code.

As we have already discussed in Sec. 3.4.2 the matrix D for $z = \mathrm{i}0^+$ and $\mathbf{q} = \mathbf{0}$ is formally singular. Numerically it features usually one eigenvalue of absolute values very close to zero ($\approx 10^{-3} - 10^{-2}$). Experience showed that the following operation (called "Goldstone correction") can improve the stability of subsequent analytical continuation. Matrix D is transformed to a diagonal representation. Subsequently its lowest eigenvalue is set to a value close to zero (typically 10^{-6}) and the matrix is transformed back to the original representation. The new matrix is used to correct the M matrix.

The case of infinitely many non-equivalent atoms is more involved. Apparently we must content ourselves with a knowledge of χ in a finite region of space called interface or center. Nevertheless the influence of the rest of the world – in the case of 2D calculations this means semi-infinite bulk region(s) –

must be also properly taken into account. For the purpose of this calculations a new scheme has been developed, which can address such semi-infinite systems. It is based on a concept similar to those of screened structure constants. One observes (see discussion below) that Kohn-Sham (non-enhanced) susceptibility is short-ranged in virtually all systems we deal with

$$\chi^0_{MN} \approx 0, \quad |\mathbf{S}_N - \mathbf{S}_M| > \zeta, \tag{5.4.8}$$

where ζ is called screening range. To be precise χ^0_{MN} stands for Y-Ch blocks of the susceptibility matrix. χ^0 is therefore effectively a tridiagonal matrix and based on this property we can determine enhanced susceptibility in the interface region by means of inversion of *finite* matrices. Figure 5.2 presents the magnetic response of bcc Fe. Magnetic field uniform within atomic sphere around site 1 was applied, the plot presents uniform component of magnetization induced on sites along (001) direction. We can see that the response is mainly localized to the given atomic sphere, being much weaker outside and decaying in an oscillatory manner. There exists a conceptual difference between the screening formalism for the susceptibility Dyson equation and screened structure constants. In the latter case one introduces a reference system, which provides screening. In our case we assume the "natural screening", which however, as we have seen, is expected.
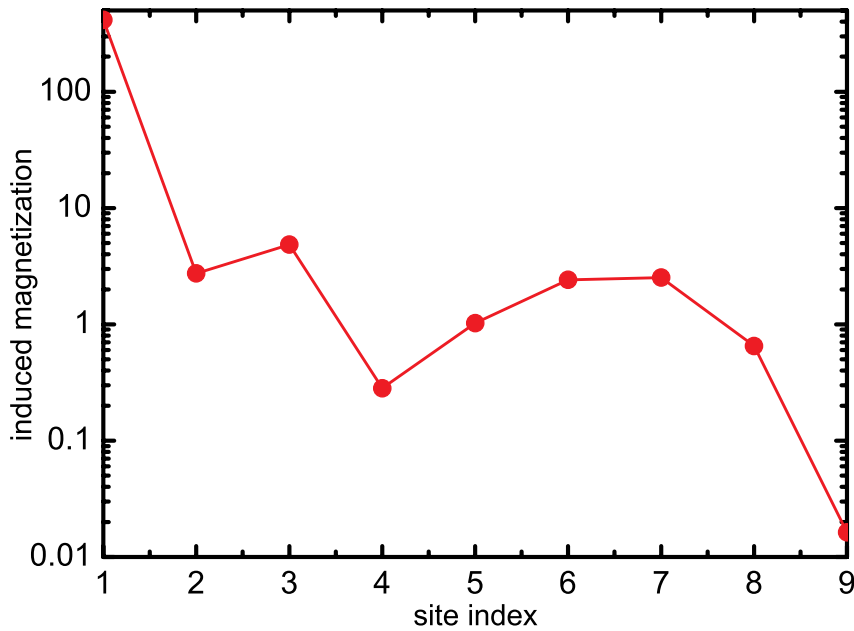

Figure 5.2: The magnetic response of bcc Fe, arbitrary units. The applied magnetic field was uniform the within atomic sphere around site 1. The plot presents the absolute value of uniform component of magnetization induced on sites along (001) direction.

The sites in an infinite system are located in three regions: left (L), center (I) and right (R), see Fig. 5.3. Additionally in the semi-infinite regions L and R we distinguish finite tangential (Lt and Rt) and extended (Le and Re) parts. The thickness of tangential parts must be larger than the range of screening of χ_0. Similarly the center part is assumed to be thicker than ζ.

We adopt one more plausible assumption that in the left and right regions the susceptibility are bulk-like; the tridiagonal structure of χ_0 repeats itself periodically deep in the bulk. The left and right regions can be composed of different bulk materials. One or both of them can be also substituted by the vacuum, in the case of adsorbed film or slab geometry, respectively. The susceptibility in the vacuum region away
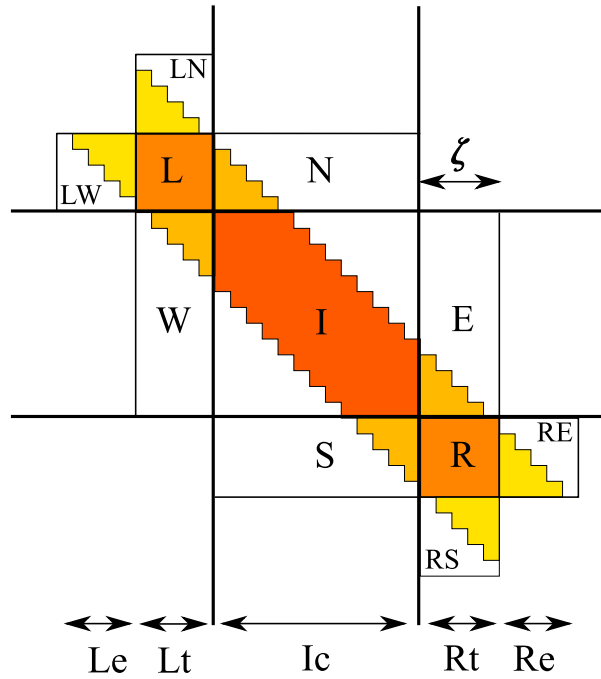
Figure 5.3: The computational domain used to solve two-dimensional susceptibility Dyson equation. The *sites* are grouped in three major regions: two semi-infinite right and left regions and a finite interface region (I). Four finite subsets of right and left sites are distinguished; they are tangential (Lt and Rt) and extended (Le and Re) regions. The *pairs of sites* are grouped in 11 regions. Due to the short-range character of χ_0 there is no need to compute susceptibility for every site pair in the computational domain; only Y-Ch blocks corresponding to colored pairs are determined. They are determined by the screening range ζ.
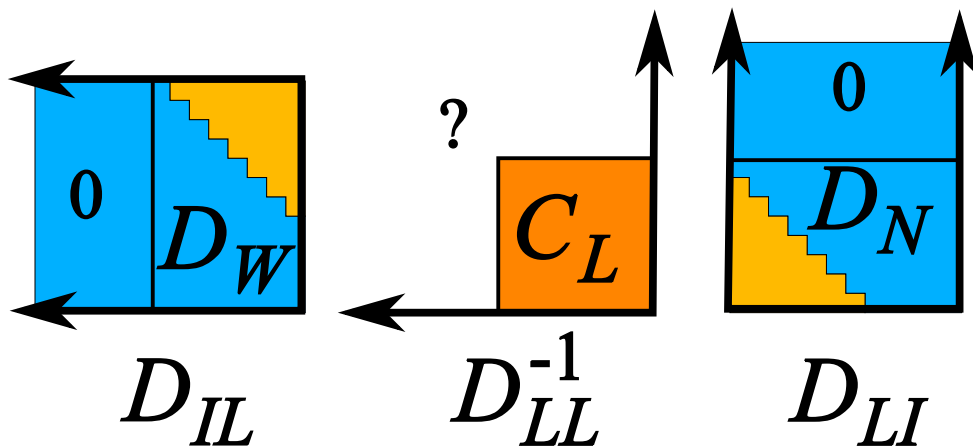
Figure 5.4: A schematic representation of $D_{IL}D_{LL}^{-1}D_{LI}$ multiplications. Due to the short-range character of χ_0 one needs only the "corner" block C_L of the semi-infinite matrix D_{LL}^{-1}.
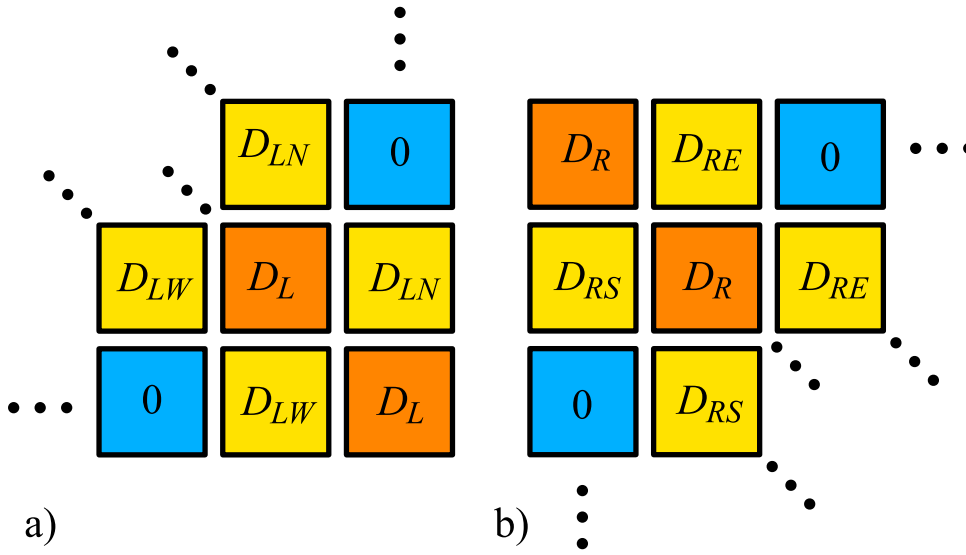
Figure 5.5: The self-repeating structure of a) LL and b) RR semi-infinite fragments of D and χ_0 allows to determine $C_{L,R}$.

from the surface can be simply equated to zero. The computational domain contains 11 finite regions, depicted in the Fig. 5.3. Under the assumptions listed above (screening and bulk like susceptibility deep in the bulk regions) the knowledge of χ_0 in these regions suffices to determine enhanced susceptibility in the center region.

A remark on notation. In this section we continue to work with composite block 2D matrices. The regions mentioned above group pairs of sites. An element of a composite matrix corresponding to such a pair of sites should be regarded as a Y-Ch block.

Both the non-enhanced susceptibility and the Dyson matrix are tridiagonal infinite matrices

$$\chi^0 = \begin{pmatrix} \chi^0_{LL} & \chi^0_{LI} & 0 \\ \chi^0_{IL} & \chi^0_{II} & \chi^0_{IR} \\ 0 & \chi^0_{RI} & \chi^0_{RR} \end{pmatrix}, \tag{5.4.9}$$

$$\mathsf{D} = \begin{pmatrix} \mathsf{I} - \chi^0_{LL}M_L & -\chi^0_{LI}M_I & 0 \\ -\chi^0_{IL}M_L & \mathsf{I} - \chi^0_{LL}M_L & -\chi^0_{IR}M_R \\ 0 & -\chi^0_{RI}M_I & \mathsf{I} - \chi^0_{RR}M_R \end{pmatrix} \equiv \mathsf{E}^{-1}. \tag{5.4.10}$$

The enhanced susceptibility in the center region reads

$$\chi_{II} = E_{IL}\chi^0_{LI} + E_{II}\chi^0_{II} + E_{IR}\chi^0_{RI}. \tag{5.4.11}$$

In order to proceed we must learn how to invert the tridiagonal matrix. We put $\mathsf{E} \equiv \mathsf{D}^{-1}$

$$\mathsf{D} = \begin{pmatrix} D_{LL} & D_{LI} & 0 \\ D_{IL} & D_{II} & D_{IR} \\ 0 & D_{RI} & D_{RR} \end{pmatrix}, \quad \mathsf{E} = \begin{pmatrix} E_{LL} & E_{LI} & E_{LR} \\ E_{IL} & E_{II} & E_{IR} \\ E_{RL} & E_{RI} & E_{RR} \end{pmatrix} \tag{5.4.12}$$

to obtain

$$E_{II} = \left(D_{II} - D_{IL}D_{LL}^{-1}D_{LI} - D_{IR}D_{RR}^{-1}D_{RI}\right)^{-1}, \tag{5.4.13a}$$

$$E_{IL} = -E_{II}D_{IL}D_{LL}^{-1}, \tag{5.4.13b}$$

$$E_{IR} = -E_{II}D_{IR}D_{RR}^{-1}. \tag{5.4.13c}$$

We see that the above evaluation involves products of infinite matrices, which can however be reduced to finite multiplications

$$D_{IL}D_{LL}^{-1}D_{LI} = D_W C_L D_N, \tag{5.4.14a}$$

$$D_{IR}D_{RR}^{-1}D_{RI} = D_E C_R D_S, \tag{5.4.14b}$$

$$D_{IL}D_{LL}^{-1}\chi_{LI}^0 = D_W C_L \chi_N^0, \tag{5.4.14c}$$

$$D_{IR}D_{RR}^{-1}\chi_{RI}^0 = D_E C_R \chi_S^0, \tag{5.4.14d}$$

where $C_{L,R}$ are "corner" blocks of D_{LL}^{-1} and D_{RR}^{-1} matrices respectively. Fig. 5.4 presents schematically multiplication $D_{IL}D_{LL}^{-1}D_{LI}$, please refer to the caption for details. Analogical argumentation can be used to reduce multiplications in every other case listed above.

The determinations of coupling matrices $C_{L,R}$ poses a bit involved issue. Let us remind ourselves that D_{LL} and D_{RR} have the characteristic self-repeating form presented schematically in the Fig. 5.5. Additional short contemplation of Eq. 5.4.13a leads us to the following self-consistent equation for E_L

$$C_L = (D_L - D_{LW} E_L D_{LN})^{-1}, \tag{5.4.15}$$

where we took $D_{IR} = D_{RI} = 0$. By the same token we obtain

$$C_R = (D_R - D_{RE} E_R D_{RS})^{-1}. \tag{5.4.16}$$

Let us remark at the end of this section that the Dyson equation can be solved directly on the imaginary axis. The non-enhanced susceptibility can also be first analytically continued to the real axis and the equation is solved there. The commutation of these two operations follows from the absence of the energy convolution in the susceptibility Dyson equation. We usually choose the first option, which gives better numerical accuracy.

5.5   Postprocessing

Once the susceptibility Dyson equation is solved we have determined the enhanced susceptibility *matrix* either for a set of Bosonic frequencies or points slightly above the real axis. This information itself is not very useful. The further analysis can go in two directions.

One can compute the Fourier transformation of the susceptibility

$$\chi(\underline{\mathbf{q} + \mathbf{K}_1}, \underline{-\mathbf{q} - \mathbf{K}_2}, \mathbf{q}) \equiv \iint_{\Omega_{\mathrm{WS}}^2} d\mathbf{r}_1 d\mathbf{r}_2 e^{-i(\mathbf{q}+\mathbf{K}_1)\cdot\mathbf{r}_1} \chi(\mathbf{r}_1, \mathbf{r}_2, \mathbf{q}) e^{i(\mathbf{q}+\mathbf{K}_2)\cdot\mathbf{r}_2}, \tag{5.5.1}$$

$\mathbf{K}_1, \mathbf{K}_2 \in \mathcal{L}^{-1}$. This quantity has a direct physical interpretation in the case of bulk systems. Its imaginary part is directly proportional to the cross-section in the scattering experiments (for $\mathbf{K}_1 = \mathbf{K}_2$, Eq. 3.3.10).

Extracting the excitations energies from this expression is rather cumbersome when there are many non-equivalent atoms in the system or we work with a film geometry. In this case one can determine the *eigensystem* of $\chi^\pm$ and trace the frequency dependence of the corresponding eigenvalues, $\chi^\lambda(\mathbf{q}, z)$. For a fixed $\mathbf{q}$ an extremum of the imaginary part of an eigenvalue signifies strong absorption and thus a spin excitation. The eigenvector corresponding to this eigenvalue (for the resonant frequency) determine the shape of the resonant magnetic field.

When the susceptibility Dyson equation is solved on the imaginary axis one must perform the analytic continuation (AC) to extract the real time dynamics. It has been recognized that AC of data is an ill-posed numerical problem [82]. The input data (given for Matsubara frequencies) must be highly accurate. The maximum entropy method [83], widely used by quantum Monte Carlo community, is not of particular

advantage in our calculations, since it was primarily devised to deal with noisy data (uncorrelated errors). In our case the errors are expected to be strongly correlated, coming for example from the basis cut-offs.

In most cases we employ a rational function approximation [84, 85, 82], where a complex function $f(z)$ is represented by a ratio of two polynomials. The procedure works fine providing one imposes the exact asymptotic behavior of the interpolating function, namely

$$\lim_{z \to \infty} \chi_{ij}(z) z^2 = 1, \quad i, j = x, y, z. \tag{5.5.2}$$

Additionally, as discussed in Ref. [28], the coefficients of the rational expansion should be restricted so certain sum rules (Kramer-Kronig relations) are fulfilled.

Let us note that the asymptotic behavior of the susceptibility $\chi^{\pm}$ given in the circular coordinates is different; it is governed effectively (as discussed in Sec. 4.3) by a single pole. The behavior of a dominant eigenvalues $\chi^{\lambda}(\mathbf{q}, z)$ in the spin-wave region *close to the singularity* can be represented by a single pole function

$$\chi^{\lambda}(\mathbf{q}, z) \approx \frac{A^{\lambda}(\mathbf{q}) \mathfrak{e}^{\mathrm{i}\delta(\mathbf{q})}}{z - \omega_0^{\lambda}(\mathbf{q}) + \mathrm{i}\beta^{\lambda}(\mathbf{q})}. \tag{5.5.3}$$

$A\mathfrak{e}^{\mathrm{i}\delta}$ can be regarded as the amplitude, ω_0 as the frequency and β as the damping parameter (proportional to the inverse life-time) of the spin-wave[2]. These symbols are used consistently in the following chapters. Summing up, the susceptibility χ_{ij} is analytically continued using the rational approximation. In the next step one constructs $\chi^{\pm}$ and determines its behavior near the pole.

The rule of thumb for performing AC is to choose enough Matsubara frequencies ($n_{max} = 9 \div 15$) and the temperature such that all interesting feature on the real axis are within the range $\left[0, \omega_{n_{max}}^b\right]$.

5.6   Remarks on the development of the code

The KKR engine providing us with the Green's function is based on Hutsepot environment. The Hutsepot code is developed in Halle and it is a modern and computationally efficient implementation of the KKR method. Apart from the standard capabilities like full potential/full charge mode, possibility of the semi-relativistic calculations and Lloyd counting of states, it features several unique improvements, most important being self-interaction correction treatment of strongly correlated systems [43, 44]. The code is particularly well suited for computations of the properties of magnets, including spin dynamics. At present it features around 10^5 lines of Fortran95 code.

The part Susc, being an extension of Hutsepot, contains the implementation of linear response DFT as presented in this and preceeding chapters. The program has been developed since February 2006 and at the moment has around $22 \cdot 10^3$ lines of Fortran95 code.

Susc is parallelized using Message Passing Interface (MPI) [86, 87, 88], most importantly in the case of the Brillouin zone convolutions. Similarly constructing Y-Ch matrix elements can be spread over many processors. The large number of necessary $\mathbf{k}$-points makes the scaling almost linear up to the 64 processors (the largest number tested). The calculations of non-enhanced susceptibility for every $\mathbf{q}$-$\mathrm{i}\omega$ pair are essentially independent from each other and they can be run independently. This "by hand" mode of parallelization is proffered on machines with smaller or limited number of processors, since it saves the time for interprocessor communication.

The tracking of code version is facilitated using `cvs`. Build is supported by `make` and since the code consists of 1693 files the makefile is auto-generated. Some highly repetitive parts of the code (especially those designed for reading and writing configuration files) are auto-generated as well. This reduces greatly the development time and increases flexibility.

---

[2]We use symbol β also to denote the inverse temperature, but the distinction is always clear from the context.

5.7 Testing

During a development of a large computer code an attention must be paid to ensure that the code is error free. In our case it was done on two levels. First, single small pieces of code were tested. For example the part responsible for calculating overlap of basis function was tested against analytic expression generated using `Mathematica`. In the second stage the code was tested as a whole, using known analytic expressions for polarized free electron gas. This on one hand allows debugging and on the other establish the convergence properties.

For the purpose of the test we used polarized electron gas with paramagnetic Fermi energy $\epsilon_F \approx 0.112$ and half-splitting $\Delta = 0.04$. The chemical potential settles in this case to $\mu \approx 0.108$. BCC lattice with constant $a = 5.41$ was used. Test calculations were performed in slab geometry (2D) or for simple cubic lattice with two atoms mimicking BCC (3D). The temperature used was 400 K. The potential was set to be constant everywhere, different for every spin channel. Subsequently standard susceptibility calculations were performed, with $l = 2$ cut-off for the KKR Green's function. The results are presented below.
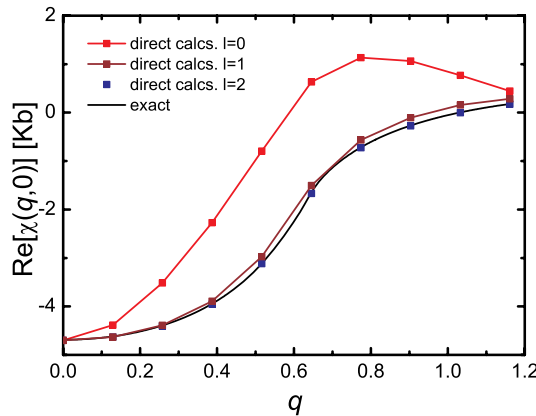

Figure 5.6: Non-interacting static susceptibility of polarized free electron gas computed starting from constant spin polarized potential using full standard calculation scheme. 8 Chebyshev polynomials were used. The l convergence to exact value can be clearly seen. Calculations were based on 2D geometry. It can be see that for larger **q** vectors a larger number of spherical harmonics must be used.

Figure 5.6 presents static susceptibility computed based on 2D geometry for different l cut-offs. We see that the increasing size of the basis brings the results closer to its exact value. Similar test (not shown) was performed in order to check Chebyshev polynomial convergence (8 polynomials was necessary in this case to provide convergence).

Figures 5.7ab present susceptibility computed for the first 6 lowest Bosonic frequencies, again based on 2D geometry. Once again an agreement (relative discrepancy smaller than 0.1%) between numerical and analytic result can be seen. The discrepancy arises from several sources: Green's function l cut-off, Y-Ch basis cut-off, **k** integration, energy integration and Sommerfeld expansion, ASA geometry, determination and approximation of screened structure constant. As we see all this approximation are controlled and the error can be made arbitrarily small. The computations of susceptibility based on our numerical scheme pertain to a finite temperature. We compare these results to the susceptibility of the free electron gas at 0 K, where the Fermi-Dirac function is approximated by a unit step. Such comparison is justified for temperatures small comparing to ϵ_F/k_B, as it is the case here.

Similar test was used to prove the correctness of the susceptibility Dyson equation engine. Please refer to the caption of Fig. 5.8 for details.
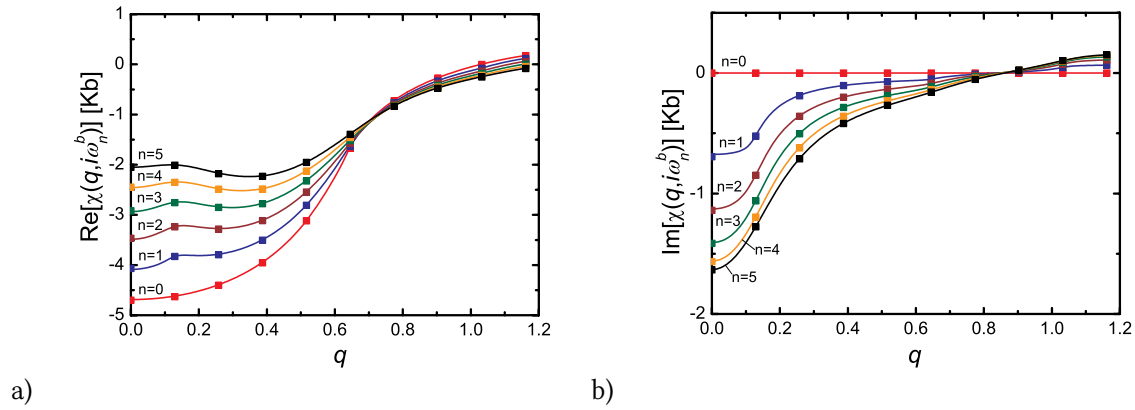
Figure 5.7: Real (a) and imaginary (b) part of non-interacting susceptibility of polarized free electron gas computed starting from constant spin polarized potential using full standard calculation scheme (scatter points) for different Bosonic frequencies n. 8 Chebyshev polynomials and $l = 2$ expansion for susceptibility were used. Exact values (lines) are provided for comparison.
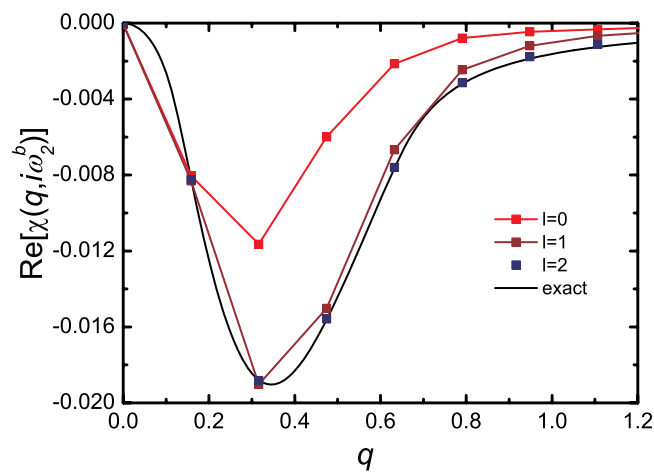

Figure 5.8: The enhanced susceptibility of polarized free electron gas computed using Y-Ch basis and susceptibility Dyson equation solver for 2nd Bosonic frequency. 8 Chebyshev polynomials were used. The l convergence to exact value can be clearly seen. The susceptibility is in Kb.

SPIN-WAVES IN BULK PHASES OF COBALT

Bulk cobalt has been chosen as the first application of our scheme for two major reasons. First, there exists a rather limited number of theoretical studies devoted to spin excitations in this system. Second, spin-waves in various phases of Co have been explored using inelastic neutron scattering; owing to the moderate damping of SWs and the complex unit cell of hcp Co, the latter material is the only known example, where for certain wave-vector $\mathbf{q}$ two spin-wave branches – acoustic and optical – have been observed. Therefore, despite simplicity of this well known system the study can yield new and non-trivial results, being partially a confirmation of the present method.

At the ambient pressure and low temperature cobalt is a ferromagnet featuring ε (hcp) structure [89]. As the temperature increases a transition to γ (fcc) structure occurs at around 750 K and above Curie temperature of around 1400 K the systems becomes paramagnetic. In this chapter we discuss the spin-wave spectrum of the both mentioned magnetically ordered phases.

6.1 ε(hcp)-Co

The experimental lattice constant of hcp cobalt was used, which reads $a_{\mathrm{hcp}} = 4.738$ Bh [90]. The real lattice is spanned on vectors (in units of a_{hcp}) $(0,1,0)$, $\left(\frac{\sqrt{3}}{2},\frac{1}{2},0\right)$ and $(0,0,\eta)$, where the $\eta \equiv c/a_{\mathrm{hcp}}$ ratio reads $2\sqrt{\frac{2}{3}}$ for perfect hcp structure, c being the lattice constant in the z- (or c-) direction. There are two atoms in the primitive cell at positions (again in units of a_{hcp}) $\left(\frac{1}{\sqrt{12}},\frac{1}{2},\frac{\eta}{4}\right)$ and $\left(\frac{1}{\sqrt{3}},0,\frac{3\eta}{4}\right)$. The reciprocal space is spanned on the following vectors (in units of $2\pi/a_{\mathrm{hcp}}$): $(1,0,0)$, $\left(\frac{1}{2},\frac{\sqrt{3}}{2},0\right)$ and $\left(0,0,\eta^{-1}\right)$. The calculated magnetic moment per Co atom is 1.61 μ_{B}.

The susceptibility matrix $\chi(\mathbf{r},\mathbf{r}',\mathbf{q},z)$ features two dominating eigenvalues for $\mathbf{q}$ in the first Brillouin zone. Their energy dependence close to maximum is analyzed using effective pole scheme, as discussed in Sec. 5.5. The eigenvalues can be interpreted as acoustic and optical SW branches. Figure 6.1ab presents respective parameters extracted from the present calculations. The eigenvalues for $q_z = \frac{\pi}{c}$ plane are degenerated within numerical error. Theoretical SW energies correspond very well to the experimental results along ΓM direction, but are larger along c-axis (ΓA) direction. For small momentum transfer the peak position can be very well described by the following experimental biquadratic *ansatz*

$$\omega_0(q) = Dq^2\bigl(1 - \gamma q^2\bigr). \tag{6.1.1}$$

Table 6.1 presents results of the fit for $q \leq 0.3\frac{2\pi}{a_{\mathrm{hcp}}}$ along different directions. D can be interpreted as an approximation to SW stiffness constant. Let us note that the dispersion relation for vanishing q in the basal plane is isotropic for hcp system. Our parameters D depend on the direction due to the limited adequacy of the biquadratic fitting function and numerical accuracy.
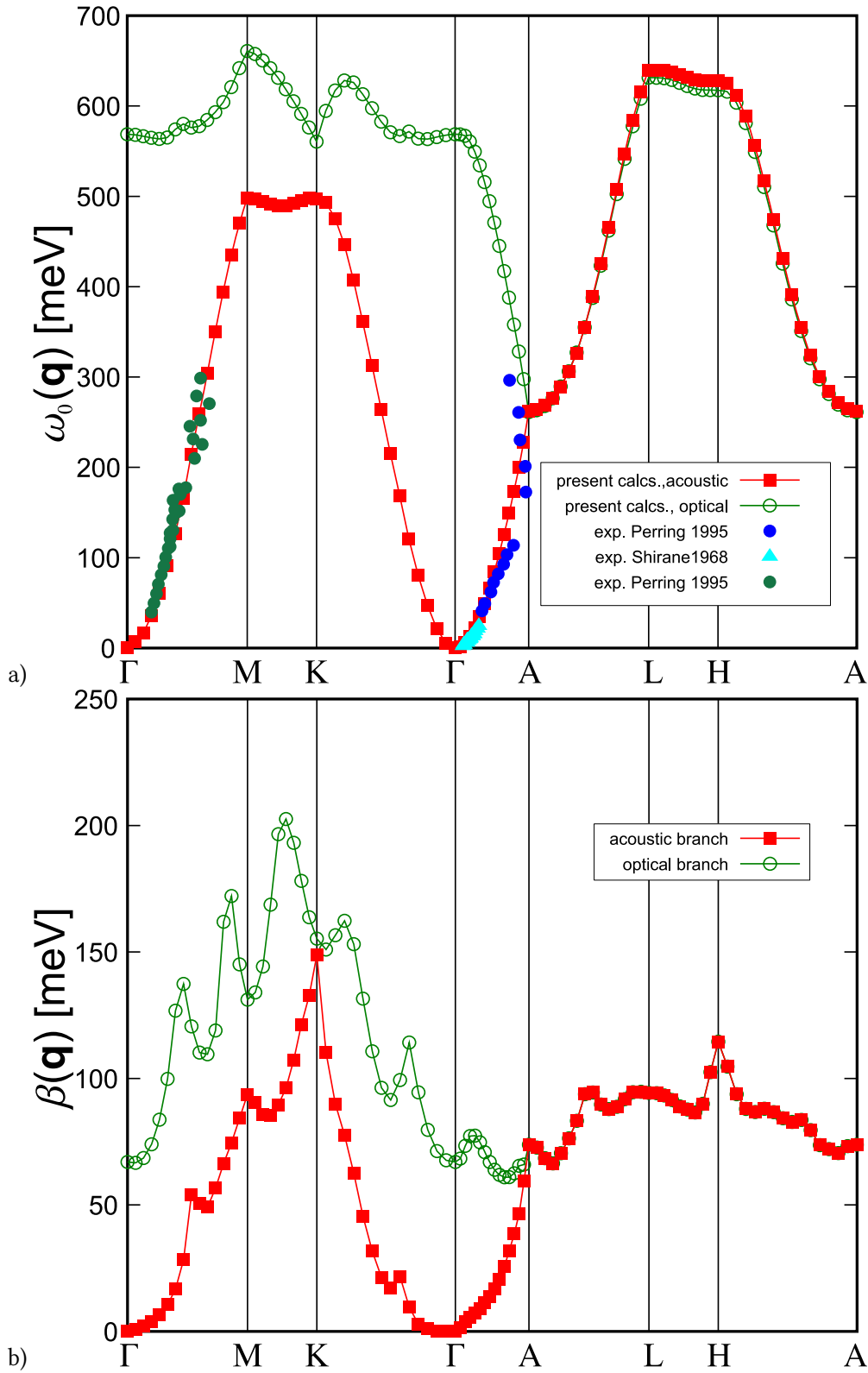
Figure 6.1: Energies (a) and half-widths at half maximum (b) of two SW peaks in hcp cobalt. High symmetry points in the first Brillouin zone are (in units of $2\pi/a_{\mathrm{hcp}}$) Γ $(0,0,0)$, M $\left(\frac{1}{2},0,0\right)$, K $\left(\frac{1}{2},\frac{1}{\sqrt{12}},0\right)$, A $\left(0,0,\frac{1}{2\eta}\right)$, L $\left(\frac{1}{2},0,\frac{1}{2\eta}\right)$ and H $\left(\frac{1}{2},\frac{1}{\sqrt{12}},\frac{1}{2\eta}\right)$. The experimental energies come from Refs. [91, 92].

direction	$D \left[\mathrm{Ry\,Bh}^2\right]$	$\gamma \left[\mathrm{Bh}^2\right]$
ΓM	0.14153(72)	0.952(12)
ΓK	0.1366(13)	0.937(12)
ΓA	0.13895(98)	1.147(54)

Table 6.1: Parameters of the biquadratic fit of Eq. 6.1.1 for different direction in Brillouin zone in hcp Co. To obtain the value of D in $\mathrm{meV\AA}^2$ it should be multiplied by 3809.981748(95) and the value of γ in $\mathrm{\AA}^2$ by 0.28002851809(38).

Perring *et al.* [92] managed to detect spin-waves for **q** beyond the first Brillouin zone along (00ξ) direction, thus accessing the optical SW branch of ΓA segment. One sees therefore that the optical SW modes are indeed a physical reality, even if the present calculations overestimate somewhat the energy of the mode. It is a rare example, in fact the only one, where an optical SW mode was experimentally detected. Nickel is sometimes said to exhibit an optical SW branch, but there the effect originates from complex energy dependence of the susceptibility; in some limited range of wave-vectors SW peak of Ni is of a complex double-maximum form. The situation in hcp Co is different, as the two branches – up to the degeneracy – are expected to exist in the whole Brillouin zone. The acoustic mode corresponds to the moments oscillating in phase and optical to the anti-phase case. Clearly, this cannot be the case in Ni, since it features only one non-equivalent atom in its primitive cell.

The damping of SWs is moderate in the case of Co. Long wave-length acoustic magnons are, as expected, long-living. Decay of SW asserts itself for larger q's. Optical branch is of much shorter life-time because of much higher Stoner states density expected at higher energies. Characteristic peaks in $\beta(\mathbf{q})$ function correspond to peaks in the density of Stoner states.

Theoretical works on spin excitations in hcp cobalt utilize empirical tight binding scheme [93, 94]. They predict correctly the energies of acoustic modes, yielding however much too low values of optical modes, in fact in a range where they were not detected despite being experimentally observable. Except for ΓA segment the optical branch energies predicted in this study lie above 0.5 eV, the maximal energy addressed in the calculations mentioned and one guesses that certain complex structure of SW spectrum was erroneously identified as the optical mode.

6.2 γ(fcc)-Co

Face centered cubic direct lattice is spanned on vectors (in units of a_{fcc}) $\left(\frac{1}{2}, \frac{1}{2}, 0\right)$, $\left(\frac{1}{2}, 0, \frac{1}{2}\right)$ and $\left(0, \frac{1}{2}, \frac{1}{2}\right)$, while the reciprocal lattice on vectors (in units of $2\pi/a_{\mathrm{fcc}}$) $(1, 1, -1)$, $(1, -1, 1)$ and $(-1, 1, 1)$. There is only one Co atom in the primitive cell. The lattice constant was determined from the condition of equal atomic volumes for hcp and fcc systems, yielding $a_{\mathrm{fcc}} = 8^{1/6}a_{\mathrm{hcp}}$. Ground state magnetic moment is very close to the one obtained for hcp phase.

Due to one non-equivalent atom in the unit cell the spectrum features only one large eigenvalue, the parameters of which are presented in figure 6.2. Comparing to the adiabatic study of ref. [95] high wave-vectors magnons are a bit more energetic in the present calculations, but the shift may be due to SW self-energy arising from including hybridization with Stoner states. Characteristic kink-like feature along ΓK is present in both approaches. D and γ parameters of Eq. 6.1.1 are gathered in Table 6.2; parameter D is significantly smaller (average value $D = 492 \mathrm{\ meV\AA}^2$) than the isotropic stiffness constant of the reference mentioned. Similarly to hcp case the damping is not very much pronounced.

Inelastic neutron scattering experiments revealed clearly softer magnons, characterized by $D = 369 \mathrm{\ meV\AA}^2$ (ref. [96], simple quadratic fit) and $D = 384 \mathrm{\ meV\AA}^2$ and $\gamma = 3.13 \mathrm{\ \AA}^2$ (ref. [97]). One notes the pronounced deviation from quadratic dispersion law in the latter study. As it has been mentioned γ-Co does not occur in nature in 0 K, our calculations therefore pertain to a somewhat fictitious material. In general the temperature influences the SW spectrum, but owing to the large Curie tempera-
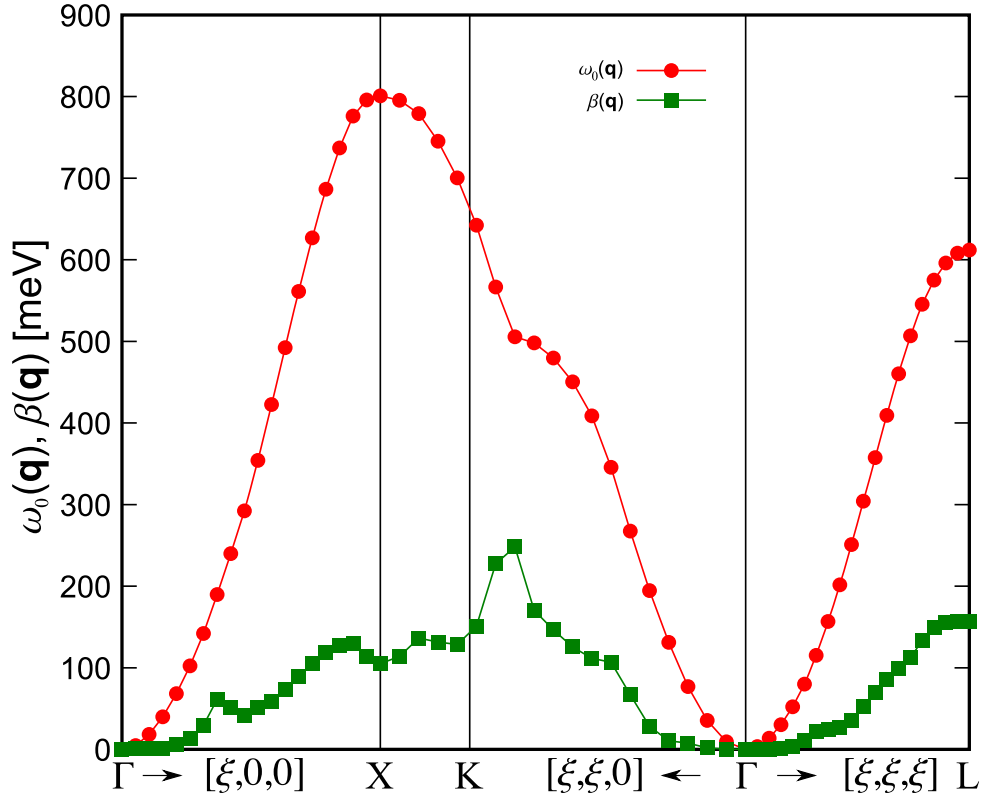
Figure 6.2: Spin wave mode of fcc Co. High symmetry points in the first Brillouin zone are (in units of $2\pi/a_{\text{fcc}}$) Γ $(0,0,0)$, X $(1,0,0)$ equivalent to $(1,1,0)$, K $\left(\frac{3}{4},\frac{3}{4},0\right)$ and L $\left(\frac{1}{2},\frac{1}{2},\frac{1}{2}\right)$.

direction	D $\left[\text{Ry Bh}^2\right]$	γ $\left[\text{Bh}^2\right]$
ΓX	0.1205(12)	0.423(27)
ΓK	0.1326(12)	0.871(28)
ΓL	0.13419(65)	0.513(25)

Table 6.2: Parameters of the biquadratic fit of Eq. 6.1.1 for different direction in Brillouin zone in fcc Co.

ture of cobalt the room temperature of experiment is not expected to be of a great importance. There is however an important factor making any direct comparison difficult; Co must be alloyed with about 6% of Fe for the sake of stability. It seems that future calculations must take the effect into account. Additionally there is no information available about the actual lattice constant influenced, among others, by temperature and composition. Interestingly, the results of SPEELS of thin fcc Co film [5] match rather well the neutron scattering data mentioned above.

SPIN DYNAMICS OF SELECTED HEUSLER PHASES

Cubic phases of general composition XYZ and X_2YZ, where X and Y stand for d- or f-electron transition metals and Z denotes a p-electron element, attract much attention ever since they were first considered by Heusler in 1903 [98], due to their remarkable magnetic and electrical transport properties [99, 100]. Both structures can be described as four interpenetrating fcc lattices, characterized by positions X $(0, 0, 0)$, Y $\left(\frac{1}{4}, \frac{1}{4}, \frac{1}{4}\right)$, X or void $\left(\frac{1}{2}, \frac{1}{2}, \frac{1}{2}\right)$ and Z $\left(\frac{3}{4}, \frac{3}{4}, \frac{3}{4}\right)$.

Full Heusler phases (Cu_2MnAl or $L2_1$ type, space group $Fm\bar{3}m$) usually show metal like conductivity. Within the series several superconductors were discovered, most spectacular being $ErPd_2$Sn [101] and Pd_2YbSn [102], where superconducting state was found to coexist with long-range magnetic ordering. Equiatomic (or semi-Heusler) compounds crystallize with the MgAgAs type of structure ($C1_b$, space group $F\bar{4}3m$) and feature wide variety of interesting properties as well, including heavy fermion state [103, 104, 105, 106], shape memory effect [107], giant magnetoresistance [108, 109] and semimetallic and semiconducting behavior [110]. The vacant site causes smaller overlap between 3d wave functions in these materials and may lead to even more localized magnetism and narrower bands than in full Heusler phases [111].

In 1983 de Groot *et al.* [112] predicted NiMnSb to be *half-metallic ferromagnet*. In this class of materials the minority spin electrons are semiconducting while the majority spin electrons feature metallic behavior. As a consequence such materials have integer magnetic moment (slight deviations may occur due to polarization of inner filled shells or off-stoichiometry [111]) and feature full polarization of electrons at the Fermi level at 0 K. Many full-Heusler compounds were predicted to be half-metallic, too, e.g. Co_2MnZ (Z=Si,Ge) [113, 114]. Materials for which half-metalicity could be combined with high Curie temperature are attractive for applications in the field of spintronics [115], therefore considerable attention was paid to the description of magnetic properties of these materials [116, 117, 118, 119, 120, 121, 122, 123, 124]. There exists both theoretical and experimental evidence that Heusler phases are promising systems also in this respect.

There are three relevant energy gaps in a half-metal, see fig. 7.1. The effective band splitting 2Δ determines the position of long-wavelength Stoner states. The half-metallic gap γ is the difference in energy between the bottom of the conduction band and the top of the valence band in the minority spin channel. Finally, the distance between Fermi level and the bottom of the conduction band in the minority channel determine the activation energy δ for the Stoner excitations ("Stoner gap"). The electronic structure implies that the total magnetic moment of a half-metal is an integer.

In the semi-Heusler phases "[t]he [semi-metallic] gap basically arises from the covalent hybridization between the lower-energy d states of the high-valent transition metal (TM) atom [e.g. Ni] [...] and the higher-energy d states of the lower-valent TM atom [e.g. Mn], leading to the formation of bonding and anti-bonding bands with a gap in between." (Citation from Ref. [126].) Somewhat more complex is the origin of the gap in the full Heusler alloys, since it involves, according to Ref. [127], hybridization of states between three atoms (Co-Co-Mn in the case of Co_2MnSi). The Fermi level must of course be located in
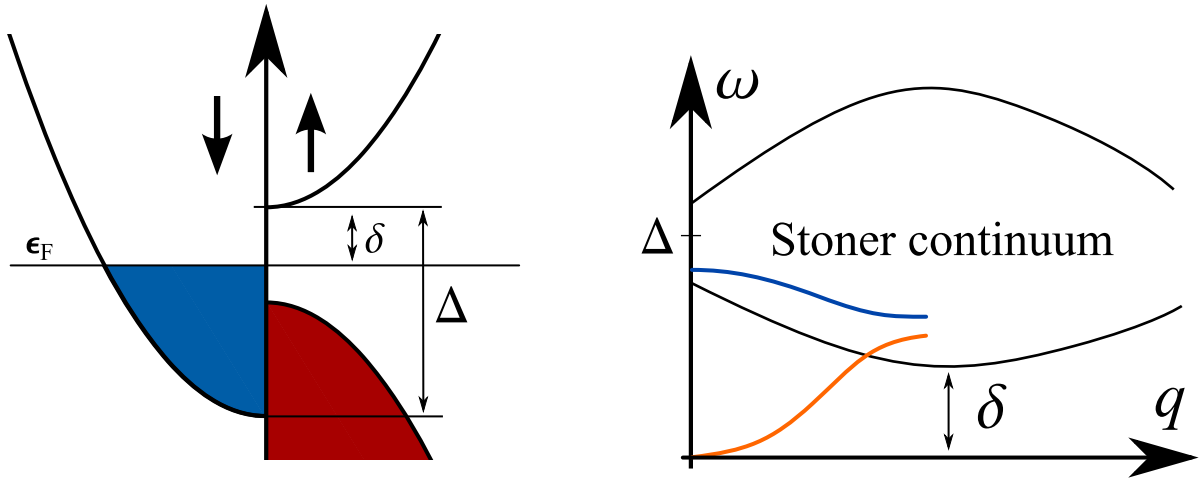
Figure 7.1: (a) The energy gaps in a half-metal relevant for spin dynamics. Please refer to the text for discussion. (b) The general structure of magnetic excitations. Somewhat modified, the figure comes from Ref. [125].

the gap for the half-metalicity to appear. Kübler *et al.* have shown that magnetism in full Heusler phases is of localized character, which follows from the exclusion of minority spin electrons from Mn 3d shell [122].

Heusler alloys are also very interesting from the point of view of spin dynamics. The existence of the Stoner gap δ allows for a existence of SW branches undamped in the whole BZ. The coexistence of damped and infinitely-long living SWs modes is possible. Due to the complex unit cell multiple SW branches can be observed. In what follows, we concentrate on three exemplary systems. First, NiMnSb is considered, since this material proved to be a quite difficult one to be studied through HH mapping. In subsequent section we compare and contrast its behavior to Co$_2$MnSi with its rich zoo of SWs modes. The spectrum of another Heusler phase (Cu$_2$MnAl) is also determined and compared to experiment.

7.1   NiMnSb

7.1.1   General properties

The structure of the unit cell was confirmed by Helmholdt and coworkers [128]. The experimental lattice constant obtained by them reads $a = 11.174$ Bh and it is used in this calculations. The reference states also that "it is rather unlikely that there is much site interchange of the atoms in the atomically ordered structure of NiMnSb". In units of a the atomic positions read: Ni $(0, 0, 0)$, Mn $\left(\frac{1}{4}, \frac{1}{4}, \frac{1}{4}\right)$, empty sphere $\left(\frac{1}{2}, \frac{1}{2}, \frac{1}{2}\right)$ and Sb $\left(\frac{3}{4}, \frac{3}{4}, \frac{3}{4}\right)$.

The average band magnetic splitting is large (2 eV) at low temperatures [125]. LDA calculation predict half-metallic gap to be around 0.4 eV, which is in a good agreement with experiment [129]. The gap is indirect. The Stoner gap has been estimated to be 163 meV.

Kübler [130] estimated the Curie temperature of the system be 601 K or 701 K depending on the approach used. Şaşıoğlu *et al.* [117] have found T_C between 880 K and 1112 K depending on the method applied and assumptions regarding interactions between moments. Experimentally T_C around 730 K was established [111].

The total magnetic moment at 2 K is an integer equal to $4\mu_B$ ($m_{0Mn} = 3.8\mu_B$, $m_{0Ni} = 0.2\mu_B$, [131]), as expected for a half-metal. LDA produces values of $m_{0Mn} = 3.74\mu_B$ and $m_{0Ni} = 0.26\mu_B$. A weak magneto-crystalline anisotropy favors $\langle 110 \rangle$ axes and no change in the easy axis can be detected up to
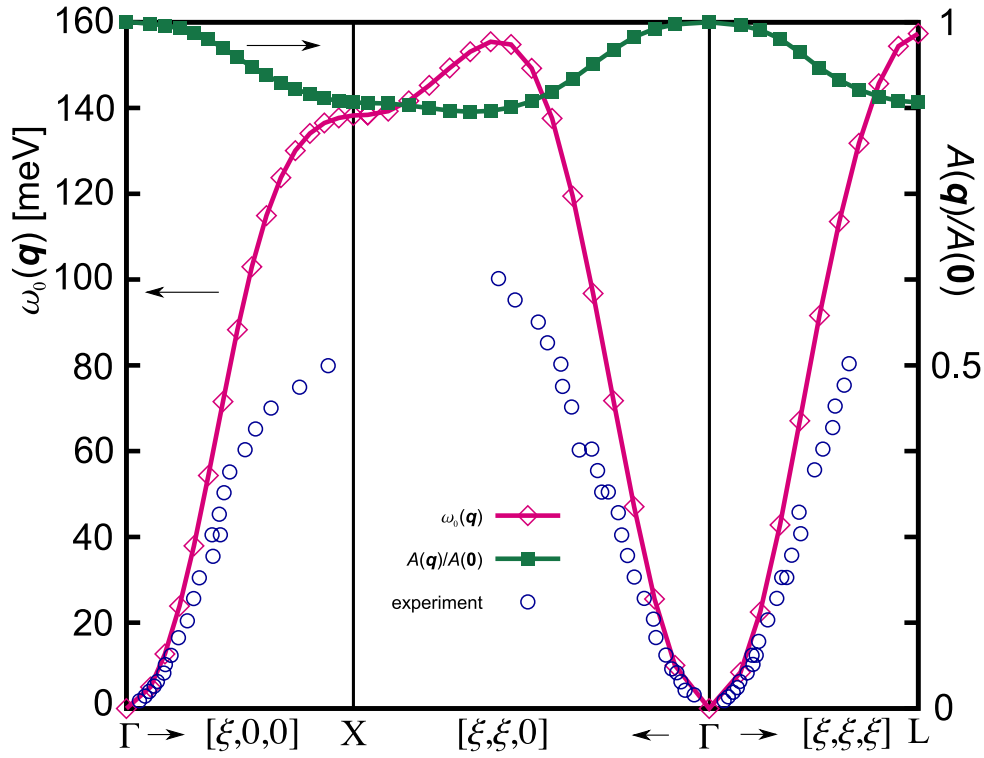
Figure 7.2: The tranverse susceptibility of NiMSb in the magnon energy range. The magnon energy $\omega_0(\mathbf{q})$ is compared to the experiment from ref. [133].

120 K, where the anisotropy becomes negligible. NiMnSb does not obey Curie-Weiss law above T_C, having significant upward curvature.

Magnetic and transport properties of NiMnSb were thoroughly studied experimentally [132, 133, 111, 125]. At low temperatures the material was confirmed to be half-metal. With the increasing temperature cross-over to a normal ferromagnet is believed to occur near 80 K, but this statement is disputable. Strictly speaking, half-metalicity is lost at any finite temperature, the relevant question being of the density of states in the minority channel. DFT predicts half-metalicity at 0 K. The study of Ležaić *et al.* revealed a collapse of Fermi level polarization at elevated temperatures [134]. At finite temperatures many body effects are believed to influence electronic structure; e.g. in Ref. [135] a presence of non-quasiparticles states (a superpositions of spin-up electron excitations and virtual magnons) in the gap near the Fermi level was predicted.

7.1.2 Transverse magnetization dynamics

The transverse susceptibility matrix $\chi^+(\mathbf{r}, \mathbf{r}', \mathbf{q}, z)$ of NiMnSb has one dominating eigenvalue in the magnon energy range. It is singular and the behavior near the singularity is analyzed using the single pole scheme of Sec. 5.5. Magnon energy and amplitude are presented in Fig. 7.2. The maximum magnon energy along the directions considered is 155 meV around K point in BZ. The imaginary part of the pole, β, is zero within the numerical noise. Magnon states happen to appear for this material in the Stoner gap δ, which explains why they do not decay into Stoner excitations. The strength of the pole, $A(\mathbf{q})$, varies weakly with $\mathbf{q}$. According to Goldstone theorem for $\mathbf{q} = \mathbf{0}$ all the spectral strength of the enhanced susceptibility is contained in the SW pole. The variation of $A(\mathbf{q})$ can be interpreted as the transfer of the spectral power between SW and Stoner states, signifying that the contribution of the latter is small. Stoner states have negligible density below 270 meV, even though their presence for lower energies is not forbidden by the value of δ.

The theoretical magnon energies are larger than those extracted from neutron scattering experiments [133]. The discrepancy can be partially attributed to the elevated temperature 300 K of the experiment. According to Ref. [111] the spin-wave stiffness decreases from 320 ± 20 meVÅ^2 at 25 K to 280 ± 20 meVÅ^2 for 300 K. The agreement with experiment can therefore be regarded as satisfactory.

The measurements have shown that the SW states acquire a finite life time for energy transfers larger than 60 meV; between points K and X, where the most energetic magnons are expected, no SW's were found whatsoever. This effect originates from the the finite temperature of the experiment as well. As it has been discussed, away from absolute zero there are necessarily electronic states appearing in the half-metallic gap, which in turn close the Stoner gap δ and allow the decay to the low lying Stoner states, absent at 0 K. Interestingly, the temperature of 300 K corresponds to the onset of the polarization collapse predicted by Ležaić.

A really striking feature of the spectrum is the presence of only one SW branch. A brute-force mapping of NiMnSb system onto a Heisenberg model would result in two branches corresponding to the two magnetic atoms in the primitive cell. The branches would be separated by a gap, a feature unobserved experimentally. It has been already recognized [136] that the Ni moment, being induced by the d-d hybridization with neighboring Mn atoms, should not be regarded as an independent degree of freedom. The present calculation naturally grasps this peculiar aspect of the spin dynamics in the systems with induced magnetic moments.

The susceptibility matrix has infinitely many eigenvalues, but one shall not expect that there should be infinitely many SW branches. Strong intra-atomic exchange implies a great stiffness of atomic magnetic moments; they behave as rigid entities, which results in the wide applicability of adiabatic spin dynamics based on the Heisenberg Hamiltonian mapping. Somewhat pictorially the situation can be compared to the system of coupled harmonic oscillators, let us carry on with two for the sake of simplicity. Each mass is attached to a spring and they are coupled with a third one of strength K. As long as K is finite the systems features two eigenmodes and two eigenfrequencies. When K becomes large comparing to the other two elastic constants – two masses become effectively connected by a rod – the system looses one of its eigenvalues and behaves as a single mass on a spring.
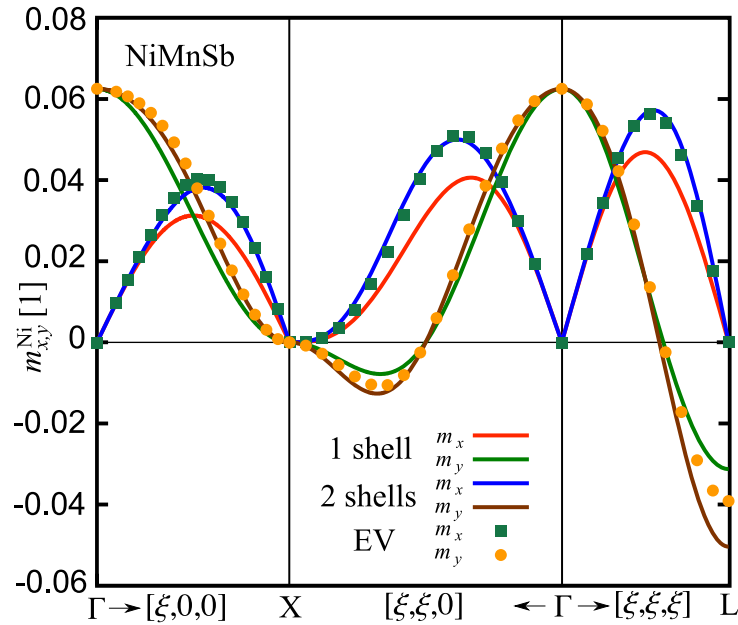

Figure 7.3: The deviation of the Ni moment in NiMnSb follows roughly the molecular field of Mn. A good fit can already be obtained taking into account only two nearest neighbor shells in equation 7.1.1, with ratio $w_2/w_1 = -0.0781$. The inclusion of the second shell visibly improves the fit.

Due to the induced character of Ni moments NiMnSb looses one more degree of freedom; the Ni sublattice is unable to support an optical SW branch. Upon analyzing the shape of the eigenvector $\varpi_0(\mathbf{r}, \mathbf{q}, \omega_0 + \mathrm{i}0^+)$ of $\chi^+(\mathbf{r}, \mathbf{r}', \mathbf{q}, \omega_0 + \mathrm{i}0^+)$ corresponding to the leading eigenvalue, we see that the dynamics of this system is dominated by the Mn sublattice. Figure 7.3 presents the transverse deviation of magnetization associated with ϖ_0 integrated over Ni atomic sphere. ϖ_0 has been normalized such that the deviation integrated over Mn sphere centered at $\mathbf{r}_0 = (1, 1, 1)a/4$ was $(1, 0)$. The induced transverse Ni moment $m_{x,y}^{\mathrm{Ni}}$ tends to align itself along the molecular field originating from Mn sublattice

$$m_x^{\mathrm{Ni}} + \mathrm{i}m_y^{\mathrm{Ni}} = \frac{m_{0\mathrm{Ni}}}{m_{0\mathrm{Mn}}} \frac{1}{\sum_s n_s w_s} \mathfrak{e}^{-\mathrm{i}\mathbf{q}\cdot\mathbf{r}_0} \sum_s w_s \sum_{l=1}^{n_s} \mathfrak{e}^{\mathrm{i}\mathbf{q}\cdot\mathbf{r}_{ls}}, \tag{7.1.1}$$

where s labels the shells of Mn atoms surrounding Ni atom located at $\mathbf{r} = \mathbf{0}$. w_s are coupling constants between Ni and Mn atoms and n_s stands for the number of Mn atoms on the given shell. $\mathbf{r}_{ls}$ are the positions of the Mn atoms. (First three shells are in the distance $\sqrt{3}a/4$, $\sqrt{11}a/4$ and $\sqrt{19}a/4$, having multiplicity 4, 12 and 12, respectively.) Such behavior is expected since Ni atoms are almost completely magnetically decoupled and it is characteristic for acoustic SW modes, in which the most stiff sublattice dominates and other try to accommodate to its dynamics; we will see it on the example of Co_2MnSi. What distinguishes these two materials is the ability of the secondary magnetic sublattice to support optical SWs.

The analysis favors the so called SF1 scenario of Ref. [136]. A similar picture of the dynamics of the induced sublattice entirely driven by the primary one has been suggested by Mrasov in the case of FePt and FeRh [137, 138]. In the latter case the role of the softer sublattice is to alter the effective interaction of the stiffer sublattice. In the case of NiMnSb this might concern only the small transverse fluctuations; as suggested by Ležaić *et al.* [134] the length of Ni moment should be treated as a separate degree of freedom.

shell	no. of atoms	distance	$Jm_{0\mathrm{Mn}}^2$ [Ry] Mn-Mn, 4 n.n. shells	$Jm_{0\mathrm{Mn}}^2$ [Ry] Ref. [20]
1	12	$a/\sqrt{2}$	0.550	0.532
2	6	a	0.473	0.356
3	24	$a\sqrt{3/2}$	0.023	0.033
4	12	$a\sqrt{2}$	-0.056	0.027

Table 7.1: Effective exchange integrals for a simple fcc lattice of NiMnSb. A reasonable fit can be obtained assuming that only Mn sublattice contributes to the dynamics and the exchange interaction is limited to the four nearest neighbor shells. The results are compared to the Mn-Mn exchange integrals obtained from magnetic force theorem of ref. [20].

Since there is *effectively* only one magnetic atom per cell in NiMnSb it is easy to extract the corresponding coupling constants by fitting the dispersion relation using adiabatic spin dynamics. The results are summarized in Table 7.1, please refer to the caption for further details. Let us remark that the values should be taken with a grain of salt. To perform reliably the necessary back Fourier transformation one should have in disposition more $\mathbf{q}$ points in the whole Brillouin zone. The analysis was included to show that when necessary the results of the susceptibility calculations can be mapped onto classical Heisenberg Hamiltonian.

7.2 Co_2MnSi

Recently the ternary Heusler phase Co_2MnSi attracts much attention, since it is the technologically most promising half-metal, featuring large half-metallic gap ($\gamma = 0.419$ eV [114]) and the highest known Curie temperature among Heusler alloys (exp. 985 K [139], theory 740 K-857 K [117]). It can be grown in the form of thin films [140] thus offering a possibility of constructing real spintronic devices.
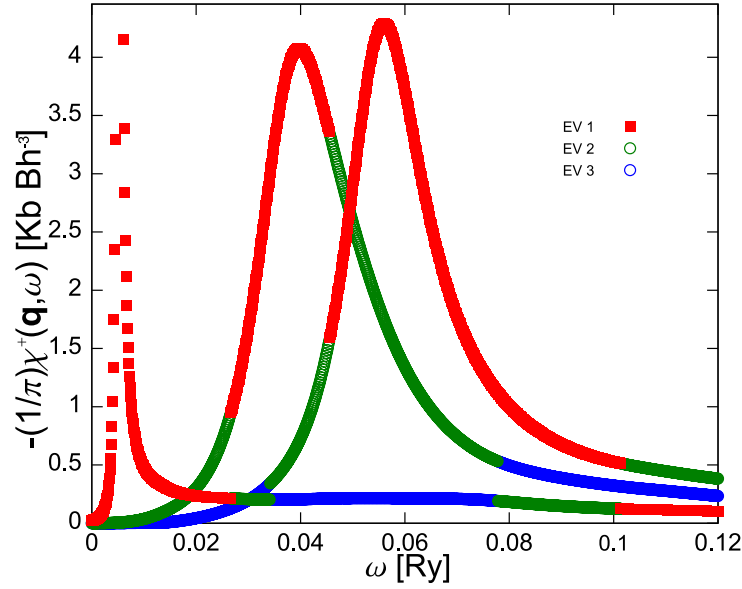
Figure 7.4: Imaginary parts of three dominant eigenvalues of Co$_2$MnSi for $\mathbf{q}_0 = 0.28(1,1,0)\frac{2\pi}{a}$ as a function of frequency. Other eigenvalues are of negligible magnitude. Only in this figure the eigenvalues are labeled according to its absolute value, 1 corresponds to the largest one. The apparent width of the acoustic (the least energetic) mode is a result of artificial broadening $0^+ = 10^{-6}$ Ry, the mode has vanishing width.

The lattice constant of this material reads 10.677 Bh [139]. There are three magnetic atoms in the unit cell. Two Co atoms at positions $\left(\frac{1}{4}, \frac{1}{4}, \frac{1}{4}\right) a$ and $\left(\frac{3}{4}, \frac{3}{4}, \frac{3}{4}\right) a$ are equivalent and carry a magnetic moment of 1.0 μ_B. Mn atom at $\left(\frac{1}{2}, \frac{1}{2}, \frac{1}{2}\right) a$ has a moment of 3.0 μ_B. The moment of Si atom at $\left(\frac{1}{2}, \frac{1}{2}, \frac{1}{2}\right) a$ is negligible.

All moments in the unit cell are autonomous in the sense they come from the on-site exchange interaction. This fact is reflected in the spectrum of the spin-wave excitations. In the low energy regime the susceptibility matrix features *three* dominant eigenvalues, other being of insignificant magnitude. They are well defined SW peaks. An example of spectral function for $\mathbf{q}_0 = 0.28(1,1,0)\frac{2\pi}{a}$ is presented in the Fig. 7.4. The situation should be compared to the NiMnSb system studied in the previous section, where despite the presence of two non-equivalent magnetic atoms only one SW branch exists.

The acoustic magnons are separated from two optical branches by a gap of almost 350 meV, cf. Fig. 7.5. The maximum energy in the acoustic branch is slightly less than 200 meV. According to author's knowledge, magnons in Co$_2$MnSi have not been studied experimentally.

Similarly to the case of NiMnSb the dynamics of the acoustic mode is determined by the Mn sublattice, the deviation of Co moments decreases for increasing momentum transfer. One of the optical modes resembles the acoustic one with Co moments being in the antiphase to Mn moment. The second optical mode involves Co moments only – the Mn stays parallel to the GS magnetization direction. An example of these modes can be found in Fig. 7.6.

The calculations of Isida *et al.* [114] predict the γ gap to be 0.419 eV; the present KKR calculations give considerably lower value of around 0.2 eV. Both approaches place the Fermi level close to the top of the gap, resulting in the Stoner gap of $\delta \approx 55$ meV. Despite being more energetic, the acoustic SWs are not significantly broadened, their width is smaller than 5 meV. One must note that the δ gap represents only the lower bound for the Stoner states' energy. For particular $\mathbf{q}$ they may appear at much higher energies. In the contrary to the acoustic mode the two optical branches are for every vector $\mathbf{q}$ immersed in a dense Stoner continuum and are strongly broadened, cf. Fig. 7.7. Again the behavior close to the center of the peak was modeled using the single pole scheme.
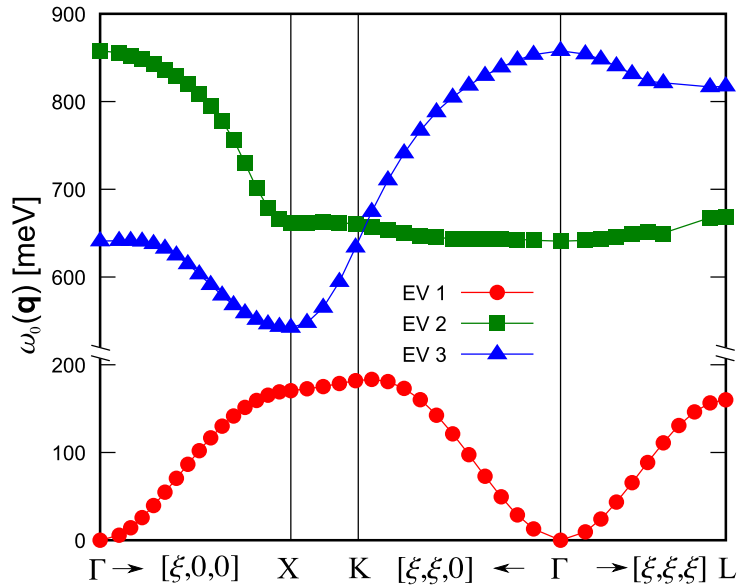
Figure 7.5: Positions of 3 SW peaks of Co_2MnSi. The enumeration of eigenvalues was introduced to make correspondence between the energies and peaks' with from Fig. 7.7 and does not imply any symmetry properties of them. Note that the optical branches are separated by a significant gap.

It is not very likely that the optical modes could be experimentally detected in typical neutron scattering experiments. First of all they very energetic and of substantial width. Second, long wave-length neutrons are unable to probe them. Figure 7.8 presents the imaginary part of Fourier transformed susceptibility for $\mathbf{q}_0 + \mathbf{K}$, where $\mathbf{K} \in \mathcal{L}^{-1}$. While the acoustic peak is present (with different intensity) for every $\mathbf{K}$, the optical branches could be resolved only for extremely large momentum transfers.

7.3 Cu_2MnAl

Cu_2MnAl is a normal ferromagnet of relatively high Curie temperature 630 K. It has been a subject to inelastic neutron scattering study [141], its structure, lattice constant and magnetic properties were also investigated [142, 143]. Earlier theoretical studies of spin dynamics were based either on semiempirical models or adiabatic approximation [144, 145, 146].

Figure 7.9 presents results based on susceptibility calculations compared to experiment and adiabatic studies. Only one SW branch is present. LDA predicts correctly the energies along $[\xi, 0, 0]$ direction. Small renormalization of adiabatic energies is observed due to the self-energy arising from the hybridization with Stoner continuum; the correction brings the results closer to the experimental values. There exists rather serious discrepancy along $[\xi, \xi, 0]$ direction; both adiabatic and dynamic approach yield similar results. A deeper understanding of the discrepancy will be subject to a further study. The line-width is small and increases monotonically with q.

7.4 Summary

Not all Heusler are alloys are half-metallic, but the general tendency to hybridization, outlined in the introduction of this chapter, implies a small density of low-energetic Stoner states resulting in long-living acoustic SW mode. In the case of half-metals featuring a Stoner gap δ these states can live infinitely long. On the contrary the high energetic optical modes appearing as a consequence of the presence of two or more non-equivalent magnetic atoms in the unit cell are rather strongly damped due to the hybridization with high density Stoner continuum. The situation is completely different from the one encountered in
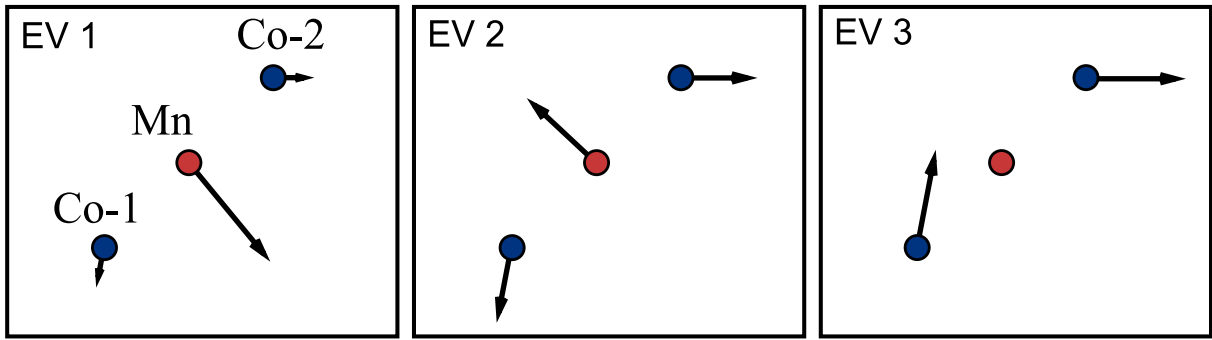
Figure 7.6: The shape of three eigenvectors of Co_2MnSi for $\mathbf{q}_0 = 0.28(1, 1, 0)\frac{2\pi}{a}$. The eigenvectors of the acoustic branch (EV 1, 5.4 mRy peak of figure 7.4) have typical shape where moments deviate roughly like $e^{i\mathbf{q}_0 \cdot \mathbf{r}_i}$; for larger momentum transfers the Co moments' contribution decreases and vanish for high symmetry points like X (they stay parallel to the GS magnetization direction). One of the optical branches (EV 2, 39 mRy) can be regarded as a counterpart to it – Co moments oscillate in the antiphase with respect to Mn moments. The third mode involves Co moments only (EV 3, 56 mRy). Eigenvectors are normalized such that the biggest deviation (Mn moment for EV 1 & 2) is (1,0).

simple metallic ferromagnets. Particularly in Fe the Stoner states have pronounced density even for small energies, leading to a severe damping of SW.
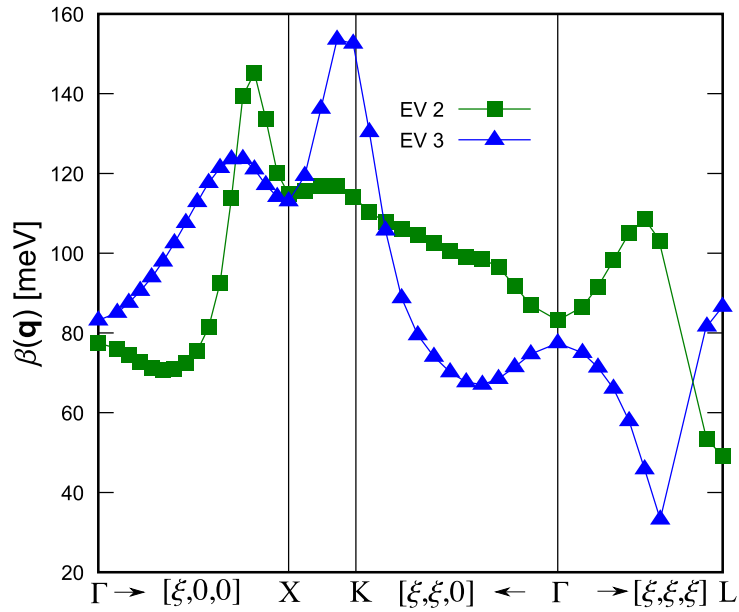
Figure 7.7: Half-width at half maximum ($\beta(\mathbf{q})$) for two optical branches of Co$_2$MnSi. The width of the acoustic mode is smaller than around 5 meV.
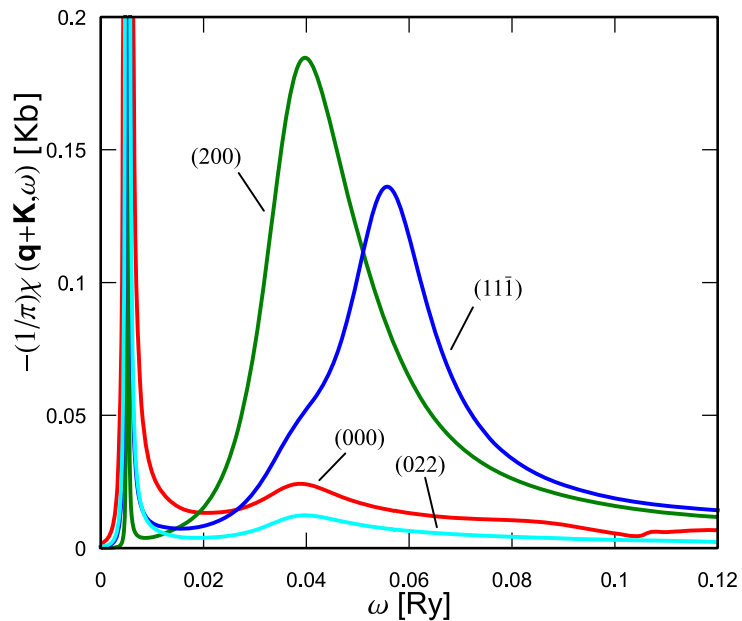

Figure 7.8: The imaginary part of Fourier transformed susceptibility of Co$_2$MnSi for $\mathbf{q}_0 = 0.28(1,1,0)\frac{2\pi}{a} + \mathbf{K}$. The triples of numbers represent $\mathbf{K}$ in units of $2\pi/a$. Different optical branches can be resolved only well outside the 1st BZ, while the optical peak is always present.
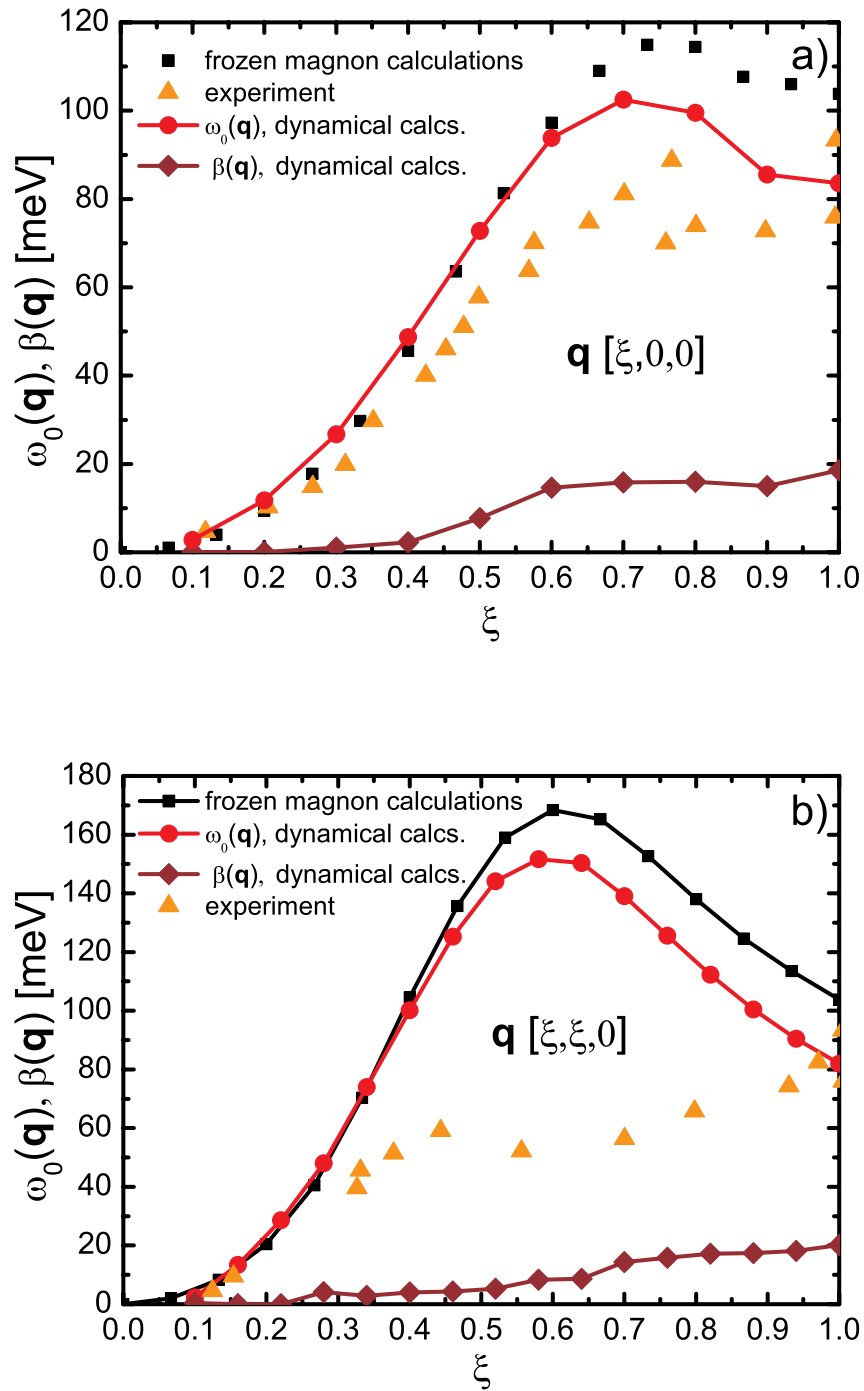
Figure 7.9: SW peak of Cu$_2$MnAl extracted from dynamic calculation compared to adiabatic treatment and experiment [141].

MAGNONS IN BULK IRON AND ITS THIN FILMS

The stable bulk phase of iron at ambient conditions is bcc and the system is often regarded a prototypical ferromagnet [17]. Density functional theory with local density approximation can predict very accurately its magnetic moment but overestimates the binding energy. The appearance of magnetism has a quantitative impact, e.g. if one restricts the bulk iron to be paramagnetic the hcp becomes the most stable phase. Many body effects may play a role in iron [147].

Modern techniques allow growing of high quality iron nanostructures. In particular, the adsorption of Fe on (110) tungsten surface has been for nearly two decades one of the most intensively studied model systems due to its mechanical and structural properties [148, 149, 150, 151] inter-playing with interesting magnetic behavior, including spin reorientation [152, 153], out-of-plane anisotropy for certain conditions [154], magnetic frustration [155] and unusual domain wall pinning [156].

Similarly involved is the spin dynamics of iron based systems. Magnetic interactions of the bcc phase feature "so-called Kohn anomalies [. . .] that are due to long-range [magnetic] interactions mediated by the RKKY interactions" as reported in Ref. [95]. The latter study is based on adiabatic treatment, formally exact in the limit of the long wave-length regime, and provides magnificent account for spin-wave stiffness, encouraging the use of ALDA. The mapping to Heisenberg Hamiltonian overlooks of course the damping of spin-waves, which proves to be severe in this material for larger frequencies, but as we will see, the dynamic treatment advertised throughout the thesis can account for the latter effect.

One does not expect the situation to be less complicated in the case of thin iron films. It was predicted that the breaking of translational symmetry in nanostructures should lead to the renormalization and enhanced damping [30] of the spin-wave states. Therefore for these systems the use of a dynamical approach is essential. Up to now the study of the dynamic magnetic susceptibility of magnetic thin films was based on the use of model Hamiltonians [30] and it is necessary to extend the LRDFT studies of magnetic excitations to the film geometry. Although the model Hamiltonian studies provide important information on general relation between parameters of the Hamiltonian and calculated observables, the self-consistent DFT calculations are inevitable for the realistic description of complex systems since the excitations depend sensitively on the detailed properties of the underlying electron structure.

In this chapter the first attempt of LRDFT calculations for a magnetic film is reported. One considers bulk bcc Fe, Fe monolayer on W(110) and the corresponding free standing Fe monolayer and finally 2 ML Fe/W(110) system. The role of low dimensionality in the properties of magnetic excitations is revealed. The study was stimulated by the SPEELS investigations of magnetic excitations in this system presented in Ref. [4].

8.1   bcc Fe

Figure 8.1 presents the calculated spin-wave spectrum of bulk bcc iron compared with experimental results [157]. The agreement of the theory and experiment is excellent. Experimentally it has been established

that in the bcc Fe the well defined SW excitations are observed only for small $\mathbf{q}$ vectors, because the short wave-length SWs are severely damped. Our calculations confirm this: for $q > 0.4$ Å^{-1} the imaginary part of the SW pole increases and for larger $\mathbf{q}$ the damping is so strong that the SW excitations cannot be considered as well defined. No further discussion is intended here as the dynamic susceptibility of the system has been already a subject of numerous studies, e.g. [21, 158, 159, 95].
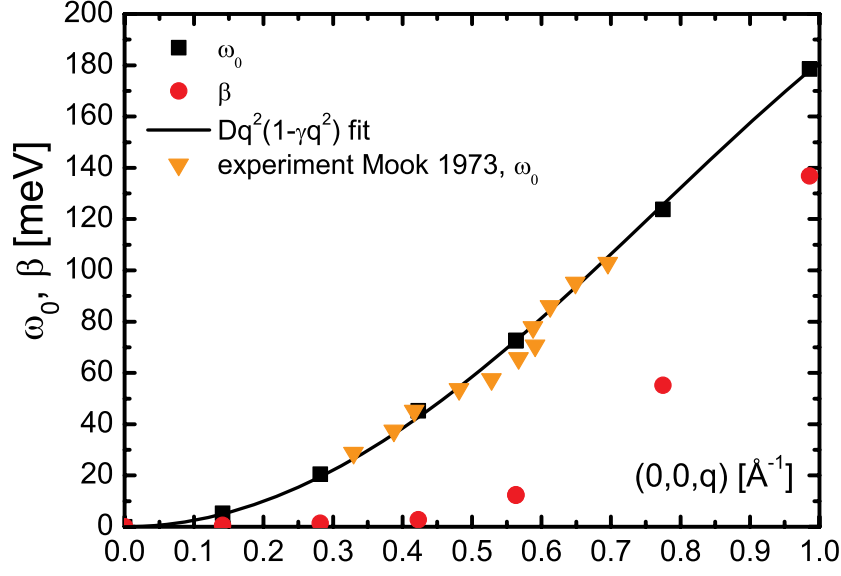

Figure 8.1: Spin-waves of bulk bcc Fe. Squares represent the SW peak positions ($\omega_0(\mathbf{q})$), black line the biquadratic fit to the data with parameters $D = 252$ meVÅ^2 and $\gamma = 0.28$ Å^2. This should be compared to the value $D = 250$ meVÅ^2 of Ref. [95]. Triangles stand for the experimental peak centers [157]. The values of D and γ extracted from the experiment are 260 meVÅ^2 and 0.47 Å^2, respectively. Circles present the imaginary part of SW poles ($\beta(\mathbf{q})$). The figure presents only about one-half of the interval between the center and the boundary of the Brillouin zone.

8.2 Fe/W(110)

We turn now to the consideration of Fe(110) thin films. Experimentally it was established that the system features strong in-plane magnetic surface anisotropy with and easy axis $[1\bar{1}0]$ [160], but these relativistic effects are not included in our model. Despite serious misfit (9.4%, $a_W = 3.161$Å, $a_{Fe} = 2.866$Å) first monolayer of Fe grows pseudomorphically [161]. Transition from pseudomorphic to nonpseudomorphic growth occurs at 1.2 ML coverage [151] and at higher coverages a regular array of misfit dislocations sets in. Also vertical lattice relaxations were observed [162, 163].

In out model the system is translationally invariant in the film plane and the direct lattice is spanned on the vectors $\left(-\frac{\sqrt{2}}{2}, \frac{1}{2}\right)$ and $\left(\frac{\sqrt{2}}{2}, \frac{1}{2}\right)$ (all distances in units a_W). The reciprocal space vectors (all reciprocal space vectors in units $\frac{2\pi}{a_W}$) read $\left[-\frac{1}{\sqrt{2}}, 1\right]$ and $\left[\frac{1}{\sqrt{2}}, 1\right]$. The system features series of alternating atomic planes parallel to the interface. *In-plane* atomic positions are $(0,0)$ for even layers and $\left(0, \frac{1}{2}\right)$ for odd layers. For perfect bcc structure interlayer distance reads $\frac{a_W}{\sqrt{2}}$, but in our calculations the experimental distances were taken, as provided in Ref. [162, 163].

The ΓH direction (H ≡ $\left[0, \frac{3}{4}\right]$) in 2D Brillouin zone (2D BZ) is perpendicular to the easy $[1\bar{1}0]$ axis; **q**'s along this direction can be probed in SPEELS experiments. The ΓN direction (N ≡ $\left[\frac{\sqrt{2}}{2}, 0\right]$) is perpendicular to ΓH.

8.2.1   1 monolayer Fe/W(110)

The vertical lattice relaxations discussed at the beginning of the section were taken into account. The magnetic moment of Fe monolayer reads 2.17 μ_B and 3.11 μ_B for the supported and free monolayer respectively. The interface layer of W in the supported case has negative polarization of -0.16 μ_B. The antiferromagnetic coupling of W interfacial layer agrees with the calculations from Ref. [164].
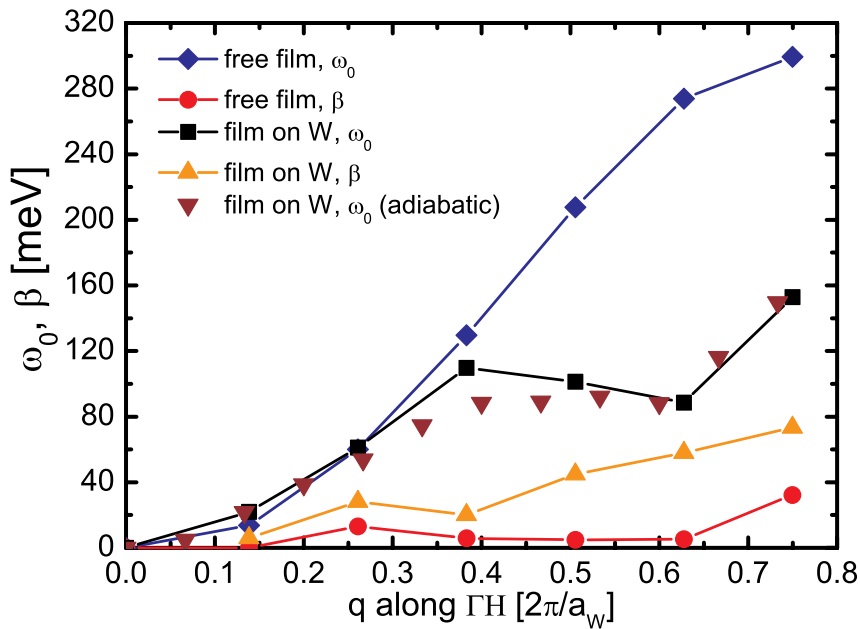

Figure 8.2: Energies and inverse life-times of magnons of iron monolayer. $\omega_0(\mathbf{q})$ and $\beta(\mathbf{q})$ have the same meaning as in Figure 8.1, cf. Sec. 5.5.

In Figure 8.2, the calculational results for the ΓH direction in the 2D BZ are presented. There is only one dominating eigenvalue with standard single-pole energy behavior. We begin with the discussion of supported monolayer Fe/W(110). The estimated SW stiffness assumes the value $D_{\Gamma H} = 278$ meVÅ^2. The dispersion curve deviates strongly from simple cosine-type behavior characteristic for Heisenberg models with the exchange interaction between nearest neighbors only. Instead of a monotonous increase with increasing q the spin wave energy decreases somewhat in the interval of q from 0.4 to 0.6 (unless differently specified wave-vectors are given in units $2\pi/a_W$) staying close to 90 meV. For larger q values the SW energy increases again assuming the value of 150 meV at the H point. The properties of the freestanding Fe film are essentially different. In this case the dispersion curve is close to a simple cosine-form. In the low-q region the SW energies are smaller than for the supported film that gives a lower stiffness $D_{\Gamma H}^{\text{free}} = 102$ meVÅ^2. The curves intersect at about $q = 0.25$. For larger q the SW energies of freestanding film exceed considerably the corresponding energies of Fe/W(110).

Also the life time of magnon states depends strongly on the presence of substrate – the damping of the SW excitations of the supported film is much stronger than in the case of free standing film. The origin of the effect can be traced back to the Fe-W substrate hybridization. Similarly to the case of (001) surface

[165] the unsupported (110) film features much narrower bands and larger spin splitting, cf. Fig. 8.3. As a result the density of low-energy Stoner states contributing to the damping is reduced.

Presently there is no experimental data for 1 ML of Fe/W(110) which could be used for direct comparison with our results. The energies we obtain are smaller than the energies observed for 2 ML [4]. This result can be explained by reduced number of neighboring magnetic Fe atoms in the case of 1 ML compared to the 2 ML film. The SW energies obtained in the model-Hamiltonian approach by Muniz *et al.* [30, 166] exceed substantially our values. Also the form of the dispersion curve reported in that paper is less complex. We relate these differences to the complexity of the Fe-W hybridizations that play crucial role in the establishing of the properties of magnetic excitations. The details of these hybridizations are better captured by the parameter-free DFT calculations.

The structural anisotropy of the (110) surface is reflected in the anisotropy of the SW dispersion; the energy of spin-waves depends on the direction of its wave-vector. The magnons for ΓN direction has higher energies compared to the ΓH direction. This is valid for both supported and free standing films. The presence of the substrate enhances this effect. The dispersion curve along ΓN is qualitatively similar to the curve for ΓH direction discussed above. The values of the stiffness constants are in this case $D_{\Gamma N} = 589$ meVÅ^2 and $D_{\Gamma N}^{\text{free}} = 233$ meVÅ^2. Similar to the ΓN case the damping is enhanced for adsorbed film.
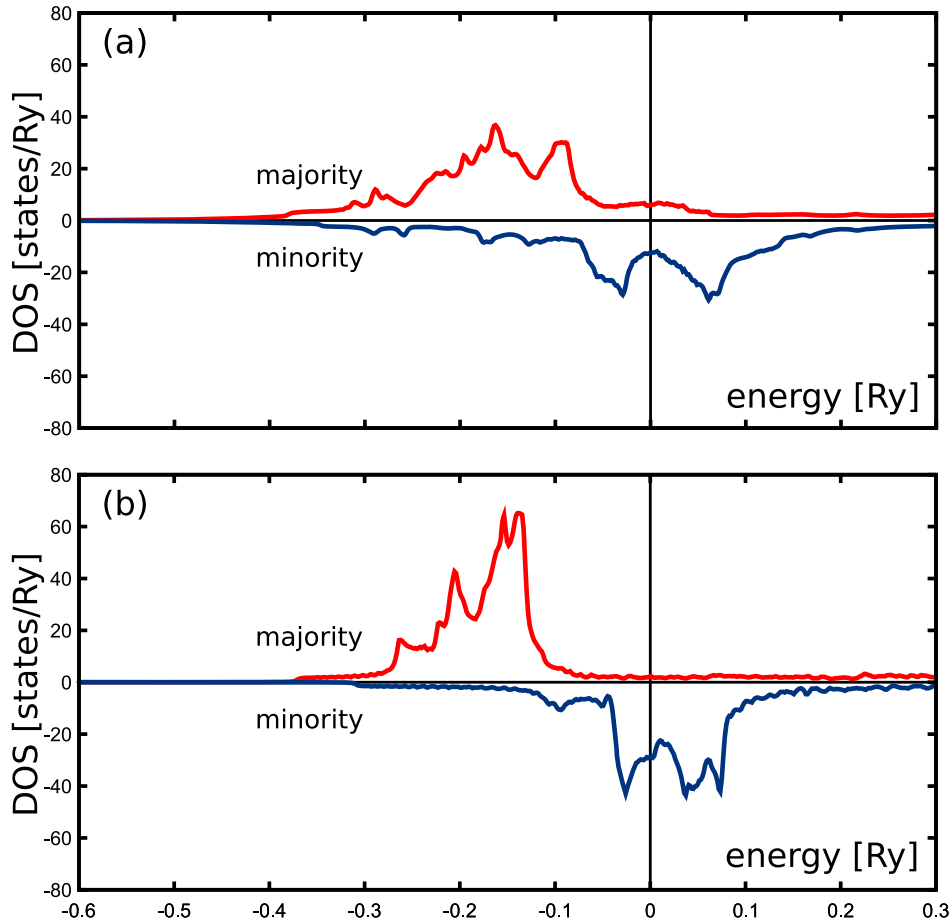

Figure 8.3: Density of majority and minority states of monolayer of iron: a) supported on W, b) free standing. The energies are given with respect to the Fermi level. One notices much narrower bands and larger band splitting in the case of free standing monolayer, yielding lower density of low energy Stoner states.

It is also worth noting that the spin-wave dispersion obtained within adiabatic frozen-magnon calculations is very close to the dispersion obtained from the calculation of the dynamic susceptibility. This means that the exchange parameters obtained by the mapping of the one Fe ML on the Heisenberg Hamiltonian capture important features of the exchange processes in the film although do not allow the estimation of the life-time of the magnons.

8.2.2   2 monolayers Fe/W(110)

In the following calculations the experimental atomic positions were used [162, 163]. The ground state atomic magnetic moments read 2.69 μ_B (top-most Fe layer), 2.16 μ_B (second Fe layer) and -0.14 μ_B (induced moment of interface W layer).

The susceptibility matrix features clearly two dominant eigenvalues; they have been analyzed using single the pole model and the results are given in Figure 8.4. Along the ΓH direction the two branches cross at $q \approx 0.6$. For small q the mode lower in energy of acoustic character, while the more energetic eigenvector is characterized by the moments of iron oscillating in anti-phase. Similar situation occurs in ΓN direction, but the two levels repel each other. Interestingly, the dispersion relation for two monolayers is almost isotropic[1]. None of the modes can be regarded as confined to the surface (surface spin-wave state) for any $\mathbf{q}$, both featuring strong deviations in both magnetic layers.

Similar to the 1 ML case magnons here are well defined in the whole Brillouin zone. As expected, the acoustic branch live very long close to the zone center and the optical magnons are damped even for $\mathbf{q} = \mathbf{0}$. For large wave-vectors the damping is more pronounced for the 2 ML case, mainly due to the fact that the spin-waves are more energetic and thus lie deeper in the Stoner continuum, but the long wave-length acoustic magnons live somewhat longer than for the thicker film.

The observed magnon energies along ΓH [4] are smaller than predicted by our theory. The reason of the discrepancy in not clear, especially in the light of good performance of ALDA for bulk iron. Furthermore, the experiment did not reveal any presence of an optical branch. It has been conjectured that SPEELS could probe only the modes with significant amplitude in the top layer, because of a limited penetratin depth of electrons. Since we predict no clear surface spin-wave state one should look for an explanation elsewhere and there exists by now no definitive answer. This discussion will be continued in the summary of this chapter.

8.3   Summary

Although the damping of the spin-wave states increases with the increasing the wave-vector they remain well defined throughout the whole 2D Brillouin zone. This property is in a striking contrast to the bulk case. The effect of the low dimensionality on the life-time of spin-waves obtained in our calculations is opposite to the effect proposed in the literature [168]. The broken translational symmetry in the direction perpendicular to the film surface destroys the conservation of the crystal momentum in this direction and should lead to the increased damping for a given in-plane wave vector. However this consideration does not take into account the decrease of the number of the Bloch states with the transition from a bulk system to a monolayer. This leads to the decrease of the number of Stoner excitations contributing to the damping.

The role of the non-magnetic substrate in the establishing of the properties of magnetic excitations should be emphasized. The hybridization of the Fe and W states modifies the electronic structure of the Fe layer leading to a more complex pattern of the effective interatomic exchange interactions between spin moments of Fe atoms and enhances damping.

The comparison with SPEELS study shows that not the whole physics of in the experiment is accounted for in our treatment. The absence of the optical mode is puzzling. For large momentum transfers,

---

[1]A fact noted already by Muniz *et al.* [167]. The latter study shows that the anisotropy asserts itself again for thicker films and for 10 ML thick film bulk (isotropic) behavior is still not observed.
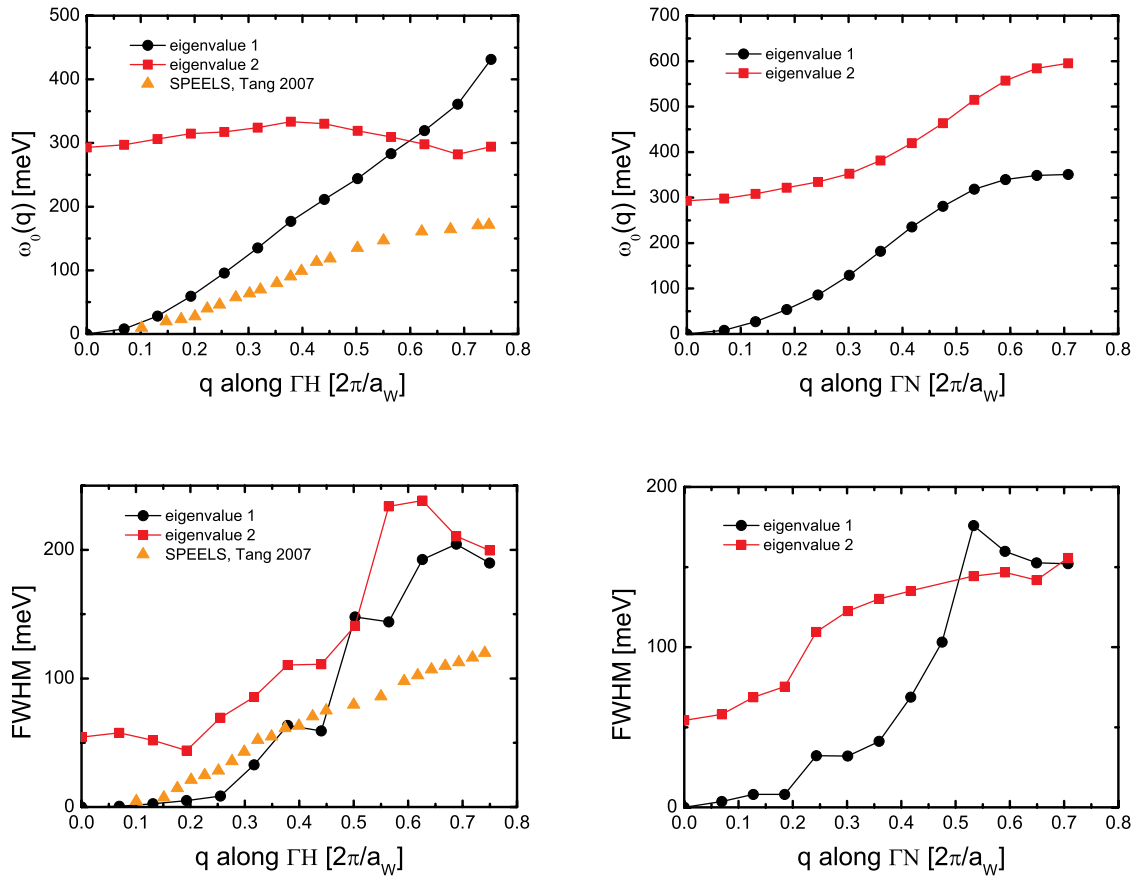
Figure 8.4: Spin-waves of 2 ML Fe/W(110) system along ΓH (left column) and ΓN direction (right column). The energies of the modes are presented in the first row and the full-widths at half-maximum (FWHM≡ $2\beta(\mathbf{q})$) in the second. Experimental points come from Ref. [4]. The last point to the right represents the boundary of 2D Brillouin zone.

where the states are close in energy, they are also substantially broadened and might appear as a single feature in the spectrum especially when one takes into account the finite resolution of SPEELS spectrometer. Nevertheless, close to the center of the zone the optical mode should be discernable. A possible explanation would be the one, in which the optical mode, being substantially broadened even for $\mathbf{q} = \mathbf{0}$, is lost in the background of the signal dominated by the acoustic mode.

The difference between the experimental and theoretical magnon energies needs further effort to be understood, too. First of all, one must make sure that the electronic structure of the sample is correctly reproduced. As we have seen it can be influenced by the details of the interface, but also by impurities and lattice imperfections. This seems to be the first direction of joint experimental and theoretical effort. It should be once more recalled that theory of SPEELS can be much more intricate than the one suggested by a simple equivalence with inelastic neutron scattering. No attempt is made at this point to give this remark any quantitative character since the detailed SPEELS theory has not become a *leitmotiv* of this work. Finally, one cannot exclude that the adiabatic local density approximation fails for the iron surfaces because of strongly enhanced or modified correlation effects. This in turn goes quite much beyond the modern state-of-art realistic electronic calculations.

Despite the limited quantitative agreement with experiment the study proves that LRDFT can be effectively applied to the systems with reduced dimensionality.

SUMMARY AND OUTLOOK

A dynamic method of studying the spectrum of spin-flip fluctuations has been presented. It is based on the numerical evaluation of magnetic susceptibility within the linear response density functional theory in adiabatic local density approximation. Similarly to the adiabatic spin dynamics based on the mapping to Heisenberg model it is parameter free, can provide us with the energies of spin-waves and uses realistic electronic structure calculations, which makes it sensitive to the geometrical boundary conditions (like surfaces and interfaces), types of atomic species, structural relaxations and – not discussed in this work – substitutional disorder. Unlike the adiabatic treatment, the dynamic method can account for the decay of spin-waves into particle-hole triplet states, since these so called Stoner excitations appear naturally in the theory.

For the long-living magnons the both methods yield similar results, however the dynamic approach takes into account the energy renormalization due to the hybridization with Stoner continuum and corrections arising from Bruno's renormalized force theorem [67, 66]. The latter are often not taken into account in many implementations of the adiabatic scheme. The dynamic treatment captures some aspects of magnetization dynamics, which are rather difficult to describe in a mapping to Heisenberg Hamiltonian, an example being the behavior of induced atomic moments. In the situation when the magnons appear in an energy region with a high Stoner states density, the adiabatic methods lead to qualitatively wrong results.

The damping of magnons is their inherent property and it seems that the decay into the Stoner states is the dominant mechanism of broadening in the itinerant magnets, possibly except for the very long wavelength magnons, when it is necessarily small and other effects might be of similar magnitude. In the case of spin-wave excitations living in a gap of Stoner continuum the decay into the single particle excitations is forbidden, but the magnons coexisting with Stoner continuum might be so broad that they could not be regarded as well defined excitation. Older experimental works very often did not try to quantify the width of spin-wave peak, partially because of the absence of a quantitative theory allowing an interpretation of these results. Such quantification is present in the contemporary experimental studies and it is hoped that the work can serve as a guide for them.

The dynamic formalism was applied to the three mono-elemental bulk systems: bcc iron, and hcp and fcc phases of cobalt. The method can account very well for the energies of spin-waves in these materials. Experimentally the magnons were found to be damped, in the case of Fe to a point, where they were not anymore detectable for high momentum transfers. The calculations presented in this thesis confirm that this behavior is in a contrast to the cobalt phases, where the magnons were observed in the whole Brillouin zone. The method presented in this work predicts a possibility of appearance of multiple spin-wave branches, originating from the the presence of many non-equivalent atoms in the primitive cell or, equivalently, from the internal dynamics of the cell. Under propitious experimental conditions, the modes can be experimentally observed, as in hcp cobalt.

Similarly, the present model predicts multiple magnon modes in the Heusler alloys. The example of NiMnSn teaches us however that the number of branches should not be identified with the number

of magnetic atoms in the primitive cell. In the discussed case the Ni moment is induced by the Mn sublattice and cannot support an optical spin-wave branch. As far as the decay is concerned, in the Heusler phases the covalent hybridization between transition metal atoms, which can lead to the half-metalicity, generally reduces the density of low-energy Stoner states. When the alloy becomes an actual half-metal, Stoner modes acquire a finite activation energy and low energy magnons are forbidden to decay into the single particle states. As discussed above, the long-living modes can, as in the example of Co_2MnSi, be accompanied by short-living high energy magnons.

Spin excitations have been recently experimentally studied in nanostructures. This poses new exciting questions about the influence of the boundaries and reduced dimensionality on the energy and life-time of magnons. One can also look at the states localized due to the presence of interfaces or other imperfections. A new generation of experiments allows a confirmation of theoretical predictions. A part of this thesis focuses on the thin films of Fe adsorbed on W(110). It was found the magnons in these systems live longer than in the bulk, even though the broken translational symmetry makes the overlap between spin-wave and Stoner states larger. One attributes it to the reduced number of single-particle states in the geometrically confined film. The present calculations confirm the sensitivity of magnons' energies and life-times to the underlying electronic structure. The structural anisotropy of the film implies that the dispersion relation depends on the wave-vector direction.

The spin-dynamics of nanostructures is of growing relevance from the practical point of view. Magnetic devices, important for example in the storage technologies or inter-chip communication, will be faster and smaller just like their electronic counterparts, reaching a moment when exciting of magnetic states will become significant part of their operation. One sees now the necessity of reliable life-time determination. In the magnetic storage devices one would like these excitations to decay as soon as possible, leaving a bit after a read-in or a read-out in a steady state. Here the damping due to the coupling to the Stoner states can effectively transfer the unwanted energy to the electron gas. On the contrary, if we wished to use the magnons as a medium to communicate two chips, we would look for energies corresponding to small density of Stoner states ("spin-wave windows"), so the signal could travel undistorted between emitter and antenna. For small frequencies this is easy to achieve since generally Stoner states are pronounced at higher energies, but as the operational frequency rises one might wish to look for high energy windows, existence of which is not easily predictable without performing explicit calculations. Some nano-devices could make use of localized magnon states or their specific shape involving only some atomic moments, etc. All the necessary physics could be tackled in the dynamic susceptibility calculations.

In the end let us focus on the future. No additional development is necessary to study antiferromagnets and the first application will be thin antiferromagnetic Mn films. It is rather straightforward to generalize the computational scheme to include one-dimensional systems and clusters. Through the inclusion of the coherent potential approximation one paves the way to study disordered systems and ultimately to include finite temperature effects in disordered local moment picture [169]. Strongly correlated materials can be now described by means of self-interaction correction (SIC) and the formalism of transverse magnetic susceptibility can be readily extended to the SIC-corrected systems [170]. Some generalization are not so straightforward. Non-collinear systems, possibly influenced by relativistic effects, require a careful reformulation of the formalism, mostly because there is a rather limited understanding, how a spin-wave should exactly look like in such cases. As far as the immediate applications of the code are concerned one will try to establish whether there is a well defined surface magnon state for different cuts of iron crystal. The study of Heusler phases will continue and include their different classes. Certain more exotic magnets will be concerned, including gadolinium or MnSi.

<div align="center">☙</div>

Our world does not allow us to doubt that the reality is more like the one of Heraclitus than of Zeno. The condensed matter theory acknowledges it and sets off to discover the lands beyond the ground state. I had the luck to witness a small part of the road and when the quantum mechanics was still young D. H. Lawrence gave an account of my wonder

I like relativity and quantum theories
because I don't understand them
and they make me feel as if space shifted about
like a swan that
can't settle,
refusing to sit still and be measured;
and as if the atom were an impulsive thing
always changing its mind.[1]

---

[1]"Relativity", David Herbert Lawrence: *Pansies: Poems.* Martin Secker, London, 1929.

RYDBERG ATOMIC UNITS

Rydberg atomic units are used in this work. In this system the numerical values of the following four fundamental constants are all unity by definition

$$\text{Coulomb's constant} \qquad \kappa \equiv \frac{1}{4\pi\varepsilon_0} = 1, \qquad\qquad \text{(A.0.1a)}$$

$$\text{Planck's constant} \qquad \hbar = 1, \qquad\qquad \text{(A.0.1b)}$$

$$\text{Bohr radius} \qquad a_0 = 1, \qquad\qquad \text{(A.0.1c)}$$

$$\text{Rydberg energy} \qquad E_\text{R} = 1, \qquad\qquad \text{(A.0.1d)}$$

which in turn fix the numerical values of the following constants

$$\text{electron mass} \qquad m_e = \frac{1}{2}\frac{\hbar^2}{E_\text{R}a_0^2} = \frac{1}{2}, \qquad\qquad \text{(A.0.2a)}$$

$$\text{elementary charge} \qquad e = \sqrt{\frac{\hbar^2}{\kappa m_e a_0}} = \sqrt{2}. \qquad\qquad \text{(A.0.2b)}$$

Table A.1 provides a short comparison of Atomic Rydberg and the International System of Units (SI), based on CODATA 2006 [171, 172]. In October 2005, the National Physical Laboratory reported initial measurements of the Planck constant using a newly improved Watt balance [173]

$$h = 6.62607095(44) \cdot 10^{-34} \,\text{J s}, \qquad\qquad \text{(A.0.3)}$$

which is significantly different (statistically) from the 2006 CODATA value.

Few remarks on unit notation and nomenclature are now in order. In ARU system most of the units do not have widely accepted names and some freedom is left. We will call the unit of length "Bohr" and denote it with Bh. The unit of time has a symbol of ch (from a Polish word meaning a short interval of time). Energy is measured in "Rydbergs" (Ry). Magnetic moment is usually given in Bohr magnetons, but let us note that this is a constant not equal to unity. Generalized density response as defined by equation 3.3.1 has units $\text{Bh}^{-6}\,\text{Ry}^{-1}\,\text{ch}^{-1}$. Its time-space Fourier transform has unit $\text{Bh}^{-3}\,\text{Ry}^{-1}$, which we call "Kubo" (Kb).

Quantity	Symbol	ARU	SI
Length ("Bohr")	[Bh]	$1 (\equiv a_0)$	$0.52917720859(36) \cdot 10^{-10}$ m
Mass		$1 (\equiv 2m_e)$	$1.82187643 \cdot 10^{-30}$ kg
Time	[ch]	$1 (\equiv \hbar/E_R)$	$4.8377687 \cdot 10^{-17}$ s
Frequency		1	$2.0670687 \cdot 10^{16}$ Hz
Energy ("Rydberg")	[Ry]	$1 (\equiv E_R)$	$2.17987197(11) \cdot 10^{-18}$ J
Charge		$1 (\equiv e/\sqrt{2})$	$1.132909859 \cdot 10^{-19}$ C
Magnetic induction		$1 (\equiv \sqrt{2} E_R/\mu_B)$	$3.3241336 \cdot 10^{5}$ T
Planck's constant	$\hbar$	1	$1.054571628(53) \cdot 10^{-34}$ J s
$2\pi\hbar$	h	2π	$6.62606896(33) \cdot 10^{-34}$ J s
Elementary charge	e	$\sqrt{2}$	$1.602176487(40) \cdot 10^{-19}$ C
Energy 1 electron volt	eV		$1.602176487(40) \cdot 10^{-19}$ J
Rydberg energy	E_R	1	$13.60569193(34)$ eV
Rec. fine structure constant	α^{-1}		$137.035999679(94)$
Electric constant	ε_0	$(4\pi)^{-1}$	$8.854187817 \cdot 10^{-12}$ F m^{-1}
Speed of light in vacuum	c	$2/\alpha$	299792458 m s^{-1}
Bohr magneton	μ_B	$\sqrt{2}$	$927.400915(23) \cdot 10^{-26}$ J T^{-1}
Electron mass	m_e	$1/2$	$9.10938215(45) \cdot 10^{-31}$ kg
Boltzmann constant	k_B	$6.333631(11) \cdot 10^{-6}$	$1.3806504(24) \cdot 10^{-23}$ J K^{-1}
Gravitation constant	G	$1.92000 \cdot 10^{-42}$	$6.67428(67) \cdot 10^{-11}$ m^3 kg^{-1} s^{-2}

Table A.1: Conversion table for Atomic Rydberg (ARU) and SI Units. Additionally the values of few constants are provided. Numbers in brackets denote standard uncertainties. Numerical values without error should be regarded as approximate with the exception of c and ε_0, which are by definition exact within SI. Data after CODATA 2006 [171].

FOURIER SPACES

Some conventions concerning Fourier transformations are specified here. In addition several useful identities (mainly sum rules and convolution theorems) are provided. Primarily I follow [31]. The symbol for function and its transformation is usually the same and they can be distinguished judging by their arguments.

B.1 τ-time functions

In the standard usage they are functions periodic with period $2\beta\hbar$, i.e.

$$f(\tau + 2\beta\hbar) = f(\tau), \quad \tau \in \mathbb{R}. \tag{B.1.1}$$

As such they can be naturally expanded in Fourier series with discrete frequencies

$$\omega_n = \frac{n\pi}{\beta}, \quad n \in \mathbb{Z} \tag{B.1.2}$$

and the following holds

$$f(\omega_n) = \frac{1}{2} \int_{-\beta}^{\beta} d\tau\, \mathfrak{e}^{\mathrm{i}\omega_n\tau} f(\tau), \quad f(\tau) = \frac{1}{\beta} \sum_{n \in \mathbb{Z}} \mathfrak{e}^{-\mathrm{i}\omega_n\tau} f(\omega_n). \tag{B.1.3}$$

If function is *periodic* with period $\beta\hbar$, $f(\omega_n)$ is non-zero only for *even (bosonic)* frequencies

$$\omega_m^b = 2m\frac{\pi}{\beta}, \quad m \in \mathbb{Z}. \tag{B.1.4}$$

An *antiperiodic* function with period $\beta\hbar$ (i.e. $f(\tau + \beta) = -f(\tau)$), $f(\omega_n)$ is non-zero only for *odd (fermionic)* frequencies

$$\omega_m^f = (2m + 1)\frac{\pi}{\beta}, \quad m \in \mathbb{Z}. \tag{B.1.5}$$

ω_m^f and ω_m^b are usually called **Matsubara frequencies**. In the both of the above cases the transformed function for its specific frequencies can be computed like follows

$$f\left(\omega_m^{b,f}\right) = \int_0^{\beta} d\tau\, \mathfrak{e}^{\mathrm{i}\omega_m^{b,f}\tau} f(\tau). \tag{B.1.6}$$

Representations of *Kronecker delta δ_{nl} Dirac's delta $\delta(\tau)$* exist

$$\frac{1}{2} \int_{-\beta}^{\beta} d\tau\, \mathfrak{e}^{\mathrm{i}(\omega_n - \omega_l)\tau} = \beta\delta_{nl}, \quad n, l \in \mathbb{Z}, \tag{B.1.7}$$

$$\delta(\tau) = \frac{1}{\beta\hbar} \sum_{n\in\mathbb{Z}} \mathbf{e}^{-\mathrm{i}\omega_n^b \tau}, \quad \tau \in [-\beta\hbar, \beta\hbar].$$ (B.1.8)

The following convolution theorem appears to be very useful. Let us put

$$g(\tau) = f_1(\tau)f_2(-\tau).$$ (B.1.9)

the τ-transform of g reads

$$g(\omega_n) = \frac{1}{\beta\hbar} \sum_{m\in\mathbb{Z}} f_1(\omega_n + \omega_m)f_2(\omega_m) = \frac{1}{\beta\hbar} \sum_{m\in\mathbb{Z}} f_1(\omega_n)f_2(\omega_n - \omega_m).$$ (B.1.10)

If f has additional symmetry such that $f_{1,2}\big(\omega_n^b\big) = 0$, then

$$g\big(\omega_n^f\big) = 0$$ (B.1.11)

and

$$g\big(\omega_n^b\big) = \frac{1}{\beta\hbar} \sum_{m\in\mathbb{Z}} f_1\big(\omega_m^f + \omega_n^b\big)f_2\big(\omega_m^f\big) = \frac{1}{\beta\hbar} \sum_{m\in\mathbb{Z}} f_1\big(\omega_m^f\big)f_2\big(\omega_m^f - \omega_n^b\big).$$ (B.1.12)

Let's note that

$$\omega_m^f - \omega_n^b = \omega_{m-n}^f.$$ (B.1.13)

B.2   Ordinary time Fourier transform

The relations between time and frequency domains are

$$f(\omega) = \int_{\mathbb{R}} dt\, \mathbf{e}^{\mathrm{i}\omega t} f(t), \quad f(t) = \int_{\mathbb{R}} \frac{d\omega}{2\pi} \mathbf{e}^{-\mathrm{i}\omega t} f(\omega).$$ (B.2.1)

For reference some transformations are explicitly given below; $\mathbb{R} \ni \Omega > 0$. Damped harmonic oscillations (no motion in the past)

$$\int_{\mathbb{R}} dt\, \mathbf{e}^{-\mathrm{i}\omega_0 t} \mathbf{e}^{-\Omega t} \theta(t) \mathbf{e}^{\mathrm{i}\omega t} = \frac{\mathrm{i}}{\omega - \omega_0 + \mathrm{i}\Omega}.$$ (B.2.2)

Heaviside function $\theta(t)$ allowing for better future can be represented as

$$\int_{\mathbb{R}} dt\, \theta(t) \mathbf{e}^{\mathrm{i}\omega t} = \frac{\mathrm{i}}{\omega + \mathrm{i}0^+},$$ (B.2.3)

while Heaviside function $\theta(-t)$ emphasizing the past as

$$\int_{\mathbb{R}} dt\, \theta(-t) \mathbf{e}^{\mathrm{i}\omega t} = -\frac{\mathrm{i}}{\omega - \mathrm{i}0^+}.$$ (B.2.4)

Useful identity involving principal value

$$\frac{1}{\omega \pm \mathrm{i}0^+} = \mathrm{Pv}\frac{1}{\omega} \mp \mathrm{i}\pi\delta(\omega).$$ (B.2.5)

B.3   Space Fourier transform

Transformations between real and reciprocal space have different sign, but the same 2π convention

$$f(\mathbf{k}) = \int_{\mathbb{R}^D} d\mathbf{x} \mathfrak{e}^{-i\mathbf{k} \cdot \mathbf{x}} f(\mathbf{x}), \quad f(\mathbf{x}) = \int_{\mathbb{R}^D} \frac{d\mathbf{k}}{(2\pi)^D} \mathfrak{e}^{i\mathbf{k} \cdot \mathbf{x}} f(\mathbf{k}). \tag{B.3.1}$$

The following Dirac's delta representations are often used

$$\int_{\mathbb{R}^D} d\mathbf{x} \mathfrak{e}^{-i\mathbf{k} \cdot \mathbf{x}} = (2\pi)^D \delta(\mathbf{k}) \tag{B.3.2a}$$

$$\int_{\mathbb{R}^D} d\mathbf{k} \mathfrak{e}^{i\mathbf{k} \cdot \mathbf{x}} = (2\pi)^D \delta(\mathbf{x}) \tag{B.3.2b}$$

Let $\mathcal{L}$ be a lattice spanned on the basis vectors $\mathbf{a}_i$. The lattice $\mathcal{L}^{-1}$ *reciprocal* to $\mathcal{L}$ is spanned on the basis vectors $\mathbf{A}_i$ such that

$$\mathbf{a}_i \cdot \mathbf{A}_j = 2\pi \delta_{ij}. \tag{B.3.3}$$

The following sum rules are called *Poisson summation formulas*

$$\sum_{\mathbf{R} \in \mathcal{L}} \mathfrak{e}^{-i\mathbf{k} \cdot \mathbf{R}} = \Omega_{\mathrm{BZ}} \sum_{\mathbf{K} \in \mathcal{L}^{-1}} \delta(\mathbf{k} - \mathbf{K}), \tag{B.3.4a}$$

$$\sum_{\mathbf{K} \in \mathcal{L}^{-1}} \mathfrak{e}^{i\mathbf{K} \cdot \mathbf{x}} = \Omega_{\mathrm{WS}} \sum_{\mathbf{R} \in \mathcal{L}} \delta(\mathbf{x} - \mathbf{R}). \tag{B.3.4b}$$

They can be used to compute Fourier transforms of the functions periodic with the periodicity of $\mathcal{L}$ or $\mathcal{L}^{-1}$. If we put

$$f(\mathbf{x} + \mathbf{R}) = f(\mathbf{x}), \quad \mathbf{R} \in \mathcal{L}, \tag{B.3.5a}$$

$$g(\mathbf{k} + \mathbf{K}) = g(\mathbf{k}), \quad \mathbf{K} \in \mathcal{L}^{-1}, \tag{B.3.5b}$$

we obtain

$$f(\mathbf{k}) = f(\underline{\mathbf{k}}) \sum_{\mathbf{K} \in \mathcal{L}^{-1}} (2\pi)^D \delta(\mathbf{k} - \mathbf{K}), \quad g(\mathbf{x}) = g(\underline{\mathbf{x}}) \sum_{\mathbf{R} \in \mathcal{L}} \delta(\mathbf{x} - \mathbf{R}), \tag{B.3.6}$$

where

$$f(\underline{\mathbf{k}}) = \frac{1}{\Omega_{\mathrm{WS}}} \int_{\Omega_{\mathrm{WS}}} d\mathbf{x} \mathfrak{e}^{-i\mathbf{k} \cdot \mathbf{x}} f(\mathbf{x}), \quad g(\underline{\mathbf{x}}) = \frac{1}{\Omega_{\mathrm{BZ}}} \int_{\Omega_{\mathrm{BZ}}} d\mathbf{k} \mathfrak{e}^{i\mathbf{k} \cdot \mathbf{x}} g(\mathbf{k}). \tag{B.3.7}$$

The inverse transform can be computed as

$$f(\mathbf{x}) = \sum_{\mathbf{K} \in \mathcal{L}^{-1}} f(\underline{\mathbf{K}}) \mathfrak{e}^{i\mathbf{K} \cdot \mathbf{x}}, \quad g(\mathbf{k}) = \sum_{\mathbf{R} \in \mathcal{L}} g(\underline{\mathbf{R}}) \mathfrak{e}^{-i\mathbf{k} \cdot \mathbf{R}}. \tag{B.3.8}$$

The following Brillouin zone convolution theorem is of particular importance

$$\sum_{\mathbf{R} \in \mathcal{L}} f_1(\mathbf{R}) f_2(-\mathbf{R}) \mathfrak{e}^{-i\mathbf{q} \cdot \mathbf{R}} = \frac{1}{\Omega_{\mathrm{BZ}}} \int_{\Omega_{\mathrm{BZ}}} d\mathbf{k} f_1(\mathbf{k}) f_2(\mathbf{k} - \mathbf{q}) = \frac{1}{\Omega_{\mathrm{BZ}}} \int_{\Omega_{\mathrm{BZ}}} d\mathbf{k} f_1(\mathbf{k} + \mathbf{q}) f_2(\mathbf{k}). \tag{B.3.9}$$

Y-CH BASIS

For the sake of clarity I present here the conventions used throughout this work and in the developed computer programs. References to `Mathematica` package in this Appendix pertain to version `6.0.1.0`.

C.1 Spherical coordinates

We use the spherical coordinates with polar (θ) and azimuthal (ϕ) angles and radial coordinate r as presented in Fig. 3.1

$$\theta \in [0, \pi], \quad \phi \in [0, 2\pi], \quad r \in [0, \infty). \tag{C.1.1}$$

The Cartesian components of position vector $\mathbf{r} = (x, y, z)$ read

$$x = r \sin\theta \cos\phi, \quad y = r \sin\theta \sin\phi, \quad z = r \cos\theta \tag{C.1.2}$$

and this transformation is characterized by the following Jacobian

$$\left| \frac{\partial(x, y, z)}{\partial(r, \phi, \theta)} \right| = r^2 \sin\theta. \tag{C.1.3}$$

In this spherical coordinates the area and volume elements read respectively

$$d\mathbf{a} = r^2 \sin\theta \, d\phi \, d\theta \, \hat{\mathbf{r}}, \quad dV = r^2 \sin\theta \, d\phi \, d\theta \, dr. \tag{C.1.4}$$

C.2 Spherical harmonics

We define standard (complex) spherical harmonics [77] following `Mathematica`

$$\widetilde{\mathcal{Y}}_{lm}(\theta, \phi) \equiv \texttt{SphericalHarmonicY}[l, m, \theta, \phi]. \tag{C.2.1}$$

The real spherical harmonics are defined as follows ((θ, ϕ) arguments are suppressed)

$$\mathcal{Y}_{lm} \equiv \begin{cases} \frac{i}{\sqrt{2}} \left(\widetilde{\mathcal{Y}}_{l,-|m|} - (-1)^m \widetilde{\mathcal{Y}}_{l,|m|} \right) & m < 0, \\ \widetilde{\mathcal{Y}}_{l0} & m = 0, \\ \frac{1}{\sqrt{2}} \left(\widetilde{\mathcal{Y}}_{l,-|m|} + (-1)^m \widetilde{\mathcal{Y}}_{l,|m|} \right) & m > 0. \end{cases} \tag{C.2.2}$$

Both $\widetilde{\mathcal{Y}}$ and $\mathcal{Y}$ are orthonormal with respect to the integration over the surface of the unit sphere.

C.3 Chebyshev polynomials

We used Chebyshev polynomials similar to those defined in `Mathematica`; only the definition of zeroth-order polynomial differ

$$\mathfrak{Ch}_\mu(\xi) \equiv \left(1 - \frac{1}{2}\delta_{\mu 0}\right)\texttt{ChebyshevT}[\mu, \xi],\tag{C.3.1}$$

where $\mathbb{Z} \ni \mu \geq 0, \xi \in [-1, 1]$. Chebyshev polynomials are orthogonal in the latter interval with weight

$$\mathcal{W}(\xi) \equiv \frac{1}{\sqrt{1-\xi^2}}.\tag{C.3.2}$$

The detailed discussion of properties of Chebyshev polynomials is beyond the scope of this short summary. They were used as a part of Y-Ch basis because it is straightforward to approximate functions using $\mathfrak{Ch}$. Additionally, it is rather easy to obtain many results (like overlap integrals or Fourier transformations of $\mathfrak{Ch}$) analytically.

A sufficiently well behaved complex function $f(z)$ given in the interval $[a, b]$ (if a and b are complex, $[a, b]$ should be understood as a contour with a and b as a beginning and an end, respectively) can be approximated by means of Chebyshev polynomials as follows

$$f(z) = \sum_{\mu=0}^{N} c_\mu \mathfrak{Ch}_\mu\big(\xi_{[a,b]}(z)\big),\tag{C.3.3}$$

where

$$c_\mu = \frac{2}{N_0}(1 + \delta_{\mu 0}) \sum_{j=1}^{N_0} f\left(\xi_{[a,b]}^{-1}(\xi_j)\right)\mathfrak{Ch}_\mu(\xi_j), \quad \xi_j = \cos\left(\frac{\pi\left(j - \frac{1}{2}\right)}{N_0}\right)\tag{C.3.4}$$

and N_0 and N are non-negative integers such that $N < N_0$. N is the order of approximating polynomial and N_0 is called approximation order. $\xi_{[a,b]}(z)$ is an invertible function mapping contour $[a, b]$ into interval $[-1, 1]$. In most cases is simply linear function.

C.4 Miscellaneous

Below I present several additional conventions and formulas. One of the spherical Bessel functions, particularly useful to us, is defined as

$$j_l(z) = \sqrt{\frac{\pi}{2z}}\texttt{BesselJ}[l + 1/2, z].\tag{C.4.1}$$

It can be used to decompose a plane wave into spherical harmonics

$$\mathfrak{e}^{\mathbf{iq}\cdot\mathbf{r}} = 4\pi \sum_{l=0}^{\infty} \mathfrak{i}^l j_l(qr) \sum_{m=-l}^{l} \mathcal{Y}_{lm}(\hat{\mathbf{q}})\mathcal{Y}_{lm}(\hat{\mathbf{r}}).\tag{C.4.2}$$

The above formula is called Bauer's identity. It can be used to compute the following integral, necessary when performing Fourier transformation of susceptibility

$$A_{\mu lm}(\mathbf{q}) = \int_0^R r^2 dr \int_0^{2\pi} d\phi \int_0^\pi \sin\theta d\theta \frac{1}{r}\mathfrak{Ch}\big(\xi_{[0,R]}(r)\big)\mathcal{Y}_{lm}(\hat{\mathbf{r}})\mathfrak{e}^{\mathbf{iq}\cdot\mathbf{r}} = \mathfrak{i}^l \pi R^2 \zeta_{\mu l}(qR)\mathcal{Y}_{lm}(\hat{\mathbf{q}}),\tag{C.4.3}$$

where

$$\zeta_{\mu l}(x) \equiv \int_{-1}^1 d\xi(1 + \xi)\mathfrak{Ch}_\mu(\xi)j_l\left(\frac{x}{2}(1 + \xi)\right).\tag{C.4.4}$$

The latter function was evaluated analytically using `Mathematica` and subsequently Chebyshev approximated in x. In such form it is directly used in the code.

[1] SEAVEY, M. H. and P. E. TANNENWALD: *Direct Observation of Spin-Wave Resonance.* Phys. Rev. Lett., 1(5):168–, September 1958.

[2] NODA, YASUHISA and YOSHIKAZU ISHIKAWA: *Spin Dynamics in a Heusler Alloy Pd_2MnSn.* Journal of the Physical Society of Japan, 40(3):699–705, March 1976.

[3] BALASHOV, T., A. F. TAKACS, W. WULFHEKEL and J. KIRSCHNER: *Magnon Excitation with Spin-Polarized Scanning Tunneling Microscopy.* Phys. Rev. Lett., 97(18):187201–4, November 2006.

[4] TANG, W. X., Y. ZHANG, I. TUDOSA, J. PROKOP, M. ETZKORN and J. KIRSCHNER: *Large Wave Vector Spin Waves and Dispersion in Two Monolayer Fe on W(110).* Phys. Rev. Lett., 99(8):087202–4, August 2007.

[5] VOLLMER, R., M. ETZKORN, P. S. ANIL KUMAR, H. IBACH and J. KIRSCHNER: *Spin-Polarized Electron Energy Loss Spectroscopy of High Energy, Large Wave Vector Spin Waves in Ultrathin fcc Co Films on Cu(001).* Physical Review Letters, 91(14):147201, 2003.

[6] KITTEL, CHARLES: *Interpretation of Anomalous Larmor Frequencies in Ferromagnetic Resonance Experiment.* Phys. Rev., 71(4):270–, February 1947.

[7] VLECK, J. H. VAN: *Concerning the Theory of Ferromagnetic Resonance Absorption.* Phys. Rev., 78(3):266–, May 1950.

[8] VLECK, J. H. VAN and J. VAN KRANENDONK: *Spin Waves.* Rev. Mod. Phys., 30(1):1–, January 1958.

[9] WALDRON, R A: *What is ferromagnetic resonance?* British Journal of Applied Physics, 11(2):69, 1960.

[10] HOVE, LÉON VAN: *Time-Dependent Correlations between Spins and Neutron Scattering in Ferromagnetic Crystals.* Phys. Rev., 95(6):1374–, September 1954.

[11] MORIYA, TORU: *Spin fluctuations in itinerant electron magnetism*, volume 56 of *Springer series in solid-state sciences.* Springer, Berlin, 1985.

[12] SCHÄFER, J., D. SCHRUPP, ELI ROTENBERG, K. ROSSNAGEL, H. KOH, P. BLAHA and R. CLAESSEN: *Electronic Quasiparticle Renormalization on the Spin Wave Energy Scale.* Phys. Rev. Lett., 92(9):097205–, March 2004.

[13] HONG, JISANG and D. L. MILLS: *Spin dependence of the inelastic electron mean free path in Fe and Ni: Explicit calculations and implications.* Phys. Rev. B, 62(9):5589–, September 2000.

[14] SCALAPINO, D. J.: *The case for $d_{x^2-y^2}$ pairing in the cuprate superconductors.* Physics Reports, 250(6):329–365, January 1995.

[15] SLONCZEWSKI, J. C.: *Excitation of spin waves by an electric current.* Journal of Magnetism and Magnetic Materials, 195(2):261–268, May 1999.

[16] KAKA, SHEHZAAD, MATTHEW R. PUFALL, WILLIAM H. RIPPARD, THOMAS J. SILVA, STEPHEN E. RUSSEK and JORDAN A. KATINE: *Mutual phase-locking of microwave spin torque nano-oscillators.* Nature, 437(7057):389–392, 2005.

[17] KÜBLER, J. K.: *Theory of itinerant electron magnetism*, volume 106 of *International series of monographs on physics.* Clarendon Press, Oxford, 2000.

[18] HALILOV, S. V., H. ESCHRIG, A. Y. PERLOV and P. M. OPPENEER: *Adiabatic spin dynamics from spin-density-functional theory: Application to Fe, Co, and Ni.* Phys. Rev. B, 58(1):293–, July 1998.

[19] Sandratskii, L. M.: *Noncollinear magnetism in itinerant-electron systems: theory and applications.* Advances in Physics, 47(1):91 – 160, January 1998.

[20] Liechtenstein, A. I., M. I. Katsnelson, V. P. Antropov and V. A. Gubanova: *Local spin density functional approach to the theory of exchange interactions in ferromagnetic metals and alloys.* Journal of Magnetism and Magnetic Materials, 67(1):65–74, May 1987.

[21] Cooke, J. F., H. L. Davis and J. W. Lynn: *Calculations of the dynamic susceptibility of nickel and iron.* Phys. Rev. B, 21(9):4118–4131, May 1980.

[22] Gross, E. K. U. and Walter Kohn: *Local density-functional theory of frequency-dependent linear response.* Physical Review Letters, 55(26):2850–2852, 1985.

[23] Gross, E. K. U. and Walter Kohn: *Erratum: Local density-functional theory of frequency-dependent linear response Phys. Rev. Lett. 55, 2850 (1985).* Physical Review Letters, 57(7):923–923, 1986.

[24] Callaway, J., D. G. Laurent and C. S. Wang: *Magnetic susceptibility and spin waves in ferromagnetic metals.* Phys. Rev. B, 24(11):6491–6496, Dec 1981.

[25] Stenzel, E. and H. Winter: *A real-space method for the evaluation of the dynamic spin susceptibility of paramagnetic metals with application to palladium.* Journal of Physics F: Metal Physics, 15(7):1571–1594, 1985.

[26] Winter, H., E. Stenzel, Z. Szotek and W. M. Temmermans: *On the evaluation of spin susceptibilities within multiple scattering theory.* Journal of Physics F: Metal Physics, 18(3):485–500, 1988.

[27] Staunton, J., B. L. Gyorffy, G. M. Stocks and J. Wadsworth: *The static, paramagnetic, spin susceptibility of metals at finite temperatures.* Journal of Physics F: Metal Physics, 16(11):1761–1788, 1986.

[28] Staunton, J. B., J. Poulter, B. Ginatempo, E. Bruno and D. D. Johnson: *Incommensurate and Commensurate Antiferromagnetic Spin Fluctuations in Cr and Cr Alloys from ab initio Dynamical Spin Susceptibility Calculations.* Physical Review Letters, 82:3340–3343, April 1999.

[29] Staunton, J. B., J. Poulter, B. Ginatempo, E. Bruno and D. D. Johnson: *Spin fluctuations in nearly magnetic metals from ab initio dynamical spin susceptibility calculations: Application to Pd and $Cr_{95}V_5$.* Physical Review B (Condensed Matter and Materials Physics), 62:1075–1082, July 2000.

[30] Muniz, R. B. and D. L. Mills: *Theory of spin excitations in Fe(110) monolayers.* Physical Review B (Condensed Matter and Materials Physics), 66(17):174417, 2002.

[31] Fetter, Alexander L. and John Dirk Walecka: *Quantum theory of many-particle systems.* International series in pure and applied physics. McGraw-Hill, New York, NY, 1971.

[32] Abrikosov, A.A., L.P. Gorkov and I.E. Dzyaloshinski: *Methods of quantum field theory in statistical physics.* Dover Books on Physics and Chemistry. Dover, New York, 1975.

[33] Mattuck, Richard D.: *A guide to Feynman diagrams in the many-body problem.* Dover science books. Dover, New York, 1992.

[34] Hedin, Lars: *New Method for Calculating the One-Particle Green's Function with Application to the Electron-Gas Problem.* Phys. Rev., 139(3A):A796–A823, Aug 1965.

[35] Aryasetiawan, F and O Gunnarsson: *The GW method.* Reports on Progress in Physics, 61(3):237, 1998.

[36] Georges, Antoine, Gabriel Kotliar, Werner Krauth and Marcelo J. Rozenberg: *Dynamical mean-field theory of strongly correlated fermion systems and the limit of infinite dimensions.* Rev. Mod. Phys., 68(1):13–125, January 1996.

[37] Kotliar, G., S. Y. Savrasov, K. Haule, V. S. Oudovenko, O. Parcollet and C. A. Marianetti: *Electronic structure calculations with dynamical mean-field theory.* Rev. Mod. Phys., 78(3):865–87, July 2006.

[38] Fock, V.: *Näherungsmethode zur Lösung des quantenmechanischen Mehrkörperproblems.* Zeitschrift für Physik A Hadrons and Nuclei, 61(1):126–148, January 1930.

[39] Hohenberg, P. and W. Kohn: *Inhomogeneous Electron Gas.* Phys. Rev., 136(3B):B864–B871, November 1964.

[40] Dreizler, R. M. and E. K. U. Gross: *Density functional theory: an approach to the quantum many-body problem.* Springer, Berlin, 1990.

[41] KOHN, W. and L. J. SHAM: *Self-Consistent Equations Including Exchange and Correlation Effects*. Phys. Rev., 140(4A):A1133–A1138, November 1965.

[42] PARR, ROBERT G. and WEITAO YANG: *Density-functional theory of atoms and molecules*, volume 16 of *International series of monographs on chemistry*. Oxford Univ. Press, Oxford, 1989.

[43] LÜDERS, M., A. ERNST, M. DANE, Z. SZOTEK, A. SVANE, D. KODDERITZSCH, W. HERGERT, B. L. GYORFFY and W. M. TEMMERMAN: *Self-interaction correction in multiple scattering theory*. Physical Review B (Condensed Matter and Materials Physics), 71(20):205109, 2005.

[44] PERDEW, J. P. and ALEX ZUNGER: *Self-interaction correction to density-functional approximations for many-electron systems*. Phys. Rev. B, 23(10):5048–, May 1981.

[45] BARTH, U. VON and L. HEDIN: *A local exchange-correlation potential for the spin polarized case: I.* Journal of Physics C: Solid State Physics, 5(13):1629–1642, 1972.

[46] PERDEW, JOHN P. and YUE WANG: *Accurate and simple analytic representation of the electron-gas correlation energy*. Phys. Rev. B, 45(23):13244–13249, Jun 1992.

[47] KUBO, RYOGO and KAZUHISA TOMITA: *A General Theory of Magnetic Resonance Absorption*. Journal of the Physical Society of Japan, 9(6):888–919, November-December 1954.

[48] KUBO, RYOGO: *Statistical-Mechanical Theory of Irreversible Processes. I. General Theory and Simple Applications to Magnetic and Conduction Problems*. Journal of the Physical Society of Japan, 12(6):570–586, June 1957.

[49] NYQUIST, H.: *Thermal Agitation of Electric Charge in Conductors*. Phys. Rev., 32(1):110–, July 1928.

[50] CALLEN, HERBERT B. and THEODORE A. WELTON: *Irreversibility and Generalized Noise*. Phys. Rev., 83(1):34–, July 1951.

[51] MA, SHANG-KENG, M. T. BEAL-MONOD and DONALD R. FREDKIN: *Spin Waves in* He^3 *in the Paramagnon Model*. Phys. Rev., 174(1):227–, October 1968.

[52] IZUYAMA, TAKEO, DUK-JOO KIM and RYOGO KUBO: *Band Theoretical Interpretation of Neutron Diffraction Phenomena in Ferromagnetic Metals*. Journal of the Physical Society of Japan, 18(7):1025–1042, July 1963.

[53] PLIHAL, M. and D. L. MILLS: *Spin-flip exchange scattering of low-energy electrons in ferromagnetic iron*. Phys. Rev. B, 58(21):14407–, December 1998.

[54] KIRSCHNER, J., D. REBENSTORFF and H. IBACH: *High-Resolution Spin-Polarized Electron-Energy-Loss Spectroscopy and the Stoner Excitation Spectrum in Nickel*. Phys. Rev. Lett., 53(7):698–, August 1984.

[55] PLIHAL, M. and D. L. MILLS: *Spin dynamics and spin-polarized EELS spectra of model itinerant-electron magnetic films*. Physical Review B (Condensed Matter), 52(17):12813–12828, 1995.

[56] PLIHAL, M., D. L. MILLS and J. KIRSCHNER: *Spin Wave Signature in the Spin Polarized Electron Energy Loss Spectrum of Ultrathin Fe Films: Theory and Experiment*. Physical Review Letters, 82(12):2579–2582, 1999.

[57] IBACH, H., D. BRUCHMANN, R. VOLLMER, M. ETZKORN, P. S. ANIL KUMAR and J. KIRSCHNER: *A novel spectrometer for spin-polarized electron energy-loss spectroscopy*. Rev. Sci. Instrum., 74(9):4089–4095, September 2003.

[58] RUNGE, ERICH and E. K. U. GROSS: *Density-functional theory for time-dependent systems*. Physical Review Letters, 52(12):997–1000, 1984.

[59] MARQUES, MIGUEL A.L.: *Time-Dependent Density Functional Theory*, volume 706 of *Lecture Notes in Physics*. Springer, Berlin, Heidelberg edition, 2006.

[60] VIGNALE, G., C. A. ULLRICH and S. CONTI: *Time-Dependent Density Functional Theory Beyond the Adiabatic Local Density Approximation*. Phys. Rev. Lett., 79(24):4878–, December 1997.

[61] ONIDA, GIOVANNI, LUCIA REINING and ANGEL RUBIO: *Electronic excitations: density-functional versus many-body Green's-function approaches*. Rev. Mod. Phys., 74(2):601–, June 2002.

[62] KATSNELSON, M. I. and A. I. LICHTENSTEIN: *Magnetic susceptibility, exchange interactions and spin-wave spectra in the local spin density approximation*. Journal of Physics: Condensed Matter, 16(41):7439–7446, 2004.

[63] GRIFFIN, A., A. J. PINDOR and G. GUMBS: *Condition for spin-rotational invariance in a semi-infinite itinerant-electron ferromagnet.* Phys. Rev. B, 36(16):8831–, December 1987.

[64] GUMBS, G. and A. GRIFFIN: *Surface spin waves in a tight-binding itinerant-electron ferromagnet.* Surface Science, 91(2-3):669–693, January 1980.

[65] ANTROPOV, V. P., M. I. KATSNELSON, M. VAN SCHILFGAARDE and B. N. HARMON: *Ab initio Spin Dynamics in Magnets.* Physical Review Letters, 75(4):729–732, Jul 1995.

[66] GROTHEER, O., C. EDERER and M. FÄHNLE: *Fast ab initio methods for the calculation of adiabatic spin wave spectra in complex systems.* Phys. Rev. B, 63(10):100401, Feb 2001.

[67] BRUNO, P.: *Exchange Interaction Parameters and Adiabatic Spin-Wave Spectra of Ferromagnets: A "Renormalized Magnetic Force Theorem".* Phys. Rev. Lett., 90(8):087205, Feb 2003.

[68] SANDRATSKII, L M: *Symmetry analysis of electronic states for crystals with spiral magnetic order. I. General properties.* Journal of Physics: Condensed Matter, 3(44):8565–8585, 1991.

[69] ISHIKAWA, Y., G. SHIRANE, J. A. TARVIN and M. KOHGI: *Magnetic excitations in the weak itinerant ferromagnet MnSi.* Phys. Rev. B, 16(11):4956–, December 1977.

[70] DONIACH, S: *Theory of inelastic neutron scattering in nearly ferromagnetic metals.* Proceedings of the Physical Society, 91(1):86, 1967.

[71] STENZEL, E. and H. WINTER: *The wave vector dependent dynamic spin susceptibilities of Pd and V and their contributions to the low temperature specific heat.* Journal of Physics F: Metal Physics, 16(11):1789–1809, 1986.

[72] THAKOR, V., J. B. STAUNTON, J. POULTER, S. OSTANIN, B. GINATEMPO and EZIO BRUNO: *First-principles relativistic theory of the magnetic response of paramagnetic metals: Application to yttrium and scandium.* Physical Review B (Condensed Matter and Materials Physics), 68(13):134412, 2003.

[73] KOHN, W. and N. ROSTOKER: *Solution of the Schrödinger Equation in Periodic Lattices with an Application to Metallic Lithium.* Phys. Rev., 94:1111–1120, 1954.

[74] KORRINGA, J.: *On the calculation of the energy of a Bloch wave in a metal.* Physica, 13(6-7):392–400, August 1947.

[75] ZABLOUDIL, J. (editor): *Electron scattering in solid matter: a theoretical and computational treatise*, volume 147 of *Springer series in solid-state sciences.* Springer, Berlin, 2005.

[76] ANDERSEN, O. KROGH: *Linear methods in band theory.* Phys. Rev. B, 12(8):3060–, October 1975.

[77] BIAŁYNICKI-BIRULA, I., M. CIEPLAK and J. KAMIŃSKI: *Teoria kwantów: mechanika falowa*, volume 13 of *Biblioteka Fizyki.* Wydaw. Naukowe PWN, Warszawa, 1991.

[78] SZUNYOGH, L., B. ÚJFALUSSY, P. WEINBERGER and J. KOLLÁR: *Self-consistent localized KKR scheme for surfaces and interfaces.* Phys. Rev. B, 49(4):2721–2729, Jan 1994.

[79] WILDBERGER, K., R. ZELLER and P. H. DEDERICHS: *Screened KKR-Green's-function method for layered systems.* Phys. Rev. B, 55(15):10074–10080, Apr 1997.

[80] ZELLER, RUDOLF: *Evaluation of the screened Korringa-Kohn-Rostoker method for accurate and large-scale electronic-structure calculations.* Phys. Rev. B, 55(15):9400–9408, Apr 1997.

[81] ZELLER, R., P. H. DEDERICHS, B. ÚJFALUSSY, L. SZUNYOGH and P. WEINBERGER: *Theory and convergence properties of the screened Korringa-Kohn-Rostoker method.* Phys. Rev. B, 52(12):8807–8812, Sep 1995.

[82] BEACH, K. S. D., R. J. GOODING and F. MARSIGLIO: *Reliable Padé analytical continuation method based on a high-accuracy symbolic computation algorithm.* Phys. Rev. B, 61(8):5147–5157, Feb 2000.

[83] JARRELL, MARK and J. E. GUBERNATIS: *Bayesian inference and the analytic continuation of imaginary-time quantum Monte Carlo data.* Physics Reports, 269(3):133–195, May 1996.

[84] ESCHRIG, H., R. RICHTER and B. VELICKÝ: *A numerical method of analytical continuation of Green-function-like expressions.* Journal of Physics C: Solid State Physics, 19(36):7173–7181, 1986.

[85] LEE, KEUN-HO and K. J. CHANG: *Analytic continuation of the dynamic response function using an N-point Padé approximant.* Phys. Rev. B, 54(12):R8285–R8288, Sep 1996.

[86] GRAHAM, RICHARD L., TIMOTHY S. WOODALL and JEFFREY M. SQUYRES: *Open MPI: A Flexible High Performance MPI.* In *Proceedings, 6th Annual International Conference on Parallel Processing and Applied Mathematics*, Poznan, Poland, September 2005.

[87] GRAHAM, RICHARD L., GALEN M. SHIPMAN, BRIAN W. BARRETT, RALPH H. CASTAIN, GEORGE BOSILCA and ANDREW LUMSDAINE: *Open MPI: A High-Performance, Heterogeneous MPI.* In *Proceedings, Fifth International Workshop on Algorithms, Models and Tools for Parallel Computing on Heterogeneous Networks*, Barcelona, Spain, September 2006.

[88] HURSEY, JOSHUA, ETHAN MALLOVE, JEFFREY M. SQUYRES and ANDREW LUMSDAINE: *An Extensible Framework for Distributed Testing of MPI Implementations.* In *Proceedings, Euro PVM/MPI*, Paris, France, October 2007.

[89] YOO, CHOONG-SHIK, PER SODERLIND and HYUNCHAE CYNN: *The phase diagram of cobalt at high pressure and temperature: the stability of γ(fcc)-cobalt and new ε'(dhcp)-cobalt.* Journal of Physics: Condensed Matter, 10(20):L311, 1998.

[90] TAYLOR, A. and R. W. FLOYD: *Precision measurements of lattice parameters of non-cubic crystals.* Acta Crystallographica, 3(4):285–289, 1950.

[91] SHIRANE, G., V. J. MINKIEWICZ and R. NATHANS: *Spin Waves in 3d Metals.* Journal of Applied Physics, 39(2):383–390, 1968.

[92] PERRING, T.G., A.D. TAYLOR and G.L. SQUIRES: *High-energy spin waves in hexagonal cobalt.* Physica B: Condensed Matter, 213-214:348–350, August 1995.

[93] TROHIDOU, K. N., J. A. BLACKMAN and J. F. COOKE: *Calculation of the high-energy spin-wave spectrum of hcp cobalt.* Phys. Rev. Lett., 67(18):2561–, October 1991.

[94] BASS, J. M., J. A. BLACKMAN and J. F. COOKE: *The role of the exchange matrix in the itinerant-electron theory of ferromagnetism.* Journal of Physics: Condensed Matter, 4(16):L275, 1992.

[95] PAJDA, M., J. KUDRNOVSKÝ, I. TUREK, V. DRCHAL and P. BRUNO: *Ab initio calculations of exchange interactions, spin-wave stiffness constants, and Curie temperatures of Fe, Co, and Ni.* Phys. Rev. B, 64(17):174402–, October 2001.

[96] SINCLAIR, R. N. and B. N. BROCKHOUSE: *Dispersion Relation for Spin Waves in a fcc Cobalt Alloy.* Phys. Rev., 120(5):1638–, December 1960.

[97] PICKART, S. J., H. A. ALPERIN, V. J. MINKIEWICZ, R. NATHANS, G. SHIRANE and O. STEINSVOLL: *Spin-Wave Dispersion in Ferromagnetic Ni and fcc Co.* Phys. Rev., 156(2):623–, April 1967.

[98] HEUSLER, F. *Verh. Dtsch. Phys. Ges.*, 5:219–, 1903.

[99] PIERRE, J., R. V. SKOLOZDRA, J. TOBOLA, S. KAPRZYK, C. HORDEQUIN, M. A. KOUACOU, I. KARLA, R. CURRAT and E. LELIÈVRE-BERNA: *Properties on request in semi-Heusler phases.* Journal of Alloys and Compounds, 262-263:101–107, November 1997.

[100] WEBSTER, P.J. and K.R.A. ZIEBECK: *Magnetic and chemical order in Heusler alloys containing cobalt and titanium.* Journal of Physics and Chemistry of Solids, 34(10):1647–1654, October 1973.

[101] SHELTON, R. N., L. S. HAUSERMANN-BERG, M. J. JOHNSON, P. KLAVINS and H. D. YANG: *Coexistence of superconductivity and long-range magnetic order in $ErPd_2Sn$.* Phys. Rev. B, 34(1):199–, July 1986.

[102] KIERSTEAD, H. A., B. D. DUNLAP, S. K. MALIK, A. M. UMARJI, SHENOY and G. K.: *Coexistence of ordered magnetism and superconductivity in Pd_2YbSn.* Phys. Rev. B, 32(1):135–, July 1985.

[103] CANFIELD, P. C., J. D. THOMPSON, W. P. BEYERMANN, A. LACERDA, M. F. HUNDLEY, E. PETERSON, Z. FISK and H. R. OTT: *Magnetism and heavy fermion-like behavior in the RBiPt series.* In *J. Appl. Phys.*, volume 70, pages 5800–5802, Pittsburgh, Pennsylvania (USA), November 1991. AIP.

[104] HUNDLEY, M. F., J. D. THOMPSON, P. C. CANFIELD and Z. FISK: *Electronic transport properties of the semimetallic heavy fermion YbBiPt.* Phys. Rev. B, 56(13):8098–, October 1997.

[105] KACZOROWSKI, D., A. LEITHE-JASPER, P. ROGL, H. FLANDORFER, T. CICHOREK, R. PIETRI and B. ANDRAKA: *Magnetic, thermodynamic, and electrical transport properties of ternary equiatomic ytterbium compounds YbTM (T=transition metal, M=Sn and Bi).* Phys. Rev. B, 60(1):422–, July 1999.

[106] SZYTUŁA, A., A. JEZIERSKI, B. PENC, A. WINIARSKI, A. LEITHE-JASPER and D. KACZOROWSKI: *Electronic structure of YbTX compounds.* Journal of Alloys and Compounds, 360(1-2):41–46, October 2003.

[107] ZHU, T. J., L. LU, M. O. LAI and J. DING: *Growth and magnetic properties of NiMnGa thin films prepared by pulsed laser ablation.* Smart Materials and Structures, 14(5):S293–S296, 2005.

[108] KARLA, I., J. PIERRE and R. V. SKOLOZDRA: *Physical properties and giant magnetoresistance in RNiSb compounds.* Journal of Alloys and Compounds, 265(1-2):42–48, January 1998.

[109] PIERRE, J. and I. KARLA: *Giant magnetoresistance in RENiSb semiconductors (RE=Tb,Dy,Ho).* Journal of Magnetism and Magnetic Materials, 217(1-3):74–82, July 2000.

[110] UHER, C., J. YANG, S. HU, D. T. MORELLI and G. P. MEISNER: *Transport properties of pure and doped MNiSn (M=Zr, Hf).* Phys. Rev. B, 59(13):8615–, April 1999.

[111] HORDEQUIN, C., J. PIERRE and R. CURRAT: *Magnetic excitations in the half-metallic NiMnSb ferromagnet: From Heisenberg-type to itinerant behaviour.* Journal of Magnetism and Magnetic Materials, 162(1):75–84, September 1996.

[112] GROOT, R. A. DE, F. M. MUELLER, P. G. VAN ENGEN and K. H. J. BUSCHOW: *New class of materials: Half-metallic ferromagnets.* Physical Review Letters, 50(25):2024–2027, 1983.

[113] ISHIDA, S., S. AKAZAWA, Y. KUBO and J. ISHIDA: *Band theory of Co_2MnSn, Co_2TiSn and Co_2TiAl.* Journal of Physics F: Metal Physics, 12(6):1111–1122, 1982.

[114] ISHIDA, SHOJI, SHINPEI FUJII, SHOEI KASHIWAGI and SETSURO ASANO: *Search for Half-Metallic Compounds in Co_2MnZ (Z=IIIb, IVb, Vb Element).* J. Phys. Soc. Jpn., 64:2152–2157, 1995.

[115] ŽUTIĆ, IGOR, JAROSLAV FABIAN and S. DAS SARMA: *Spintronics: Fundamentals and applications.* Rev. Mod. Phys., 76(2):323–, April 2004.

[116] ŞAŞIOĞLU, E., L. M. SANDRATSKII and P. BRUNO: *First-principles calculation of the intersublattice exchange interactions and Curie temperatures of the full Heusler alloys Ni_2MnX (X=Ga,In,Sn,Sb).* Phys. Rev. B, 70(2):024427–, July 2004.

[117] ŞAŞIOĞLU, E., L. M. SANDRATSKII, P. BRUNO and I. GALANAKIS: *Exchange interactions and temperature dependence of magnetization in half-metallic Heusler alloys.* Phys. Rev. B, 72(18):184415–11, November 2005.

[118] ŞAŞIOĞLU, E., L.M. SANDRATSKII and P. BRUNO: *Magnetic exchange coupling and Curie temperature of $Ni_{1+x}MnSb$ (x=0,0.25,0.5,0.75,1) from first principles.* Journal of Magnetism and Magnetic Materials, 290-291(Part 1):385–387, April 2005.

[119] ŞAŞIOĞLU, E., L. M. SANDRATSKII and P. BRUNO: *Pressure dependence of the Curie temperature in Ni_2MnSn Heusler alloy: A first-principles study.* Phys. Rev. B, 71(21):214412–7, June 2005.

[120] ŞAŞIOĞLU, E., L. M. SANDRATSKII and P. BRUNO: *First-principles study of exchange interactions and Curie temperatures of half-metallic ferrimagnetic full Heusler alloys Mn_2VZ Z (Z = Al, Ge).* Journal of Physics: Condensed Matter, 17(6):995–1001, 2005.

[121] ŞAŞIOĞLU, E., L. M. SANDRATSKII and P. BRUNO: *Pressure dependence of the Curie temperature in Ni_2MnSn Heusler alloy: A first-principles study.* Phys. Rev. B, 71(21):214412–7, June 2005.

[122] KÜBLER, J., A. R. WILLIAM and C. B. SOMMERS: *Formation and coupling of magnetic moments in Heusler alloys.* Phys. Rev. B, 28(4):1745–, August 1983.

[123] KURTULUS, YASEMIN, RICHARD DRONSKOWSKI, GERMAN D. SAMOLYUK and VLADIMIR P. ANTROPOV: *Electronic structure and magnetic exchange coupling in ferromagnetic full Heusler alloys.* Phys. Rev. B, 71(1):014425–12, January 2005.

[124] ANTROPOV, V. P., B. N. HARMON and A. N. SMIRNOV: *Aspects of spin dynamics and magnetic interactions.* Journal of Magnetism and Magnetic Materials, 200(1-3):148–166, October 1999.

[125] HORDEQUIN, C., D. RISTOIU, L. RANNO and J. PIERRE: *On the cross-over from half-metal to normal ferromagnet in NiMnSb.* The European Physical Journal B - Condensed Matter and Complex Systems, 16(2):287–293, July 2000.

[126] GALANAKIS, I., P. H. DEDERICHS and N. PAPANIKOLAOU: *Origin and properties of the gap in the half-ferromagnetic Heusler alloys.* Phys. Rev. B, 66(13):134428–, October 2002.

[127] GALANAKIS, I., P. H. DEDERICHS and N. PAPANIKOLAOU: *Slater-Pauling behavior and origin of the half-metallicity of the full-Heusler alloys.* Phys. Rev. B, 66(17):174429–, November 2002.

[128] HELMHOLDT, R. B., R. A. DE GROOT, F. M. MUELLER, P. G. VAN ENGEN and K. H. J. BUSCHOW: *Magnetic and crystallographic properties of several C1b type Heusler compounds.* Journal of Magnetism and Magnetic Materials, 43(3):249–255, August 1984.

[129] KIRILLOVA, M. M., A. A. MAKHNEV, E. I. SHREDER, V. P. DYAKINA and N. B. GORINA: *Interband Optical Absorption and Plasma Effects in Half-Metallic XMnY Ferromagnets.* physica status solidi (b), 187(1):231–240, 1995.

[130] KÜBLER, J.: *Curie temperatures of zinc-blende half-metallic ferromagnets.* Phys. Rev. B, 67(22):220403–, June 2003.

[131] HORDEQUIN, CH., E. LELIEVRE-BERNA and J. PIERRE: *Magnetization density in the half-metallic ferromagnet NiMnSb.* Physica B: Condensed Matter, 234-236:602–604, June 1997.

[132] WATANABE, KIYOSHI: *Magetic Properties of C1b-Type Mn Base Compounds.* Transactions of the Japan Institute of Metals, 17(4):220–226, 1976.

[133] HORDEQUIN, CH., J. PIERRE and R. CURRAT: *How do magnetic excitations behave in half metallic ferromagnets? The case of NiMnSb.* Physica B: Condensed Matter, 234-236:605–607, June 1997.

[134] LEŽAIĆ, M., PH. MAVROPOULOS, J. ENKOVAARA, G. BIHLMAYER and S. BLUGEL: *Thermal Collapse of Spin Polarization in Half-Metallic Ferromagnets.* Phys. Rev. Lett., 97(2):026404–4, July 2006.

[135] CHIONCEL, L., M. I. KATSNELSON, R. A. DE GROOT and A. I. LICHTENSTEIN: *Nonquasiparticle states in the half-metallic ferromagnet NiMnSb.* Physical Review B (Condensed Matter and Materials Physics), 68(14):144425, 2003.

[136] SANDRATSKII, L. M., R. SINGER and E. ŞAŞIOĞLU: *Heisenberg Hamiltonian description of multiple-sublattice itinerant-electron systems: General considerations and applications to NiMnSb and MnAs.* Phys. Rev. B, 76(18):184406–14, November 2007.

[137] MRYASOV, OLEG N.: *Magnetic interactions in 3d-5d layered ferromagnets.* Journal of Magnetism and Magnetic Materials, 272-276(Part 2):800–801, May 2004.

[138] MRYASOV, OLEG N.: *Magnetic interactions and phase transformations in FeM, M=(Pt, Rh) ordered alloys.* Phase Transitions, 78(1):197–208, 2005.

[139] WEBSTER, P.J.: *Magnetic and chemical order in Heusler alloys containing cobalt and manganese.* Journal of Physics and Chemistry of Solids, 32(6):1221–1231, 1971.

[140] SINGH, L. J., Z. H. BARBER, Y. MIYOSHI, Y. BUGOSLAVSKY, W. R. BRANFORD and L. F. COHEN: *Structural, magnetic, and transport properties of thin films of the Heusler alloy Co_2MnSi.* Appl. Phys. Lett., 84(13):2367–2369, March 2004.

[141] TAJIMA, KEISUKE, YOSHIKAZU ISHIKAWA, PETER J. WEBSTER, MICHAEL W. STRINGFELLOW, DINO TOCCHETTI and KURT R. A. ZEABECK: *Spin Waves in a Heusler Alloy Cu_2MnAl.* Journal of the Physical Society of Japan, 43(2):483–489, August 1977.

[142] PARANJPE, S.K. and R.J. BEGUM: *Magnetic properties of mixed Cu_2MnAl-Pd_2MnAl heusler alloys.* Journal of Magnetism and Magnetic Materials, 15-18(Part 1):477–478, 1980.

[143] SOŁTYS, J.: *X-ray diffraction research of the order-disorder transitions in the ternary Heusler alloys B_2MnAl (B = Cu, Ni, Co, Pd, Pt).* Physica Status Solidi (a), 66(2):485–491, 1981.

[144] ŞAŞIOĞLU, E., L. M. SANDRATSKII and P. BRUNO: *Role of conduction electrons in mediating exchange interactions in Mn-based Heusler alloys.* Phys. Rev. B, 77(6):064417–15, February 2008.

[145] KUBO, YASUNORI, SHOJI ISHIDA, JUNJI ISHIDA and SETSURO ASANO: *Dynamical Spin Susceptibility for Cu_2MnAl.* J. Phys. Soc. Jpn., 48:407–413, 1980.

[146] REITZ, JOHN R. and MARY BETH STEARNS: *Theory of spin wave spectra in Heusler alloys.* J. Appl. Phys., 50(B3):2066–2068, March 1979.

[147] LICHTENSTEIN, A. I., M. I. KATSNELSON and G. KOTLIAR: *Finite-Temperature Magnetism of Transition Metals: An ab initio Dynamical Mean-Field Theory.* Phys. Rev. Lett., 87(6):067205–4, August 2001.

[148] SANDER, D., A. ENDERS, C. SCHMIDTHALS, D. REUTER and J. KIRSCHNER: *Mechanical stress and magnetism of ferromagnetic monolayers.* Surface Science, 402-404:351–355, May 1998.

[149] SANDER, D., R. SKOMSKI, A. ENDERS, C. SCHMIDTHALS, D. REUTER and J. KIRSCHNER: *The correlation between mechanical stress and magnetic properties of ultrathin films.* Journal of Physics D: Applied Physics, 31(6):663–670, 1998.

[150] SANDER, D.: *The correlation between mechanical stress and magnetic anisotropy in ultrathin films.* Reports on Progress in Physics, 62(5):809–858, 1999.

[151] SANDER, D., A. ENDERS and J. KIRSCHNER: *Anisotropic surface stress on W(110).* EPL (Europhysics Letters), 45(2):208–214, 1999.

[152] WEBER, N., K. WAGNER, H. J. ELMERS, J. HAUSCHILD and U. GRADMANN: *Nanoscale spatial switching of magnetic anisotropy in pseudomorphic Fe(110) on W(110).* Phys. Rev. B, 55(21):14121–, June 1997.

[153] DÜRKOP, T., H. J. ELMERS and U. GRADMANN: *Adsorption-driven spin reorientation transition in sesquilayers of Fe(110) on W(110).* Journal of Magnetism and Magnetic Materials, 172(1-2):L1–L8, August 1997.

[154] HAUSCHILD, J., U. GRADMANN and H. J. ELMERS: *Perpendicular magnetization and dipolar antiferromagnetism in double layer nanostripe arrays of Fe(110) on W(110).* Appl. Phys. Lett., 72(24):3211–3213, June 1998.

[155] ELMERS, H. J., J. HAUSCHILD, H. FRITZSCHE, G. LIU, U. GRADMANN and U. KÖHLER: *Magnetic Frustration in Ultrathin Fe Films.* Phys. Rev. Lett., 75(10):2031–, September 1995.

[156] SANDER, D., R. SKOMSKI, C. SCHMIDTHALS, A. ENDERS and J. KIRSCHNER: *Film Stress and Domain Wall Pinning in Sesquilayer Iron Films on W(110).* Phys. Rev. Lett., 77(12):2566–, September 1996.

[157] MOOK, H. A. and R. M. NICKLOW: *Neutron Scattering Investigation of the Magnetic Excitations in Iron.* Phys. Rev. B, 7(1):336–, January 1973.

[158] SAVRASOV, S. Y.: *Linear Response Calculations of Spin Fluctuations.* Physical Review Letters, 81:2570–2573, September 1998.

[159] ARYASETIAWAN, F. and K. KARLSSON: *Green's function formalism for calculating spin-wave spectra.* Physical Review B (Condensed Matter and Materials Physics), 60(10):7419–7428, 1999.

[160] ANDERSEN, TORSTEN and WOLFGANG HÜBNER: *Substrate effects on surface magnetism of Fe/W(110) from first principles.* Physical Review B, 74:184415, 2006.

[161] GRADMANN, U. and G. WALLER: *Periodic lattice distortions in epitaxial films of Fe(110) on W(110).* Surface Science, 116(3):539–548, May 1982.

[162] MEYERHEIM, H. L., D. SANDER, R. POPESCU, J. KIRSCHNER, P. STEADMAN and S. FERRER: *Surface structure and stress in Fe monolayers on W(110).* Phys. Rev. B, 64(4):045414–, July 2001.

[163] POPESCU, R., H. L. MEYERHEIM, D. SANDER, J. KIRSCHNER, P. STEADMAN, O. ROBACH and S. FERRER: *Surface X-ray structure analysis of periodic misfit dislocations in Fe/W(110).* Phys. Rev. B, 68(15):155421–, October 2003.

[164] QIAN, X. and W. HÜBNER: *First-principles calculation of structural and magnetic properties for Fe monolayers and bilayers on W(110).* Phys. Rev. B, 60(23):16192–, December 1999.

[165] SANDRATSKII, L. M., E. ŞAŞIOĞLU and P. BRUNO: *Exchange interactions and Néel temperature of a Fe monolayer on W(001): A first-principles study.* Phys. Rev. B, 73(1):014430–6, January 2006.

[166] COSTA, A. T., R. B. MUNIZ, J. X. CAO, R. Q. WU and D. L. MILLS: *Magnetism of an Fe monolayer on W(110).* Phys. Rev. B, 78(5):054439–9, August 2008.

[167] MUNIZ, R. B., A. T. COSTA and D. L. MILLS: *Microscopic theory of spin waves in ultrathin ferromagnetic films: Fe on W(110).* Journal of Physics: Condensed Matter, 15(5):S495, 2003.

[168] Costa, A. T., R. B. Muniz and D. L. Mills: *Theory of spin excitations in Fe(110) multilayers.* Phys. Rev. B, 68(22):224435–, December 2003.

[169] Gyorffy, B. L., A. J. Pindor, J. Staunton, G. M. Stocks and H. Winter: *A first-principles theory of ferromagnetic phase transitions in metals.* Journal of Physics F: Metal Physics, 15(6):1337–1386, 1985.

[170] Hughes, I. D., M. Dane, A. Ernst, W. Hergert, M. Lüders, J. Poulter, J. B. Staunton, A. Svane, Z. Szotek and W. M. Temmerman: *Lanthanide contraction and magnetism in the heavy rare earth elements.* Nature, 446(7136):650–653, April 2007.

[171] *The NIST Reference on Constants, Units, and Uncertainty.* `http://physics.nist.gov/cuu/index.html`.

[172] Mohr, Peter J., Barry N. Taylor and David B. Newell: *CODATA Recommended Values of the Fundamental Physical Constants: 2006.* `http://physics.nist.gov/cuu/Constants/codata.pdf`, 2006.

[173] Steiner, Richard L., Edwin R. Williams, David B. Newell and Ruimin Liu: *Towards an electronic kilogram: an improved measurement of the Planck constant and electron mass.* Metrologia, 42(5):431, 2005.

Acknowledgments

I would like to thank my supervisors Leonid M. Sandratskii and Arthur Ernst for their support and encouragement. Every page of this work bears a sign of their knowledge and scientific intuition.

I have really enjoyed and benefited from discussions with Patrick Bruno, Markus Däne, Guntram Fischer, Balazs Gyorffy, Jürgen Henk, Wolfram Hergert, Jürgen Kirschner, Josef Kudrnovský, Martin Lüders, Ingrid Mertig, Jacek Prokop, Ersoy Şaşıoğlu, Julie Staunton, Zdzisława Szotek, László Szunyogh, Wen-Xin Tang, Walter Temmerman, Wulf Wulfhekel, and Yu Zhang. Markus, Guntram and Martin helped me a lot during the preparation of the final version of the manuscript. Jacek taught me that a sense of humor is the right perspective for judging scientific activity.

I am indebted to Ina Goffin for her help, not least for arranging countless formalities and small details, which I would never have been able to properly take care of. Many thanks to Udo Schmidt for his patience and for his taming of the computers; it is equally honest to say that he protected these vulnerable machines against me.

During these years there was a lot of life outside the institute. These people made this time enjoyable, interesting and meaningful. Without them I would have given up many times. I see no way to express my gratitude and feelings towards them here. I hope that I nevertheless managed to show it.

☙

Eidesstattliche Erklärung

Hiermit erkläre ich gemäß §5 Abs. 2b der Promotionsordnung der Naturwissenschaftlichen Fakultät II– Chemie und Physik der Martin-Luther-Universität Halle-Wittenberg vom 3.2.2004, dass ich die vorliegende Arbeit selbständig und ohne fremde Hilfe verfasst sowie keine als die von mir angegebenen Quellen und Hilfsmittel benutzt und die den benutzten Werken wörtlich oder inhaltlich entnommenen Stellen als solche kenntlich gemacht habe. Weiterhin erkläre ich, dass ich bisher keine vergeblichen Promotionsversuche unternommen habe.

Halle, den 9.10.2008

Paweł Buczek

Urtamili coming

Sbudomali orabing

To dut mrrsrtco pracude

Pracude i trude

do im tstco o to coori

Absr ram robie rrcooripi

Absr ram nie mozpi msrlec

Absr ram nie mozpi cooric

Cult, Fragment r "Modi"

Lebenslauf

Paweł Adam Buczek

pbuczek@mpi-halle.mpg.de

ANGABEN ZUR PERSON:

Geburtsdatum:	7.7.1981
Geburtsort:	Rybnik, Polen
Staatangehörigkeit:	Polnisch
Wohnsitz:	Max-Nenke-Str. 1, 06120 Halle/S., Deutschland
Geschlecht:	männlich
Familienstand:	ledig

BILDUNGSGANG

ab Oktober 2005
Doktorand (Physik) an der Martin-Luther-Universität Halle-Wittenberg (Festkörperphysik und Magnetismus). Seit Oktober 2007 wiss. Mitarbeiter am Max-Planck-Institut für Mikrostrukturphysik Halle.

September 2003 – Juni 2005
Master of Science in Physics, University of Alberta, Edmonton, Canada. (Thesis *On the drag experienced by particles in a fluid*)

Oktober 2000 – Juli 2005
Batchelor & Master of Science in Technical Physics, AGH University of Science and Technology, Kraków, Polen. (Thesis *Statistical methods in analysis of crystal imperfections*)

1996-2000
Frycz-Modrzewski Mittelschule, Rybnik, Polen. Abschluss Abitur.

1988-1996
Jan III Sobieski Grundschule, Lyski, Polen.

EIGENE VERÖFFENTLICHUNGEN

1. Buczek, P., "Can aperiodic crystals have periodic diffraction patterns?", *Zeszyty Naukowe AGH*, June 2003
2. Buczek, P., Sadun, L., Wolny, J., "Periodic diffraction patterns for 1D quasicrystals". *Acta Physica Polonica B* **36**(3), 2005.
3. Buczek, P., Wolny, J., "An extinction rule for a class of 1D quasicrystals", *Philosophical Magazine* **86**(6-8), 889-894 (2005)
4. Buczek, P., Wolny, J., "Physical space description of decorated 1D aperiodic sequences", *Philosophical Magazine* **86**(27), 4181-4194 (2006)
5. Buczek, P., Ernst, L., Sandratskii, L., Bruno, P., "The energies and life-times of magnons in bulk iron and one monolayer Fe film", *Journal of Magnetism and Magnetic Materials*, `doi:10.1016/j.jmmm.2009.03.010` (2009)
6. Buczek, P., Ernst, L., Sandratskii, L., Bruno, P., "Energies and life-times of magnons in complex ferromagnets – a first principle study of Heusler alloys", *accepted to Physical Review Letters*